IAEA-TECDOC-1410

Delayed hydride cracking in zirconium alloys in pressure tube nuclear reactors

Final report of a coordinated research project
1998–2002

IAEA
International Atomic Energy Agency

October 2004

IAEA-TECDOC-1410

Delayed hydride cracking in zirconium alloys in pressure tube nuclear reactors

Final report of a coordinated research project
1998–2002

IAEA
International Atomic Energy Agency

October 2004

The originating Section of this publication in the IAEA was:

Nuclear Power Technology Development Section
International Atomic Energy Agency
Wagramer Strasse 5
P.O. Box 100
A-1400 Vienna, Austria

DELAYED HYDRIDE CRACKING IN ZIRCONIUM ALLOYS IN PRESSURE TUBE NUCLEAR REACTORS

IAEA, VIENNA, 2004
IAEA-TECDOC-1410
ISBN 92–0–110504–5
ISSN 1011–4289

Printed by the IAEA in Austria
October 2004

FOREWORD

This report documents the work performed in the Coordinated Research Project (CRP) on Hydrogen and Hydride Degradation of the Mechanical and Physical Properties of Zirconium Alloys. The Project consisted of hydriding samples of Zr-2.5 Nb pressure tube materials used in CANDU-type and RBMK reactors, the measurement of delayed hydride cracking (DHC) rates under specified conditions, and analysis of hydrogen concentrations. The project was overseen by a supervisory group of experts in the field who provided advice and assistance to the participants as required.

All of the research work undertaken as part of the CRP is described in this report, which includes a review of the state of the art in understanding crack propagation by DHC and details of the experimental procedures that produced the most consistent set of DHC rates reported in an international round-robin exercise to this date. All of the participants and many of their co-workers in the laboratories involved in the CRP contributed results and material used in the drafting of this report, which contains compilations of all of the results, their analysis, discussions of their interpretation and conclusions and recommendations for further work.

The research was coordinated in three laboratories in industrialized Member States and seven laboratories in developing Member States. Besides the basic goal of transfer of "know-how" at the laboratory level from some experienced laboratories and the supervisory group to those starting off in the field, the CRP was set up to harmonize experimental methodologies in an attempt to produce consistent data sets, both in the results from a particular laboratory and from one laboratory to another. DHC is sensitive to the local microstructure and internal stress in the area of the crack tip as well as to the temperature history and stress state of the sample. Thus it was clear from the outset that to obtain consistency in the results and their interpretation from laboratory to laboratory, it would be necessary for each participant to work with samples of the same, well-characterized materials and to develop and follow a standard set of experimental protocols.

The basic scope of the programme was originally formulated by the IAEA with the help of the supervisory group in March 1998. It was based on the materials and experimental procedures developed over several decades at the host laboratory of the CRP, the Chalk River Laboratories (CRL) of Atomic Energy of Canada Limited (AECL). The CRP began formally with the signing of contracts and agreements in the second half of 1998. The first research coordination meeting (RCM) was held in December 1998. At this RCM, standard compact tension samples and rings cut from a single CANDU Zr-2.5Nb pressure tube were given to each participant together with detailed instructions for the measurement of DHC and for hydriding samples to a given target concentration. The second RCM was held in Pitesti, Romania, in June 2000 and at that meeting each participant was given a ring of RBMK channel tube material, kindly provided by the Lithuanian participant, for testing within the framework of the CRP. Later in 2000, each participant was provided with a bottle containing 10 standard pellets of Zr-2.5Nb material provided by the host laboratory for hydrogen analysis in a round-robin exercise. The third and final RCM was held in July 2002 in Studsvik, Sweden. Supervisory group meetings were also held at appropriate times to review the results obtained. The CRP was completed and documented at the end of 2002.

The IAEA wishes to thank all of the participants in the CRP for their contributions to this publication. In particular, the IAEA is grateful to the host laboratory (CRL, Canada) that generously provided most of the materials and standard samples for testing during the CRP.

Special thanks are also due to C.E. Coleman (AECL, Canada) who represented the host laboratory and led the supervisory group and to M. Roth (Pitesti, Romania) and V. Grigoriev (Studsvik, Sweden) for their outstanding contributions to the CRP in organizing the RCMs at their institutes. The IAEA officer responsible for this publication was I.G. Ritchie of the Division of Nuclear Fuel Cycle and Waste Technology.

EDITORIAL NOTE

CONTENTS

CHAPTER 1. INTRODUCTION 1
References to Chapter 1 4

CHAPTER 2. DELAYED HYDRIDE CRACKING TESTING – STATE OF THE ART 5

2.1. General description of the phenomenon 5
2.2. Models of DHC cracking 7
2.3. Hysteresis in the solubility of hydrogen in zirconium 9
2.4. Solubility hysteresis and DHC testing 12
2.5. Conditions for crack tip hydride fracture 15
2.6. co-ordinated research program testing 16
2.7. Summary 16
References to Chapter 2 16

CHAPTER 3. EXPERIMENTAL PROGRAM 19

3.1. Philosophy 19
3.2. Materials 19
3.3. Specimen preparation and testing 26
3.3.1. Adding hydrogen 26
3.3.2. Test specimen 30
3.3.3. DHC testing 30
3.4. Hydrogen analysis 32
References to Chapter 3 33

CHAPTER 4. RESULTS AND DISCUSSION 35

4.1. Source of test data 35
4.2. Phase 1: Tests at 250°C on CANDU pressure tube 36
4.3. Phase 2: Tests at other temperatures on CANDU pressure tube 42
4.3.1 Specimen preparation 42
4.3.2. Results of DHC tests 46
4.4. Phase 3: Tests on other materials 47
4.4.1. RBMK Zr-2.5 Nb with TMT-1 heat-treatment 47
4.4.2. CANDU tube from Cernavoda 55
4.4.3. HWR tube from India 56
4.4.4. Other RBMK materials 58
4.4.5. Alternative measurement method – CANDU tube RX094 58
4.5. Striations 59
4.6. Inter-laboratory comparison on hydrogen analysis 62
4.6.1. Precision 64
4.6.2. Bias 64
4.7. Discussion 66
References to Chapter 4 73

CHAPTER 5. MEASUREMENT OF DHC VELOCITY IN FUEL CLADDING USING THE PIN-LOADING TENSION TEST 77
5.1. Method 77
5.2. Results 79
5.3. Summary 80
References to Chapter 5 81

CHAPTER 6. CONCLUSIONS AND RECOMMENDATIONS 83

LIST OF PARTICIPANTS 87

APPENDICES ON CD-ROM

APPENDIX I: PREPARATION OF MATERIAL AND SPECIMENS

APPENDIX II: DHC AXIAL VELOCITY TEST PROCEDURE

APPENDIX III: PROCEDURE FOR ADDING HYDROGEN TO SMALL SECTIONS OF ZIRCONIUM ALLOYS

APPENDIX IV: DETAILS OF DHC TEST RESULTS

CHAPTER 1

INTRODUCTION

Zirconium alloys are used in water reactors because of their low capture cross-section for thermal neutrons and good mechanical and corrosion properties. Early in their application, hydrogen was identified as an embrittling agent. The source of the embrittlement was hydride precipitates that formed as platelets [1.1] Usually, low ductility was found below about 150°C with impact testing or in tensile testing when the normal to the hydride plates was parallel to the tensile stress. Much effort was expended in keeping the hydrogen concentration low and ensuring that any hydrides were in a benign orientation. Results from a few laboratory experiments hinted that zirconium alloys may also fracture by a time-dependent mechanism involving hydrogen, but the first practical confirmation of such a mechanism was the cracking of experimental fuel cladding made from Zr-2.5 Nb [1.2]. Cracks were found in the heat-affected zone in the weld between the cladding and its end-cap after several months of storage at room temperature. Hydrides were associated with the cracks and the process was called Delayed Hydride Cracking – DHC.[1] A factor contributing to the fracture was high residual tensile stress from the welding.

Later, high residual stresses were shown to be responsible for DHC in Zr-2.5 Nb pressure tubes. In CANDU, the pressure tubes are about 6 m long, 104 mm inside diameter and 4 mm thick and are made from cold-worked material. They are joined to the reactor at their ends by a mechanical joint. The tube end is placed inside a thick-walled tube of 403 stainless steel containing three internal, circumferential grooves and the pressure tube is internally rolled to make a seal at the grooves; this configuration is called a rolled-joint. If the rolls are advanced too far, part of the pressure tube is deformed without support from the stainless steel and large residual tensile stresses, up to 700 MPa, arise. Consequently, cracks may initiate. When a crack penetrates the tube wall, heat-transport water leaks and is detected, and the reactor is shutdown. Once the leaking tubes are identified, they are removed and replaced. Twenty tubes out of 780 in Pickering Units 3 and 4 leaked [1.3]. The cracks initiated on the inside surface and grew by DHC radially and axially in a series of bands, Fig. 1.1. The interpretation was that the cracks grew at low temperatures by DHC, but once the reactor was at power and the pressure tubes were at a high temperature, >250°C, cracking stopped because the low hydrogen concentration, <15 ppm, was all in solution. The crack surface oxidized. Cracking continued during subsequent reactor shutdowns and the stopped crack continued to oxidize during power production. Each band on the fracture surface corresponded with a reactor shutdown and period of operation, with cracking at the expected rates for DHC at the temperature of the shutdown [1.4]. To prevent further occurrences of such cracking, depending on the reactor, the residual stresses were minimized by stress-relief or redesign of the rolled-joint [1.5].

Cracking in the pressure tubes in RBMK reactors had a similar cause. These tubes have a length of about 8 m, an inside diameter of 80 mm and a wall thickness of 4 mm, and the Zr-2.5 Nb is partly recrystallized. The final stage of fabrication involved straightening that induced residual tensile stresses of about 350 MPa. Twenty tubes out of a population of 20,000 leaked because of cracking by DHC initiated on the outside surface. Most of the failures were in the first two years of operation of the Kursk and Chernobyl reactors [1.6].

[1] In the literature on zirconium alloys, the time-dependent cracking involving hydrogen has had several names but the accepted one is delayed hydride cracking or DHC.

Similar cracking was observed in guide tubes. Stress relief after straightening has prevented further cracking.

Fig. 1.1. Through-wall crack in a CANDU Zr-2.5 Nb pressure tube, showing oxidized crack growth bands. The crack initiated at the inside surface just inboard of the rolled joint.

These failures prompted much research on the phenomenology and mechanisms of DHC in zirconium alloys. Although no new cracks have been observed in CANDU or RBMK reactors during the past 18 years, as the reactors age the spectre of DHC looms because of increasing hydrogen concentration from corrosion and potential mechanical damage to the surfaces of the pressure tubes. Thus constant vigilance is required. The results of the research are used to determine the life of the pressure tubes due to both crack initiation and subsequent DHC propagation. Should a crack initiate and penetrate the tube wall, water leaking from the through-wall crack is detected and the reactor must be capable of being shut-down before the critical crack length is reached and the pressure tube ruptures. This sequence is the basis for Leak-Before-Break (LBB) [1.7]. The values required to support LBB are knowledge of the length of the crack at leakage, the critical crack length for rupture and the velocity of DHC in the axial direction of a tube. The latter quantity is the focus of this project. The IAEA set up a co-ordinated research programme (CRP) on Hydrogen and Hydride Induced Degradation of the Mechanical and Physical Properties of Zirconium-based Alloys the objective of which was to transfer "know-how" on laboratory practices to member states who have pressure tube reactors but were unfamiliar with DHC testing. The participating Institutes in the CRP are listed in Table 1.1[2]. The major goal of the programme was to establish a uniform and consistent laboratory practice to determine the DHC velocity in the axial direction of pressure tubes to be followed internationally so that meaningful inter-laboratory comparison of the results could be made. Two reference materials were tested – CANDU cold-worked Zr-2.5 Nb and RBMK Zr-2.5 Nb in the TMT-1 heat-treated condition. Participants were encouraged to test examples of their own material for comparison with the reference materials.

As an extension of this CRP, preliminary development of a test method for fuel cladding is in progress [1.8]. In some Zircaloy nuclear fuel cladding used in boiling water reactors (BWR), hydride cracking is strongly implicated in long splits that allowed substantial leakage of fission products [1.9–1.11]. Cladding in BWRs is usually a tube with diameter of about

[2] The names of the participating Institutes and their usual acronyms are given in the list of Contributors, page 101. For simplicity in the text participants are simply referred to by their country and the Republic of Korea is given as ROK.

TABLE 1.1 Participating Institutes, countries and their reactor types of interest

INSTITUTE[2]	COUNTRY	REACTOR TYPE
CNEA	Argentina	CANDU, PWR (D_2O moderated)
AECL	Canada	CANDU
NPIC	China	CANDU, PWR
BARC	India	Indian HWR
KAERI	ROK	CANDU, PWR
LEI	Lithuania	RBMK
PINSTECH	Pakistan	CANDU
INR	Romania	CANDU
VNINM	Russia	RBMK, WWER
STUDSVIK	Sweden	BWR, PWR, surveillance on RBMK

10 mm, wall thickness of about 0.6 mm and length of about 4 m. The Zircaloy is usually recrystallized and in some designs of fuel rod the inside surface is lined with another zirconium alloy or pure zirconium, to prevent stress corrosion cracking by fission products, such as iodine [1.12]. If the cladding wall is penetrated during operation, for example by fretting, water from the heat-transport system can enter the fuel cavity where, because of the low pressure, steam is produced. Much hydrogen is generated because the steam oxidizes the fuel and the inside surface of the cladding, reducing the partial pressure of oxygen and leaving a gas rich in hydrogen. This process is called "oxygen starvation". At some distance from the primary defect the gas stream becomes almost pure hydrogen, and with break down of the protective oxide layer, copious quantities of hydrogen may be absorbed by the cladding [1.13]. Sometimes, "sunbursts" of hydride are formed on the inside surface. Although the pure Zr liner was often found to be completely corroded, and therefore contributed hydrogen to the inventory and stress through expansion via the oxide, it is not a necessary requirement for the secondary damage because unlined fuel cladding behaves in a similar manner. With fuel expansion during fuel shuffling, the hydrided cladding is stressed which leads to crack initiation. The cracks grow through-wall and may be over 1 m long. The fractures are characterized by brittle regions in "striations" or "chevrons", with the crack front often leading towards the outside surface of the cladding [1.14]. The lower bounds of the crack velocities were in the range 4×10^{-8} to 5×10^{-7} $m.s^{-1}$ based on assuming constant growth rates in the time between first detection of the defect and removal of the fuel. The mechanism of cracking appears to be a form of DHC [1.10, 1.15] perhaps exacerbated by a continuous additional supply of hydrogen from the steam inside the fuel element [1.16]. Careful reactor core management can mitigate the consequences of a primary defect by controlling the fuel expansion.

In this report, in Chapter 2 background to DHC is provided to show the technical basis for the test procedures, Chapter 3 describes the materials, specimen preparation and test methods, and an interlaboratory comparison of hydrogen analysis, the test results are discussed in Chapter 4, possible future work on fuel cladding is described in Chapter 5 while in Chapter 6 conclusions and recommendations are made.

REFERENCES TO CHAPTER 1

[1.1] MUDGE, W.L, Effect of hydrogen on the embrittlement of zirconium and zirconium-tin alloys, Symposium on Zirconium and Zirconium alloys, ASM, Metals Park, OH, (1953) 146–167.

[1.2] SIMPSON, C.J., ELLS, C.E., Delayed hydrogen embrittlement of Zr-2.5wt.%Nb, J. Nucl. Mater., **52**, (1974) 289–295.

[1.3] PERRYMAN, E.C.W., Pickering pressure tube cracking experience, Nucl. Energy, **17**, (1978) 95–105.

[1.4] CAUSEY, A.R., URBANIC, V.F., COLEMAN, C.E., In-reactor oxidation of crevices and cracks in cold-worked Zr-2.5 wt.% Nb, J. Nucl. Mater., **71**, (1977) 25–35.

[1.5] DUNN, J.T., KAKARIA, B.K., GRAHAM, J., JACKMAN, A.H., CANDU-PHW fuel channel replacement experience, AECL-Report, AECL-7538, Atomic Energy of Canada, Ltd., Sheridan Park, Mississauga, Ontario, (1982)

[1.6] PLATONOV, P.A., RYAZANTSEVA, A.V., SAENKO, G.P., KNIZHNIKOV, Y.N.,VIKTOROV, V.F., The study of the cause of cracking in zirconium alloy fuel channel tubes, Poster paper at ASTM Zirconium in the Nuclear Industry – 8th International Symposium, available as AECL report RC-87, (1988).

[1.7] MOAN, G.D., COLEMAN, C.E., PRICE, E.G., RODGERS, D.K., SAGAT, S., leak-before-break in the pressure tubes of CANDU reactors, Int. J. Press. Ves. Piping., **43**, (1990) 1–21.

[1.8] GRIGORIEV, V., JAKOBSSON, R., Application of the pin-loading tension test to measurements of delayed hydride cracking velocity in Zircaloy cladding, Studsvik Report SKI 00:57, (2000).

[1.9] JONSSON, A., HALLSTADIUS, L., GRAPENGIESSER, B., LYSELL, G., Failure of a barrier rod in Oskarshamn, in Fuel in the '90's, International Topical Meeting on LWR Fuel Performance, Avignon, France, ANS and ENS, (1991), 371–377.

[1.10] SCHRIRE, D., GRAPENGIESSER, B., HALLSTADIUS, L., LUNDHOLM, I., LYSELL, G., FRENNING, G., RONNBERG,G., JONSSON, A., Secondary defect behaviour in ABB BWR fuel, International Topical Meeting on LWR Fuel Performance, West Palm Beach, ANS, (1994) 398–409.

[1.11] ARMIJO, J.S., Performance of failed BWR fuel, International Topical Meeting on LWR Fuel Performance, West Palm Beach, ANS, (1994), 410–422.

[1.12] ARMIJO, J.S., COFFIN, L.F., ROSENBAUM, H.S., Development of zirconium-barrier fuel cladding, Zirconium in the Nuclear Industry – 10th International Symposium, ASTM STP 1245, eds, A.M. Garde and E.R. Bradley, ASTM, West Conshohocken, PA, (1994), 3–18.

[1.13] CLAYTON, J.C., Internal hydriding in irradiated defected Zircaloy fuel rods, Zirconium in the Nuclear Industry – 8th International Symposium, ASTM STP 1023, eds. F.P. Van Swam and C.M. Eucken, ASTM, West Conshohocken, PA, (1989), 266–288.

[1.14] LYSELL, G., GRIGORIEV, V., Characteristics of axial splits in failed BWR fuel rods, Ninth International Symposium on Environment Degradation of Materials in Nuclear Power Systems – Water Reactors, AIME-TMS, (1999), 1.169–1.175.

[1.15] EFSING, P., PETTERSSON, K., Delayed hydride cracking in irradiated Zircaloy cladding, Zirconium in the Nuclear Industry – 12th International Symposium, ASTM STP 1354, eds. G.P. Sabol and G.D. Moan, ASTM, West Conshohocken, PA., (2000), 340–355.

[1.16] EDSINGER, K., DAVIES, J.H., ADAMSON, R.B., Degraded fuel cladding fractography and fracture behavior, Zirconium in the Nuclear Industry – 12th International Symposium, ASTM STP 1354, eds. G.P. Sabol and G.D. Moan, ASTM, West Conshohocken, PA., (2000), 316–339.

CHAPTER 2

DELAYED HYDRIDE CRACKING TESTING – STATE OF THE ART

2.1. General Description of the Phenomenon

Delayed hydride cracking is a sub-critical crack growth mechanism occurring in zirconium alloys as well as other hydride-forming materials that requires the formation of brittle hydride phases at the tip of a crack and subsequent failure of that hydride resulting in crack extension. The basic process is illustrated in Fig. 2.1.

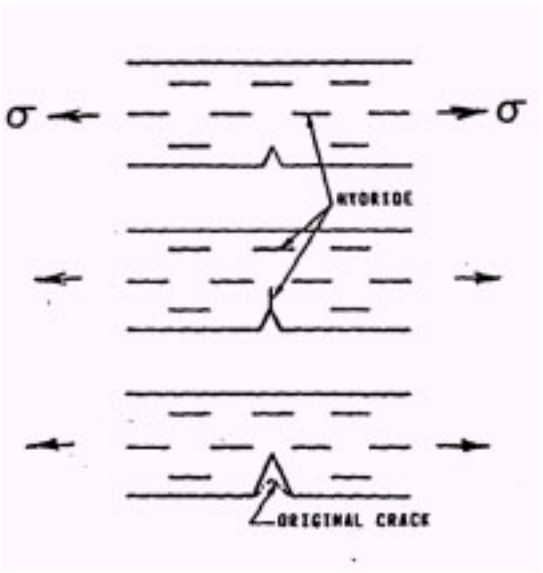

Fig. 2.1. A schematic illustration of a single step in DHC starting with a notch under stress (top), hydride precipitation at the notch (middle) and fracture of hydride and crack extension from the notch (bottom).

Hydrogen in solution in the zirconium alloy is transported to the crack tip by diffusion processes where it precipitates as a hydride phase. When the precipitate attains a critical condition, related to its size and the applied stress intensity factor, K_I, fracture ensues and the crack extends through the brittle hydride and arrests in the matrix. Each step of crack propagation results in crack extension by a distance approximately the length of the hydride. This step-wise progression may leave striations on the fracture surface corresponding to each step that can often be observed with a low power light microscope.

As with many other stable crack propagation mechanisms, the phenomenon of cracking can be generally described by the dependence of the crack growth rate or crack velocity on the applied stress intensity factor. The general shape of such a relationship has been shown to be similar to that demonstrated in many forms of environmentally assisted cracking and is illustrated in Fig. 2.2 [2.1, 2.2, 2.3]. This figure shows that, at stress intensities below a threshold, K_{IH}, cracks do not grow even though a quantity of hydride may accumulate at a crack tip under stress. In DHC, the transition to the plateau velocity portion of the velocity vs K_I curve is quite abrupt [2.4] and then the velocity does not change significantly with increasing K_I until the applied K_I approaches the fracture toughness corresponding to the initiation of unstable fracture for the material under test.

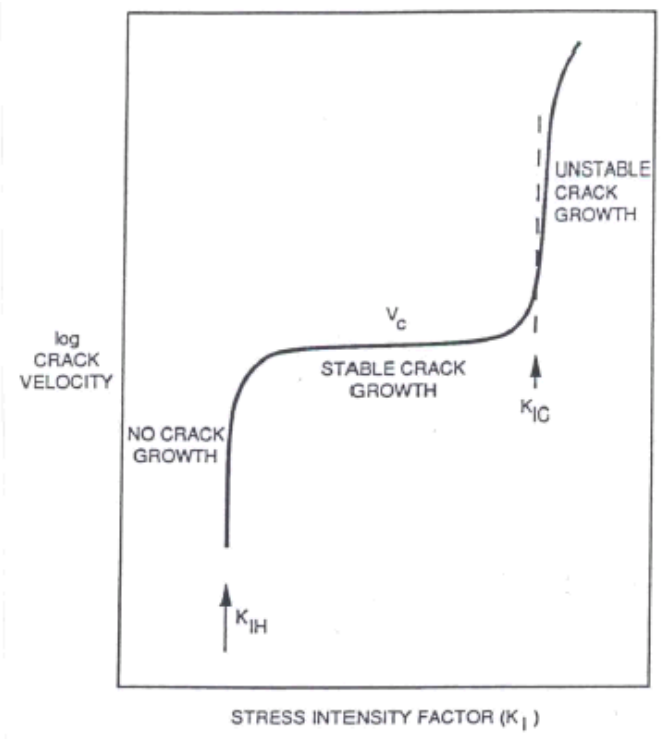

Fig. 2.2. A schematic representation of the relationship between crack velocity and stress intensity factor exhibited by the DHC phenomenon.

The velocity of the crack in the plateau region of the velocity-K_I curve has been found to have strong temperature dependence, as shown in Fig. 2.3. This temperature dependence reflects both the rate at which hydrogen in solution can be transported to the crack tip and the amount of hydride required to be formed for each fracture step in the propagation. Together, these determine the amount of hydrogen required to be transported per unit distance of crack growth The rate of transport of hydrogen to the crack tip is dependent upon the diffusion coefficient of hydrogen in the material, the amount of hydrogen available to be transported (the hydrogen dissolved in the metal) and the driving force for moving the hydrogen to the crack tip. Because the diffusion coefficient and the maximum amount of hydrogen available to be transported are both thermally activated phenomena, the crack velocity has the temperature dependence of a thermally activated process, decreasing with decreasing temperature.

The driving force for movement of hydrogen in solution to the crack tip is the gradient in the chemical potential of the hydrogen in solution that is determined by both the concentration and the stress state [2.5]. Hydrostatic tension reduces the chemical potential of hydrogen in solution in the material. Since the stress state near a crack tip under load is dependent upon the material yield stress, there is an expectation that the driving force can be higher in materials with higher yield strength. This would lead to a higher rate of diffusion of hydrogen to the crack tip and a higher crack velocity even if other factors (such as the amount of hydrogen required per unit length of crack extension) were unchanged.

These general features of the crack growth process were recognized in some of the initial studies of the phenomenon. However, understanding many of the details of the process remains an active area of investigation [2.6–2.10].

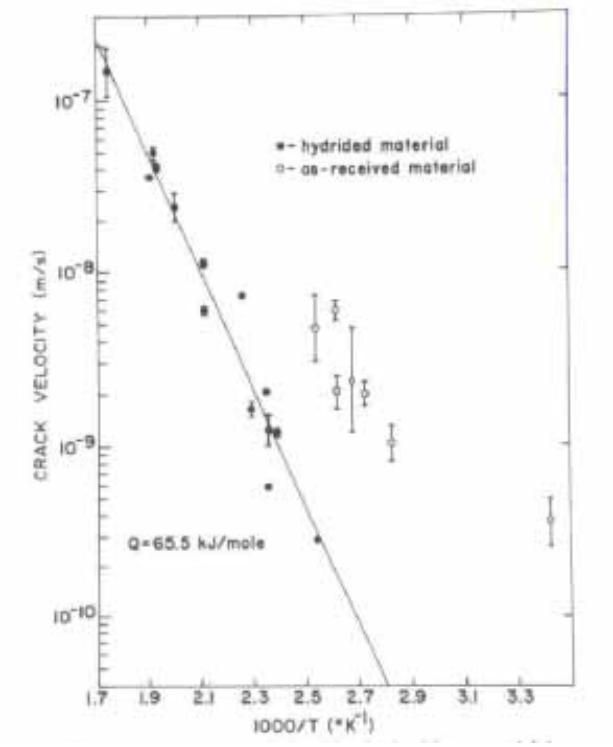

Fig. 2.3. The temperature dependence of the plateau in DHC velocity vs K_I [Ref. 2.4].

The amount of hydrogen dissolved in the metal and available for diffusion to the crack tip is a critical determinant of the cracking phenomenon. Some of the earliest experimental work on DHC, demonstrated that the upper temperature limit at which DHC could be observed corresponded closely with the temperature at which all hydrides could be dissolved on heating [2.11]. The hysteresis of the solubility of hydrogen in zirconium alloys [2.12–2.14], affects the crack growth rate that are relevant both to measurements of crack growth rates and to their prediction for the operating conditions of zirconium components in nuclear reactors. DHC crack growth rates have been observed to be dependent upon whether the crack growth temperature is approached by cooling or by heating [2.15]. These observations are a direct result of the hysteresis of the solubility of hydrogen in the material [2.16].

The purpose of this chapter is to review the phenomenon of DHC with emphasis on current understanding and how that understanding was used to establish a program of testing for this coordinated research project.

2.2. Models of DHC Cracking

The initial theoretical description of DHC was based on the model illustrated in Fig. 2.4 [2.2]. In this model, there is a hydride growing in the stress field of the crack tip.

The crack tip hydride grows due to the migration of hydrogen from hydrides in the bulk of the material at some characteristic distance from the crack tip. The driving force for the diffusion of the hydrogen is the difference in the chemical potential of hydrogen in the crack tip hydride due to the local hydrostatic stress field and the chemical potential of hydrogen in the hydrides under a reduced hydrostatic stress at the characteristic distance from the crack tip. Due to the positive partial molar volume of hydrogen in the hydrides, increasing tensile hydrostatic stress on a hydride reduces the chemical potential of hydrogen in that hydride. Therefore there exists

a chemical potential difference between hydrogen in the hydride at the crack tip compared with hydrogen in a hydride in the bulk. Assuming a condition of local chemical equilibrium of hydrogen at the interfaces between hydride and matrix, a chemical potential difference between these locations must exist for hydrogen in solution as well. This chemical potential difference drives the migration of the hydrogen in solution to the crack tip where it precipitates. In this model, the hydrides in the bulk dissolve to maintain the local hydrogen concentration in solution in the matrix at the hydride interface at the solubility limit for the temperature at which the cracking is occurring.

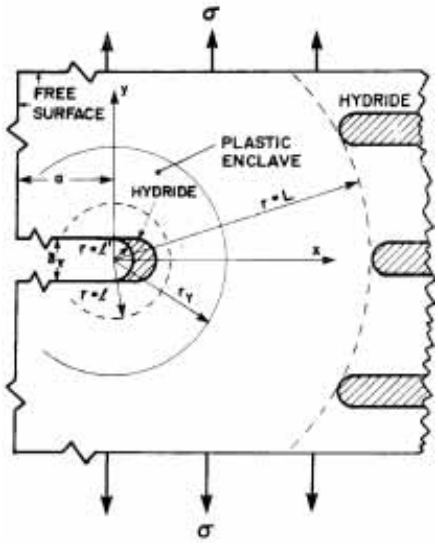

Fig. 2.4. The initial model for DHC developed by Dutton and Puls [Ref.2.2] showing the hydride growing at the crack tip and the hydrides in the matrix dissolving.

Assuming cylindrical symmetry about the crack tip, an expression for the crack velocity, V, according to this model was derived which had the following form:

$$V = G\, D_H C_H \{\exp(^hV_H\, \Delta p/RT)$$

where:

- G is a function that includes geometry factors as well as the molar volumes of zirconium and hydride, and the composition of the hydride;
- D_H is the diffusion coefficient of hydrogen (a function of temperature);
- C_H is the solubility of hydrogen in zirconium in a stress-free state;
- ^hV_H is the partial molar volume of hydrogen in zirconium hydride;
- Δp is the difference in hydrostatic tensile stress between the crack tip and the bulk at a distance equal to the characteristic hydride spacing away from the crack tip;
- R is the gas constant; and
- T is the absolute temperature.

The dependence of the crack velocity on the diffusion coefficient and the solubility is explicit in this expression. The model assumed that the amount of hydride growth required for a given distance of crack growth was fixed and that the hydride growth could be assumed to be occurring continuously even though the process was recognized as being discontinuous in nature.

This model has been altered over the years but key features have been maintained. A major change in the model occurred when it was recognized that the assumed behaviour of the solubility of hydrogen in this model did not adequately reflect the observations and modeling of the phenomenon of hysteresis in the solubility of hydrogen in hydrogen-zirconium alloy systems. A revised model of DHC incorporating the hysteresis of the solubility was produced [2.17]. In this model, the hysteretic effects on the solubility of hydrogen are taken into account: there are two different expressions used for the solubility depending upon whether hydride is dissolving or precipitating. This model was able to provide some explanation for the different crack velocities obtained on heating and on cooling.

More recently, finite element modeling has been used to examine effects of temperature cycling and load changes on the accumulation of hydride at a flaw [2.18]. This model implicitly assumes different hydrogen solubility limits for dissolution and precipitation. It has been extended to account for the changing stress state at a flaw due to the formation of the hydride [2.19] and to model DHC velocities under temperature transients [2.20]. There are no simple expressions for crack velocities derived using these finite element models.

2.3. Hysteresis in the Solubility of Hydrogen in Zirconium

The observations of the behaviour of hydrogen in zirconium alloys indicate that there is a significant hysteresis in the solubility depending upon whether hydrides are dissolving or precipitating. These effects have been known for a long time [2.12, 2.13] and are seen using several techniques including differential scanning calorimetry, and measurements of changes in thermal expansion, electrical resistivity, and elastic modulus. In all cases, the effect is manifested as a difference between the concentration of hydrogen in solution in the metal in equilibrium with dissolving hydrides at a particular temperature and the concentration in equilibrium with precipitating hydrides at the same temperature. This is illustrated for Zircaloy material in Fig. 2.5 [2.21].

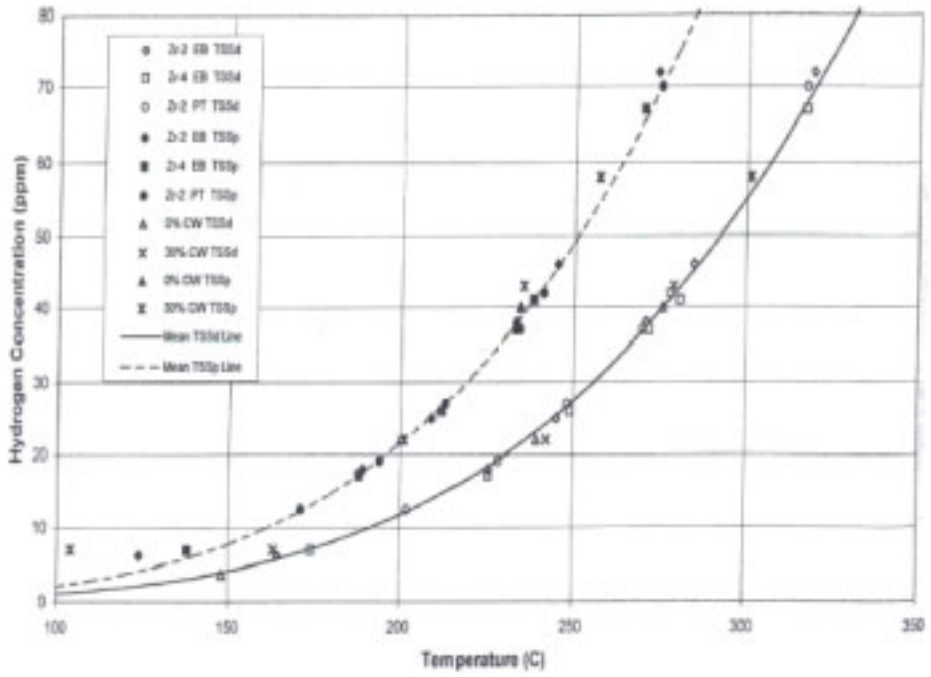

Fig. 2.5. The hysteresis in the solubility of hydrogen in Zircaloy observed using differential scanning calorimetry [Ref. 2.21].

These results were based on differential scanning calorimetry measurements of the zirconium-hydride transformation. Similar results have been obtained in Zr 2.5Nb alloys using elastic modulus measurements [2.14], (Figs 2.6 and 2.7). The modulus measurements clearly demonstrated that the amount of hydrogen in solution at a given temperature is dependent upon whether hydrides are dissolving or precipitating. Since the degree of modulus reduction is depends upon the amount of hydrogen in solution, by comparing the modulus at a given temperature with that in an unhydrided specimen, the amount of hydrogen in solution can be determined for each temperature. The complete solubility curve can be determined from a single specimen with sufficiently high hydrogen concentration. Such measurements have shown that the solubility limit associated with precipitation is itself dependent upon the thermal history of the specimen and two bounding solubility curves can be defined: one based upon precipitation of new hydrides (TSSP1) and the second based upon precipitation associated with growth of hydrides or precipitation at locations of pre-existing hydride (TSSP2).

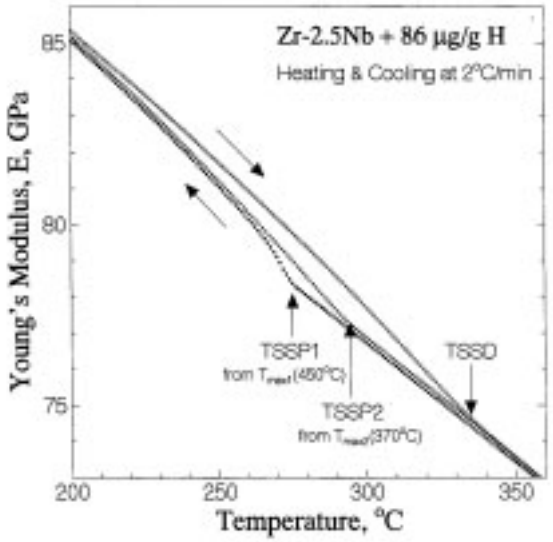

Fig. 2.6. Hysteresis in hydrogen solubility in Zr-2.5 Nb observed using dynamic elastic modulus measurements [Ref. 2.14].

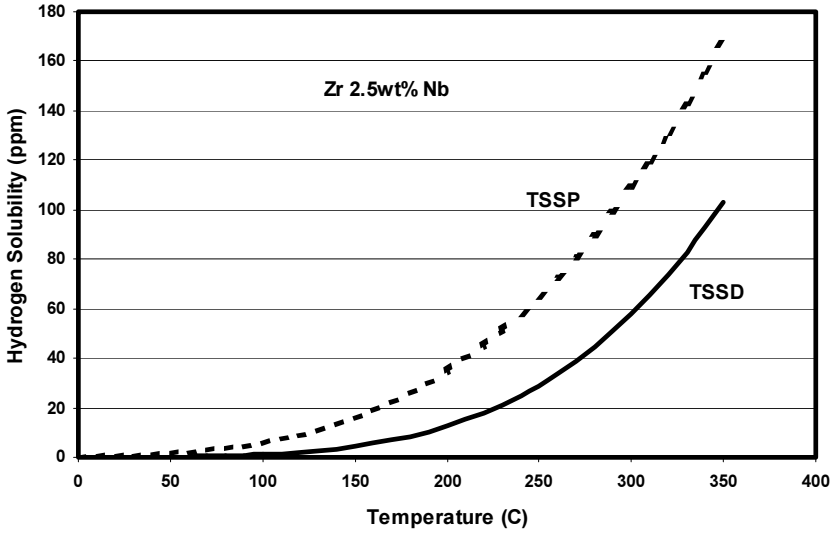

Fig. 2.7. The hydrogen solubility of Zr-2.5 Nb material measured using dynamic elastic modulus. The TSSP curve is that defined by TSSP1 in Reference 2.14.

The origin of this hysteresis is the internal stresses in the solid system developed during precipitation and dissolution of hydride caused by the 17% volume change associated with the transformation of alpha zirconium matrix to delta hydride [2.22]. If the system of hydrogen in zirconium with hydrides present could be completely stress free, (i.e. free of both internal and externally applied stresses), it would be expected that the equilibrium between hydrogen in solution and hydrogen in hydrides would be defined at a particular temperature by a single concentration of hydrogen in solution and this equilibrium would not be affected by the direction of approach in temperature to the temperature of interest. Some supersaturation could be required to nucleate hydrides on cooling due to the need to create new interfaces with characteristic surface energies. However, internal stresses develop within the system during the alpha zirconium to hydride transformation (and the reverse) and will be more intense near the hydrides themselves. These internal stresses and the plastic work associated with the formation and dissolution of hydrides are responsible for the solubility behaviour of hydrogen in zirconium alloys [2.23–2.25].

The solubility hysteresis appears to be very close to an equilibrium phenomenon because it is observed even when very slow heating and cooling rates are used or when material is charged with hydrogen isothermally [2.26]. If it is assumed that the solubility hysteresis is truly equilibrium behaviour, the chemical potential of hydrogen throughout the system can be assumed to be uniform at each temperature condition. The bulk concentration of hydrogen in solution away from the hydrides can be used as a measure of the chemical potential of hydrogen throughout the system at equilibrium. At a given temperature, the hydrogen concentration in solution in equilibrium with dissolving hydride is less that that in equilibrium with precipitating hydride. In this solid system with no externally applied stress, the chemical potential of hydrogen in a hydride undergoing dissolution is significantly lower than the chemical potential of hydrogen in a hydride that is precipitating.

It follows that non-equilibrium would exist if hydrides in a matrix were in another stress state. Chemical potential differences between hydrides in different stress states would produce local differences in the chemical potential of hydrogen in the surrounding matrices that would act to drive hydrogen towards the hydride in the higher tensile stress state.

The effect of thermal history on the concentration of hydrogen in solution of a specimen containing, for example, 60 ppm, can be illustrated by examining what occurs when the specimen is taken through a specific temperature sequence through heating and cooling. Referring to Fig. 2.8, as the temperature is increased from room temperature, the hydrogen concentration increases following the TSSD curve along AB. When the temperature begins to decrease, the concentration in solution is assumed not to change until the precipitation solvus is reached at point C. On further cooling, the concentration in solution drops following the precipitation solvus (TSSP) until point D. If the temperature is now increased again, the concentration in solution does not increase until the TSSD curve is reached. Consideration of similar temperature trajectories with different peak temperatures suggests that at a given temperature (such as the DHC test temperature), the concentration of hydrogen in solution in the bulk of the specimen could be made to vary from the TSSD concentration to the TSSP concentration. Thus the chemical potential driving force for DHC can be made to vary by changing the peak temperature attained immediately prior to the test temperature.

The difference in the stress states of the dissolving and precipitating hydrides causes the hysteresis. To change the stress state of a hydride from one state to the other, there must be a finite amount of hydrogen exchanged between the hydride and the matrix. Thus the assumption that the concentration in solution does not vary on cooling from the TSSD state to the TSSP state, i.e. along line BC in Fig. 2.8, cannot be strictly correct because a small change

in the concentration in solution is required to accommodate the hydrogen exchange between the matrix and the hydride necessary to change the stress state of the hydride.

2.4. Solubility Hysteresis and DHC Testing

Solubility hysteresis has very significant effects on DHC in zirconium alloys. The crack velocity and K_{IH} are both affected. These are discussed in turn.

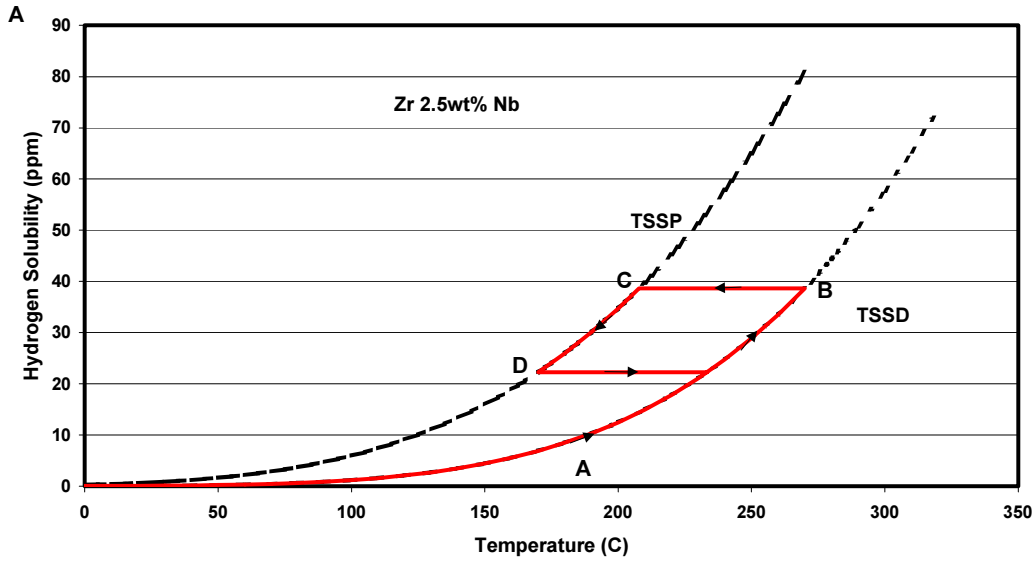

Fig. 2.8. The trajectory ABCD shows how hydrogen in solution varies during a temperature cycle.

For a DHC crack growing at isothermal conditions under a constant applied stress intensity, the rate of growth of the crack is determined by the chemical potential driving force for moving hydrogen to the crack tip from the surrounding material; the greater the chemical potential of hydrogen in the matrix, the higher the driving force and the larger velocity is a consequence. The corollary is that, at a given temperature, the DHC velocity may be a sensitive indicator of the chemical potential of hydrogen in the system.

This expectation is consistent with the observed behaviour in cracking tests. The crack velocity can be very sensitive to the precise thermal history of the test specimen immediately prior to the DHC crack growth test [2.15, 2.27]. Shek and Graham's result is shown in Fig. 2.9. In these tests, crack growth rates in unirradiated Zr-2.5 Nb specimens containing 60 ppm of hydrogen were measured at 250ºC. Each specimen was heated to a different peak temperature before cooling to the test temperature. There are very large differences in the observed crack velocities with the highest velocities being obtained in specimens in which the hydrogen was all taken into solution at the peak temperature. The presence of hydrides in the bulk of the material is not a sufficient condition for cracks to grow with a measurable velocity by DHC: hydrides would certainly have been present in the bulk material for tests in which the peak temperature was simply the test temperature of 250ºC and yet there was no indication of crack growth during the test. This result implies that the chemical potential of hydrogen in the system was too low to produce sufficient hydride at the crack tip to reach the critical state for fracture of the hydride. This result is also clear proof that the critical stress intensity factor for crack propagation is dependent upon the chemical potential of hydrogen in the system since no crack growth was observed at peak temperatures at or below 262ºC.

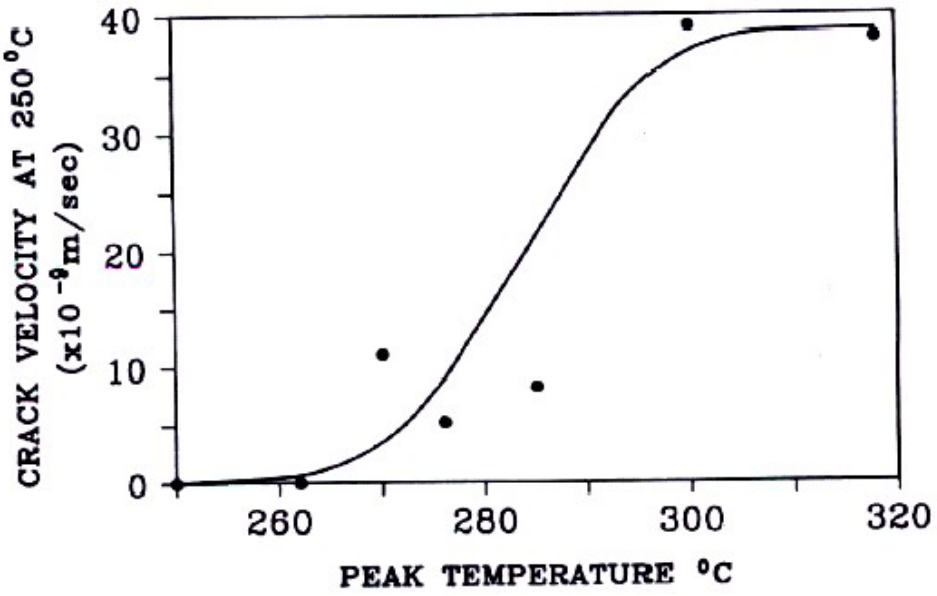

Fig. 2.9. DHC velocity measurements at 250℃ in CANDU pressure tube material showing the effect of peak temperature before testing [Ref. 2.27].

The DHC velocity measured at a test temperature will be the highest possible for that particular specimen at the test temperature when the concentration in solution (and hence the chemical potential of hydrogen in the bulk material) is maximized. Maximization for a particular specimen occurs either if all the hydrogen is in solution at the test temperature or if the hydrogen concentration in solution corresponds to the precipitation solvus. To find the maximum possible DHC velocity for a material, independent of the hydrogen concentration, there must be sufficient hydrogen in the specimens to achieve the precipitation solvus concentration at the test temperature and the thermal history of the sample must ensure that the concentration in solution is at the precipitation solvus level.

Figure 2.10 [2.16, 2.28] illustrates schematically the effects of solubility hysteresis on measure-ments of DHC crack velocities. For a specimen with a specific hydrogen concentration, the velocities can be measured after achieving the test temperature either through heating or cooling. If the specimen is heated to sequentially higher test temperatures, the velocities follow a profile similar to that described by $T_1T_2T_3T_4$. The maximum velocity occurs at T_2. When the velocities are measured after cooling from temperature T_4, the velocities follow the profile given by $T_4T_5T_6T_2$. The velocity at T_6 is the maximum for the specimen and this velocity is only achieved by cooling to T_6 from a sufficiently high temperature, T_4, such that all hydrogen was taken into solution. The decrease in velocity on heating above T_2 reflects a decreasing driving force since the total hydrogen available for transport continues to increase with increasing temperature. On cooling from T_4, the crack can grow at T_5 because there is now sufficient driving force to precipitate hydride at the crack tip in sufficient quantity to cause cracking. Upon further cooling to T_6, the velocity increases due to an increased driving force as the concentration of hydrogen required to precipitate at the crack tip decreases with temperature decrease, but the concentration in solution in the bulk material remains constant (all hydrides in the bulk dissolved).

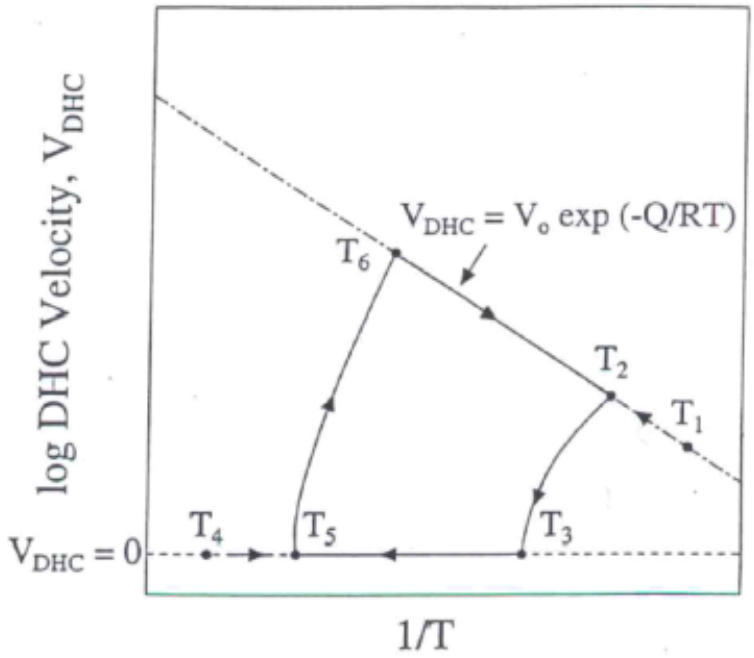

Fig. 2.10. A schematic diagram of the temperature dependence of the DHC velocity showing the effect of temperature history [Refs. 2.16, 2.28].

The schematic diagram makes it clear that the crack velocity is very dependent on the path of the temperature history immediately prior to the velocity measurement. It can be shown by consideration of other temperature histories that, at the same temperature, the velocity may be the maximum achievable or any lower velocity including zero. For this reason, to make a consistent inter-laboratory comparison of velocities, the temperature history to be followed immediately prior to the test temperature must be specified, as was done for the current co-ordinated research project.

The conditions under which hydrides nucleate and grow in the bulk of the material can influence the chemical potential of hydrogen in the bulk at a particular temperature [2.14]. Factors such as the maximum temperature to which the specimen was exposed prior to precipitation and the cooling rate, can modify the chemical potential and have been observed to modify the DHC crack growth rates [2.29]. There is a good correlation, in a specimen with fixed hydrogen concentration, between the temperature at which all hydride is dissolved on heating (the TSSD temperature) and the maximum temperature at which DHC can be observed when the test temperature is approached from a higher temperature [2.17]. In most cases the maximum temperature for DHC is slightly less than the TSSD temperature. This is the case even though, on cooling, hydrides do not form in the bulk of the specimen until the precipitation solvus temperature is attained, which can be as much as 50°C lower than the dissolution temperature. The reason for this observation has been explained by Eadie et al [2.30]. A very small difference between the partial molar volumes of hydrogen in solution in the matrix and hydrogen in the hydride means that there is little effect of stress on the solubility limit. However, the hydrostatic stress at the crack tip results in an elevated concentration of hydrogen in solution, due to the interaction of the partial molar volume of hydrogen in solution and the hydrostatic stress. The amplification is large enough at a sharp crack under load for the hydrogen concentration in solution at the crack tip to reach the precipitation solubility limit when the hydrogen concentration in solution far from the crack tip is close to the dissolution solvus concentration.

2.5. Conditions for Crack Tip Hydride Fracture

Fracture of the crack-tip hydride is a necessary requirement for the propagation of a crack by DHC. The detailed micro-mechanisms of such fracture are not yet well understood. However, a very useful approach for practical engineering assessments has been developed based on a process-zone model of hydride fracture [2.31, 2.32]. This model assumes that the hydrided zone at the crack tip can be considered as a fracture process zone similar to that proposed in the strip-yield fracture model [2.33, 2.34]. Within the process zone, the total stress acting in the crack-opening direction is a superposition of the usual K-type stress field due to the crack and a restraining stress due to the hydride. The hydride-induced restraining stress is assumed to be uniform over the process zone and decreases with an increased amount of hydride precipitation.

This assumption of stress uniformity is consistent with finite element modeling of hydride precipitation at crack tips that showed a condition of almost uniform stress in the crack-tip hydrided zone as the hydride developed [2.19]. The finite element model assumed that the hydride transformation strain was isotropic and that the condition for hydride precipitation was consistent with the precipitation solvus (i.e. the concentration in solution could not exceed TSSP for that temperature). It was observed that the stress within the crack tip region was reduced as the hydride precipitated, consistent with expectations. This same finite element model also suggested that the hydrides at the crack tip would take on a tapered shape. This shape of hydride was observed in low strength Zr-2.5Nb material in which the hydride size and shape prior to fracture could be clearly observed using light metallography [2.9]. The tapered shape of the hydride suggests that the amount of hydride required to be precipitated at the crack tip to generate a certain crack growth step length may be proportional to the square of the step length rather than simply proportional to the step length itself. The corollary of this observation is that the amount of hydrogen required to be transported to the crack tip to generate a certain amount of crack growth will be dependent on the crack-growth step size with larger steps requiring more hydrogen transport per unit length. Therefore, the expectation is that the crack velocity will be reduced in materials exhibiting large crack growth step sizes if other material characteristics are kept constant.

In the process-zone model, there are two conditions that must be met for fracture: a critical crack opening displacement, v_c, due to hydride precipitation must be attained, and, the uniform stress in the process zone must be above a critical value, p_c. The hydride must be sufficiently large and the stress along the hydride must be sufficiently high for fracture to occur. These parameters of the model are determined from values of K_{IH} and the stress required to cause fracture of long hydrides perpendicular to smooth surfaces. Good agreement between model predictions and crack initiation testing has been demonstrated for a range of flaw geometries [2.32].

During crack initiation and propagation in a DHC test, the conditions for crack tip hydride fracture must be repeatedly met for the crack to continue to propagate. When the load is first applied to a pre-cracked specimen after the DHC test temperature has been reached, there is always an incubation time required for the formation of the first hydride of the critical size required for fracture. This incubation time could be expected to be dependent upon the driving forces for hydrogen diffusion to the crack tip, the diffusion coefficient in the material and the amount of hydride required to form the critical hydride. These are the same parameters that ultimately determine the observed DHC crack velocity. In practice, incubation times are somewhat more variable than measurements of crack velocities.

Although, for simplification, the modelling of DHC has often used isotropic material properties, the crystallographic texture and material microstructure do affect the propagation of cracks by DHC. The crystallographic texture affects the precipitation of hydrides because hydride platelets have a crystallographic relationship with the metal from which they are formed. The transformation strains (metal to hydride) are also directionally related to the crystallography. The stress state of a crack tip is modified by the precipitation of hydride in a way that depends upon the orientation of the crack within the material (if that material is anisotropic). The critical hydride size and shape required for fracture will then be dependent upon the texture. DHC crack initiation and propagation in an anisotropic material will itself be anisotropic and that is what is observed [2.6, 2.7]. Crystallographic texture differences between materials will also produce differences in DHC characteristics, such as K_{IH} and crack velocity.

2.6. Co-ordinated Research Programme Testing

The testing procedure recommended for the DHC velocity measurement in the CRP was designed to maximize the velocity at each test temperature. Under all the test conditions in the test matrix (see Chapter 3, Section 3.3.3), the relationship between the hydrogen concentration in the specimen, the peak temperature achieved immediately prior to the test temperature and the DHC testing temperature were such that the concentration of hydrogen in solution was equal to the TSSP concentration at the crack tip for the test temperature.

Similarly, the applied stress intensity factor range (a minimum of 15 MPa√m) was sufficiently in excess of the usual range of K_{IH} for the materials tested (generally within a range of 4.5 to 10 MPa√m) that crack propagation should not be limited due to insufficient applied stress intensity factor.

2.7. Summary

A brief summary of the state of the art of the understanding of effects of hydrogen concentration in solution on DHC has been presented. The effects of hydrogen hysteresis on the expected driving force required to move hydrogen in solution to the crack tip have been discussed. The resulting effects on DHC testing have been shown to be consistent with observations reported in the literature. The defined test conditions for the CRP tests have been shown to meet the conditions required to maximize the crack growth rates at the test temperatures involved.

REFERENCES TO CHAPTER 2

[2.1] COLEMAN, C.E., AMBLER, J.F.R., “Delayed hydride Cracking in Zr-2.5wt%Nb Alloy”, Reviews on Coatings and Corrosion, Vol.III, Freund, Israel, (1979), 105–157.

[2.2] DUTTON, R., NUTTALL, K., PULS, M.P., SIMPSON, L.A., “Mechanism of Hydrogen-Induced Delayed Hydride Cracking in Hydride Forming Materials”, Metall. Trans.A, 8A, (1977), 1553–1562.

[2.3] COLEMAN, C.E., “Cracking of Hydride-forming Metals and Alloys”, Comprehensive Structural Integrity, Elsevier, Eds. I. Milne, R.O. Ritchie and B. Karihaloo, 2003,Chapter 6.03, pp.103–161.

[2.4] SIMPSON, L.A., PULS, M.P., “The Effects of Stress, Temperature and Hydrogen Content on Hydride-Induced Crack Growth in Zr-2.5Nb”, Metall. Trans.A, 10A, (1979), 1093–1105.

[2.5] LI, J.C.M., ORIANI, R.A., DARKEN, L.S., “The thermodynamics of a Stressed Solid”, Phys. Chem. Neue. Folge, 49, (1966) 271–290.
[2.6] KIM, Y.S., KWON. S.C., KIM, S.S., Crack growth pattern and threshold stress intensity factor, KIH of Zr-2.5Nb alloy with the notch direction, J. Nucl. Mater., 280 (2000) 304–311.
[2.7] KIM, Y.S., PERLOVICH, Y., ISAENKOVA, M., KIM, S.S., CHEONG, Y.M., Precipitation of reoriented hydrides and textural change of α-zirconium grains during delayed hydride cracking of Zr-2.5%Nb pressure tube, J. Nucl. Mater. 297 (2001) 292–302.
[2.8] SINGH, R.N., KUMAR, N., KISHORE, R., ROYCHAUDHURY, S., SINHA, T.K., KASHYAP, B.P., “Delayed hydride cracking in Zr-2.5Nb pressure tube material”, J. Nucl. Mat., 304, (2002), 189–203.
[2.9] SHEK, G.K., "The Effect of Material Properties, Thermal and Loading History on Delayed Hydride Cracking in Zr-2.5 Nb Alloys," PhD Thesis, University of Manchester, 1998.
[2.10] RESTA LEVI, M., SAGAT, S., “The Effect of Texture on Delayed Hydride Cracking in Zr-2.5Nb Alloy”, Proceedings of the International Symposium on Environmental Degradation of Materials and Corrosion Control in Metals, 38th Annual Conference of Metallurgists, 29th Annual Hydrometallurgical Meeting of CIM, 1999 August, Quebec City, Quebec Also, AECL-report AECL-12045.
[2.11] COLEMAN, C.E., AMBLER, J.F.R., “Measurement of Effective Solvus of Hydrogen in Zr-2.5wt% Nb Using Acoustic Emission”, Hydrogen in Metals, The Metallurgical Society of CIM Annual Volume, Can. Met. Quart., 17 (1978), 81–84.
[2.12] ERICKSON, W.H., HARDIE, D., “The Influence of Alloying Elements on the Terminal Solubility of Hydrogen in Alpha Zirconium”, J. Nucl. Mats. 13,(1964), 254–262.
[2.13] SLATTERY, G., “The Terminal Solubility of Hydrogen in Zirconium Alloys between 30 and 400 °C”, J. Inst. Met., 95, (1967), 43–47.
[2.14] PAN, Z.L., RITCHIE, I.G., PULS, M.P., “The terminal solid solubility of hydrogen and deuterium in Zr-2.5Nb alloys”, J. Nucl. Mat. 228,(1996) 227–237.
[2.15] AMBLER, J.F.R,. “Effects of Direction of Approach to Temperature on Delayed Hydride Cracking Behaviour of Cold Worked Zr-2.5Nb”, Zirconium in the Nuclear Industry: Sixth International Sym. STP 824, (1984) 653–674.
[2.16] SHI, S.Q., PULS, M.P., “Advances in the Theory of Delayed Hydride Cracking in Zirconium Alloys”, Hydrogen Effects in Materials. Eds. A.W. Thompson and N.R. Moody, The Minerals, Metals and Materials Society, 1996, pp.611–621.
[2.17] PULS, M.P., “Effects of Crack Tip Stress States and Hydride-matrix Interaction Stresses on Delayed Hydride Cracking”, Met. Trans. A, 21A, (1990), 2905–2917.
[2.18] EADIE, R.L., METZGER, D.R., LÉGER, M., “The Thermal Ratchetting of Hydrogen in Zirconium-Niobium – An Illustration using Finite Element Modelling”, Scr. Metall. 29, (1993), 335–340.
[2.19] METZGER, D.R., SAUVÉ, R.G., “A Self-Induced Stress Model for Simulating Hydride Formation at Flaws”, ASME PVP 326, Computer Technology:Application and Methodology”, (1996), 137.
[2.20] METZGER, D.R., EADIE, R.L., Unpublished research.
[2.21] MCMINN, A., DARBY, E.C., SCHOFIELD, J.S., “The Terminal Solid Solubility of Hydrogen in Zirconium Alloys”, Zirconium in the Nuclear Industry: Twelfth International Symposium, ASTM STP 1354, Eds. G.P. Sabol and G.D. Moan Eds., American Society for Testing and Materials, West Conshohocken, PA, 2000, 173–195.

[2.22] CARPENTER, G.J.C., “The Dilatational Misfit of Zirconium Hydrides Precipitated in Zirconium”, J. Nucl. Mats. 48, (1973), 264–266.
[2.23] PULS, M.P., “On the Consequence of Hydrogen Supersaturation Effects in Zr Alloys to Hydrogen Ingress and Delayed Hydride Cracking”, J. Nucl. Mats., 165, (1989),128.
[2.24] PULS, M.P., “The Effects of Misfit and External Stresses on Terminal Solid Solubility in Hydride Forming Metals”, Acta Metall., 29, (1981), 1961.
[2.25] PULS, M.P., “Elastic and Plastic Accommodation Effects on Metal-Hydride Solubility”, Acta Metall., 32, (1984), 1259–1269.
[2.26] PAN, Z.L., PULS, M.P., RITCHIE, I.G., “Measurement of hydrogen solubility during isothermal charging in a Zr alloy using an internal friction technique”, J. of Alloys and Compounds, 211/212, (1994), 245–248.
[2.27] SHEK, G.K., GRAHAM, D.B., “Effects of Loading and Thermal Maneuvers on Delayed Hydride Cracking in Zr-2.5Nb Alloys”, Zirconium in the Nuclear Industry: Eighth International Symposium, ASTM STP 1023, (1989), 89–110.
[2.28] CHEADLE, B.A., COLEMAN, C.E., AMBLER, J.F.R., “Prevention of Delayed Hydride Cracking in Zirconium Alloys”, Zirconium in the Nuclear Industry: Seventh International Symposium, ASTM STP 939, (1987), 224–240.
[2.29] AMOUZOUVI, K.F., CLEGG, L.J., “The Effect of Heat Treatment on Delayed Hydride Cracking in Zr-2.5 Wt.Pct.Nb”, Metall. Trans.A, 18A, (1987) 1687–1694.
[2.30] EADIE, R.L., MOK, D., SCARTH, D.A., LEGER, M., “The Hydrostatic Stress Field Around the Crack Tip in Zr 2.5% Niobium and Implications for Delayed Hydride Cracking”, Scripta Met. 25, (1991), 497.
[2.31] SCARTH, D.A., SMITH, E., "Modelling Delayed Hydride Cracking in Zirconium Alloys," Proceedings of the IUTAM Symposium on Analytical and Computational Fracture Mechanics of Non-Homogeneous Materials, Edited by B.L. Karihaloo, Cardiff, U.K., June 2001, published by Kluwer, pp. 155-166.
[2.32] SCARTH, D.A., SMITH, E., "The Effect of Plasticity on Process-Zone Predictions of DHC Initiation at a Flaw in CANDU Reactor Zr-Nb Pressure Tubes," Proceedings of the 2002 ASME Pressure Vessels and Piping Conference, Vancouver, British Columbia, Canada, August 4-8, PVP-Vol. 437, pp. 19–30.
[2.33] DUGDALE, D.S., "Yielding of Steel Sheets Containing Slits," Journal of Mechanics and Physics of Solids, 8, (1960), 100–104.
[2.34] BILBY, B.A., COTTRELL, A.H., SWINDEN, K.H., "The Spread of Plastic Yield from a Notch," Proceedings, Royal Society of London, Vol. A-272, (1963), 304–314.

CHAPTER 3

EXPERIMENTAL PROGRAM

3.1. Philosophy

A three phase programme was set up to establish, in all the countries involved, a uniform and consistent laboratory practice to determine DHC velocity in the axial direction of pressure tubes. In the first phase, AECL's CRL, (Canada), as host laboratory, supplied participating countries with machined samples of Zr-2.5 Nb alloy each containing the same amount of hydrogen [3.1], Appendix 1[3]. Each country then performed DHC tests in a prescribed manner at a single temperature, 250°C [3.2], Appendix 2. Building on this experience, the second phase of the experimental programme consisted of each country producing their own samples out of segments of the same pressure tube, developing a hydriding method and charging the samples with the desired amount of hydrogen [3.3], Appendix 3, then testing them at various temperatures. In the third phase, each country made the same determinations on Zr-2.5 Nb material supplied by Lithuania and on their own material, if available. The procedures for these activities were documented in detail to ensure consistency. As a possible extension of this CRP, the feasibility of measuring DHC velocity in fuel cladding was explored by Sweden.

3.2. Materials

For Phases 1 and 2, an 800 mm long section of CANDU Zr-2.5 Nb pressure tube, identified as RX094-C2, was used. The section started approximately 0.185 m from the back end of the tube ("Back end" refers to the end of the tube that exits the extrusion press last.) The chemical composition of the original ingot material is given in Table 3.1 and the fabrication process flow chart is shown in Fig. 3.1. The ingot was melted four times. The dimensions of the finished tube are listed in Table 3.2 and the tensile properties are provided in Table 3.3. The initial microstructure, Fig. 3.2, consists of flattened α-grains about 0.5 μm thick surrounded by a grain boundary film of β-phase. The crystallographic texture is shown in Figure 3.3 and the fraction of resolved basal plane normals, F, in the three principal directions, radial, R, transverse, T and longitudinal, L, are summarized in Table 3.4.

For the common part of Phase 3, a section of RBMK Zr-2.5 Nb pressure tube in the TMT-1 condition was used. Tubes with this production schedule are used in the Ignalina Nuclear Power Plant, Unit 1, in Lithuania. The specified chemistry and some typical values of element concentration are incorporated in Table 3.1 [3.4]. The fabrication process flow chart for each version of RBMK pressure tubes is shown in Fig. 3.4. The dimensions of the finished tube are included in Table 3.2 and the tensile properties are provided in Table 3.3 The microstructure after the TMT-1 treatment, Fig.3.5, consists of α'-phase and between 10 and 20% untransformed α-phase. The crystallographic texture is shown in Fig. 3.6 and the F-values are included in Table 3.4.

[3] Appendices to this Report can be found in the CD-ROM attached on the inside back cover.

Table 3.1. Composition of test materials

Element	Materials			
	CANDU Tube	CANDU Tube	RBMK Specification	Indian HWR Tube
	RX094 (Ingot)	N429 (Ingot)	(Typical values for TMT-1)	100-2-3 (Measurements on typical tube)
Alloy:				
Niobium (wt%)	2.6	2.55	2.4-2.7	2.53
Oxygen (ppm)	1140	1172	1000 (400-700)	1226
Impurities (ppm)				
Aluminum	35	47	80	(29)
Beryllium			30	
Boron	<0.2	<0.25		(<0.25)
Cadmium	<0.2	<0.25	0.3	(<0.25)
Calcium			300	
Carbon	90	130	200 (30-70)	(95)
Chromium	<100	<80	200 (20-50)	200
Cobalt	<10	<10		(<10)
Copper	<25	<25	50	(27)
Hafnium	39	<40	500 (230-420)	(35)
Hydrogen	2	9	5 (2-3)	10 (4)
Iron	360	590	500 (80-250)	1300
Lead	<25	<25	50	(<25)
Magnesium		<10		(<10)
Manganese	<25	<25	20	(<25)
Molybdenum	<25	<25		(<25)
Nickel	<35	<25	200 (30-90)	<7
Nitrogen	24	42	60 (30-50)	56
Silicon	26	<60	200 (20-80)	(38)
Tantalum	<100	<200		(<100)
Tin	<25	<30		180
Titanium	<25	<25	70	(<25)
Tungsten	<25	<25		(<25)
Uranium	<1.0	<1.0		(<1.0)
Vanadium	<25	<25		(<25)

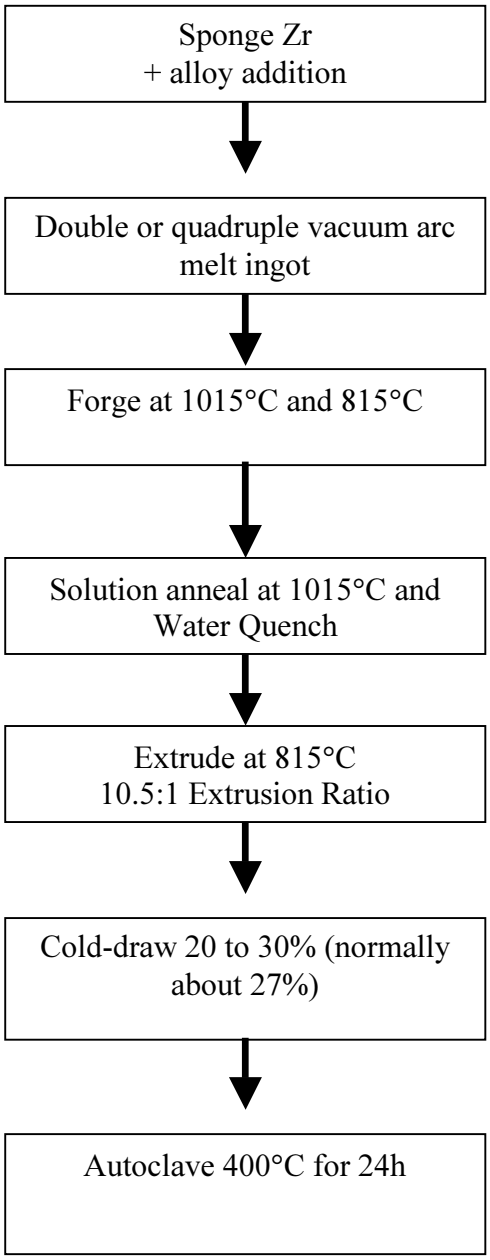

Fig. 3.1. Process flow chart for fabrication of CANDU pressure tubes.

Table 3.2. Dimensions of finished pressure tubes

Material	Inside diameter (mm)	Wall Thickness (mm)
CANDU	104	4.3
RBMK	80	4.0
Indian	82	3.7

Table 3.3. Tensile properties of test materials

Material	TEST DIRECTION L:longitudinal T:transverse	Test Temperature (°C)	0.2% Yield Stress (MPa)	UTS (MPa)	Total Elongetion (%)
CANDU Tube RX094	L	300	433	569	18
	T	20	803	889	22
	T	250	567	652	25
Tube N429	L	300	366	521	15
	T	250	585	673	13
RBMK TMT-1	L	20	580-640	680-720	20-24
	L	350	400-450	490-510	17-20
	T	20	659	760	25
	T	144	582	708	28
	T	182	546	655	24
	T	250	494	599	25
	T	300	484	555	27
Annealed	L	20	375-420	540-600	26-31
	L	300	229	336	27
	L	350	210-255	320-470	33-36
	T	20	483	520	20
	T	300	277	324	15
Indian 100-2-3	L	20	599	833	13
	L	300	426	587	14
	T	20	722	861	10
	T	250	531	641	12

Table 3.4. Resolved fraction of basal plane normals in the three principal directions of CANDU pressure tube RX094

Material	F_R	F_T	F_L
CANDU (RX094)	0.36	0.60	0.04
RBMK (TMT-1)	0.41	0.42	0.17
RBMK (Annealed)	0.47	0.46	0.07
Indian Tube	0.43	0.55	0.02

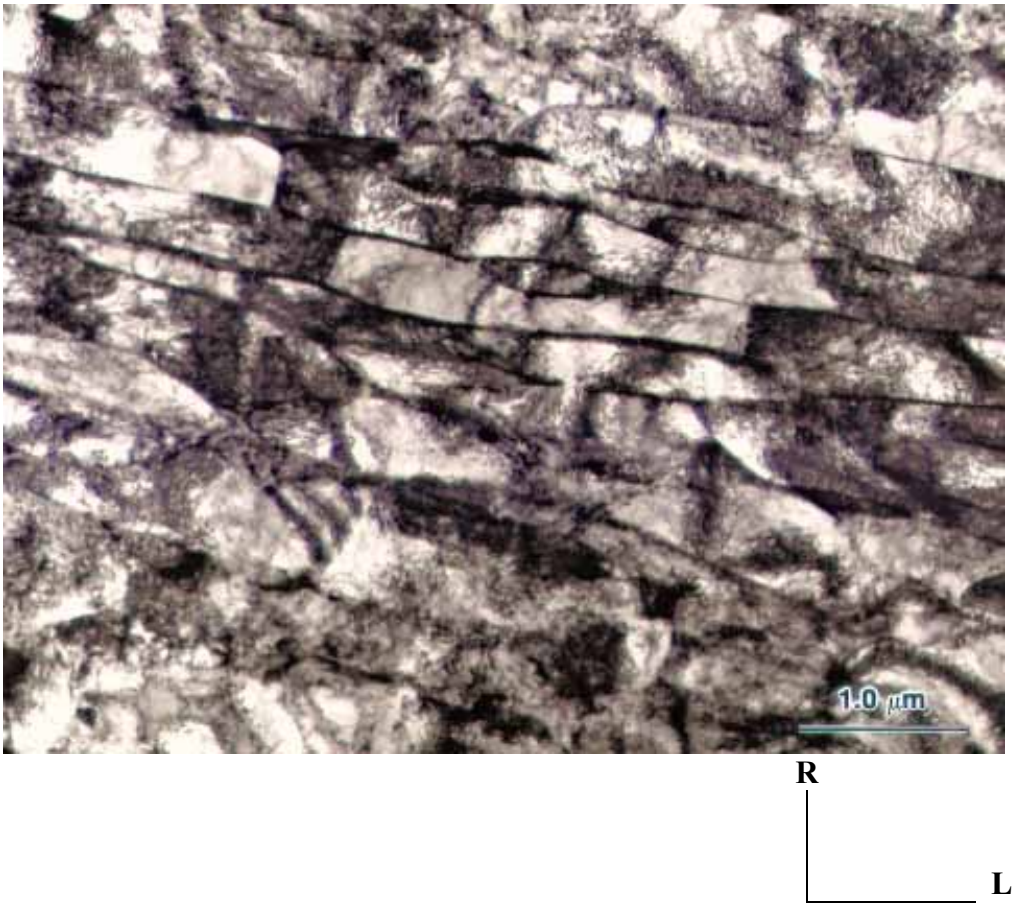

Fig. 3.2. Microstructure of CANDU pressure tube.

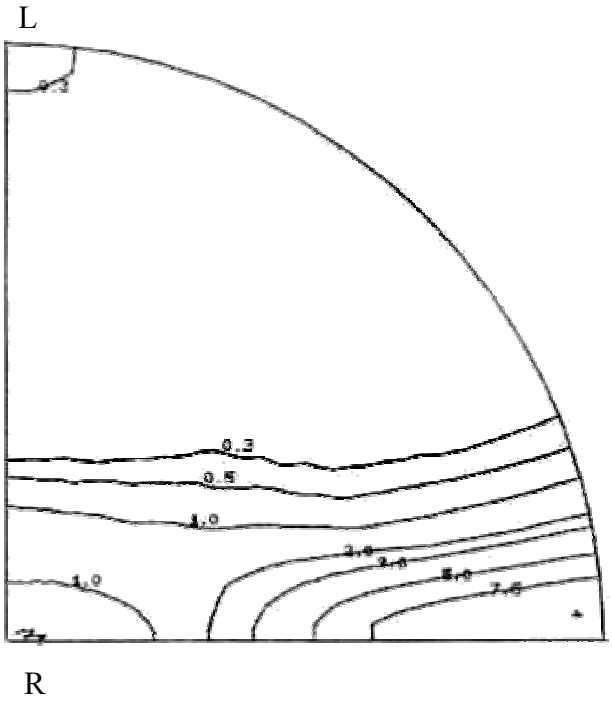

Fig. 3.3. Basal pole figure for CANDU tube RX094.

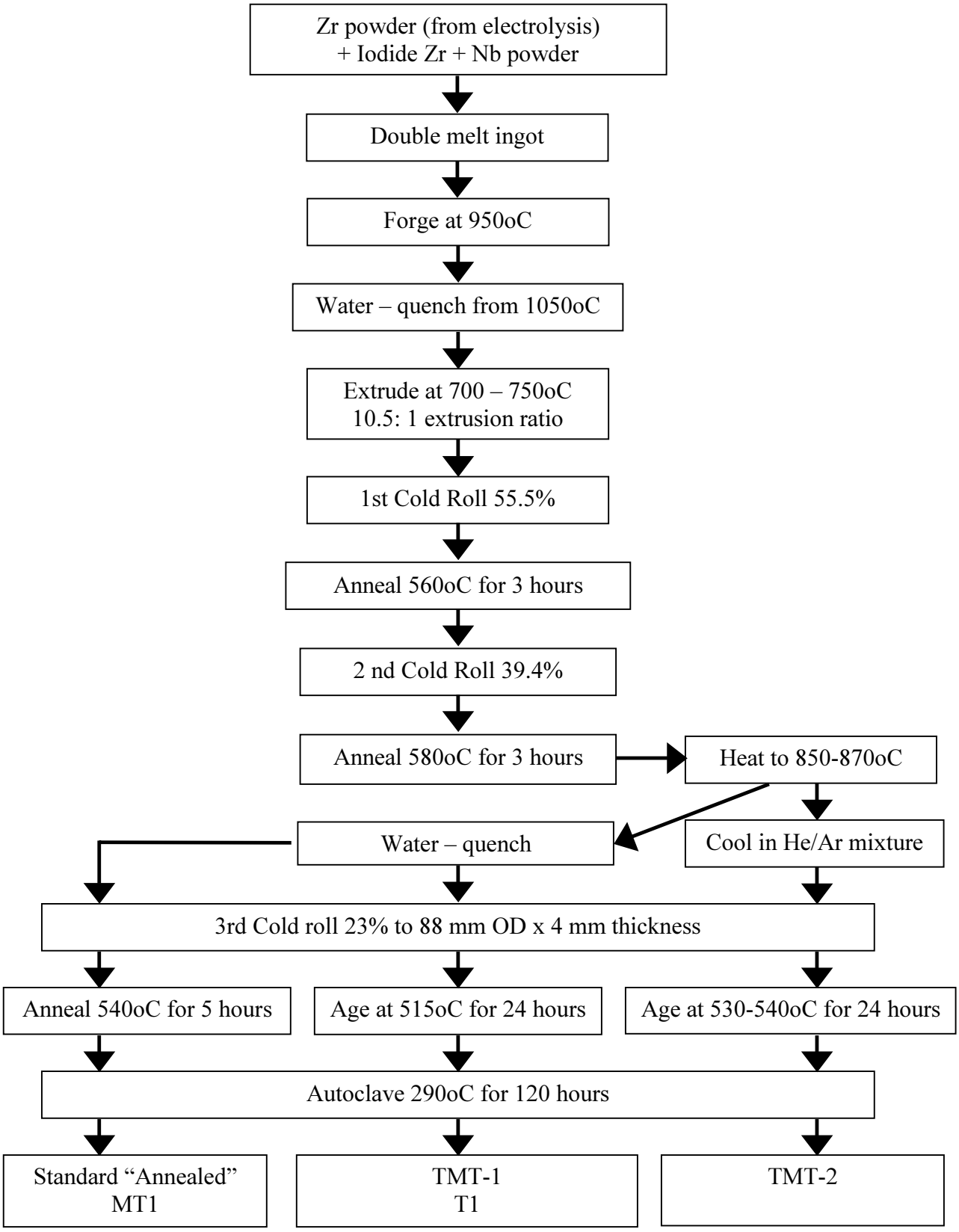

Fig. 3.4. Process flow chart for fabrication of RBMK pressure tubes.

Fig.3.5. Microstructure of RBMK pressure tube with TMT-1 treatment.

L

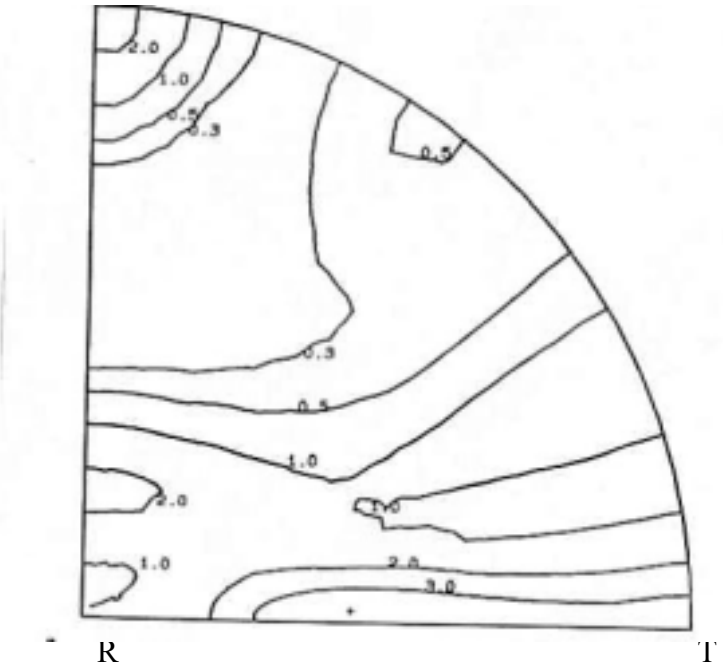

Fig.3.6. Basal pole figure for RBMK pressure tube in TMT-1 condition.

Other materials tested in Phase 3 are as follows:

Tube N429, typical of the CANDU reactor at Cernavoda, Unit 1, has attributes given in Tables 3.1 and 3.3. For this tube the ingot was melted twice. The microstructure and crystallographic texture are expected to be similar to those of Tube RX094.

Tube 100-2-3, made in India by the process depicted in Fig. 3.7, has the composition listed in Table 3.1 with dimensions and tensile properties included in Tables 3.2 and 3.3, respectively. The microstructure, Fig. 3.8, consists of elongated α-grains, 0.1 to 0.2 μm thick, surrounded by a thin layer of β-phase. The crystallographic texture, typical of this fabrication route is shown in Fig. 3.9 and the F-values are included in Table 3.4. For the tests on this material the hydrogen was added gaseously.

Some specimens were made from the other two routes for RBMK tubes, Fig. 3.4. Typical tensile properties are included in Table 3.3. The microstructure of annealed tubes contains elongated α-grains mixed with equiaxed α-grains and discontinuous β-phase at triple points and within the α-grains, Fig. 3.10. A typical crystallographic texture is shown in Fig. 3.11 with F-values in Table 3.4.

In summary, the properties of the sampled tubes were diverse. The anisotropy in properties tended to be higher in CANDU tubes than in RBMK tubes because of crystallographic texture and grain structure. The strengths at room temperature in the transverse direction were in the order CANDU (Canada), HWR (India), RBMK (TMT-1, Lithuania), RBMK (annealed, Russia). The range in strengths had several causes:

– RBMK material tends to have lower oxygen concentration than CANDU material,
– the microstructure provides lower strength in RBMK tubes than in CANDU tubes because of lower dislocation density and larger grain size,
– the high F_T in CANDU tubes leads to higher transverse strength than in RBMK tubes.

3.3. Specimen Preparation and Testing

The experiments involved adding known amounts of hydrogen to the Zr-2.5 Nb material, machining specimens and preparing a sharp crack, conducting the DHC test and evaluating the fracture surface.

3.3.1. Adding hydrogen

Several methods are available for adding hydrogen to zirconium alloys but the one chosen for this project, diffusing from a surface layer of hydride, combines good control with low temperatures [3.3]. The latter is important to minimise changing microstructure during specimen preparation, especially when dealing with irradiated materials.

The details of the procedure are given in Appendix 3. The hydride layer is formed electrolytically. After surface cleaning, the sample is placed into a bath containing 0.2 M H_2SO_4 at 65°C and electrolysis is performed at a current density of about 1.5 kA/m^2 using Pb (or other suitable metal) as anode. The hydride layer is examined metallographically to determine whether it is thick enough to supply the required concentration of hydrogen. Once a suitable layer is attained, the sample is heated, the temperature being determined by the TSS for dissolution to provide the target hydrogen concentration while the time of heating must be sufficient for the hydrogen to diffuse and attain the target concentration at the centre of the sample thickness. The efficacy of the preparation is determined by examining the resulting hydrides in the metal and by chemical analysis.

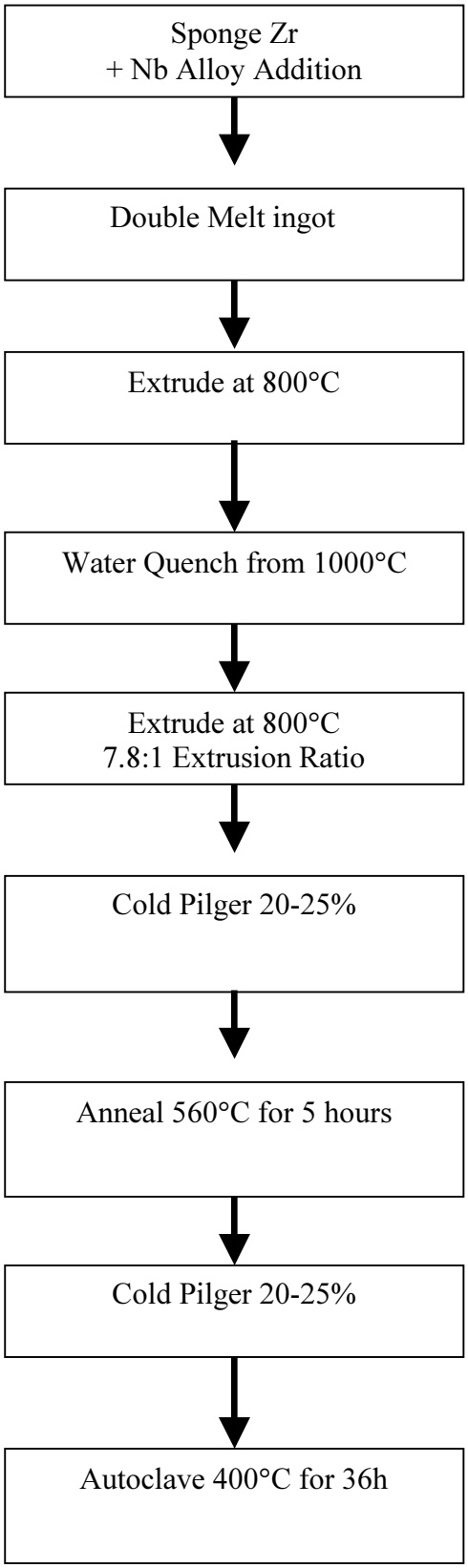

Fig. 3.7. Process flow chart for fabrication of Indian HWR pressure tubes.

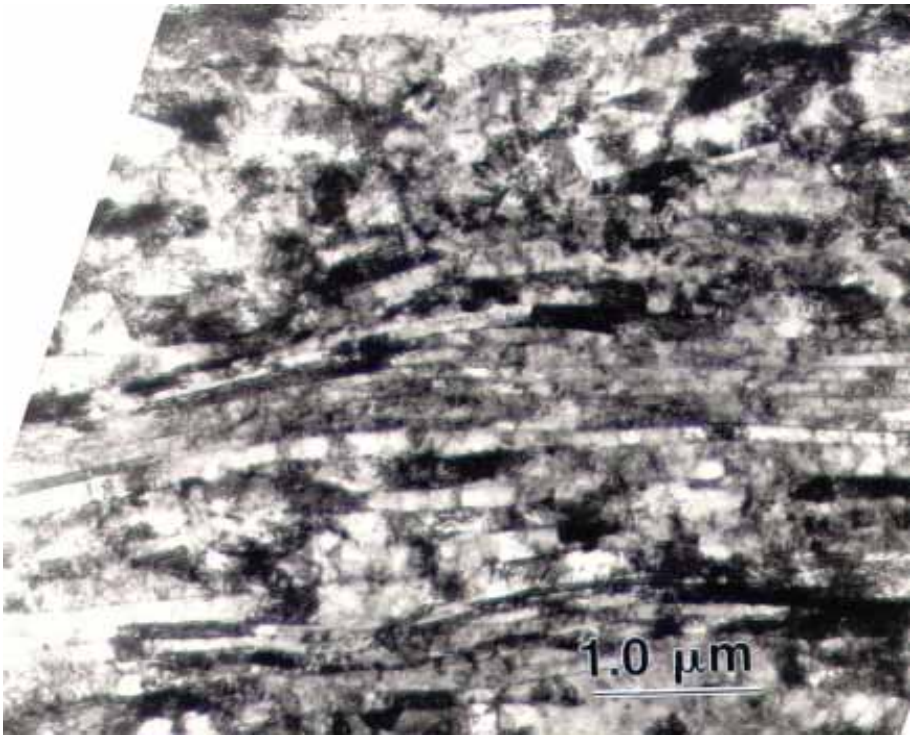

Fig. 3.8. Microstructure of Indian HWR pressure tube. (Radial direction of the tube is vertical on the page and the longitudinal direction is horizontal.)

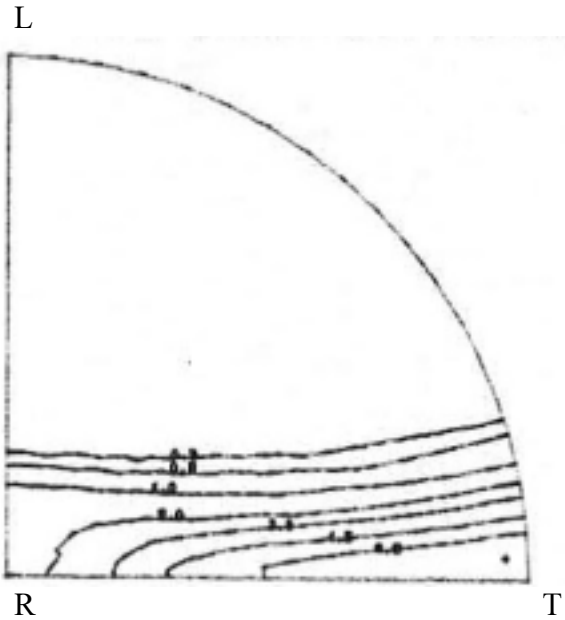

Fig.3.9. Basal pole figure for Indian HWR pressure tube.

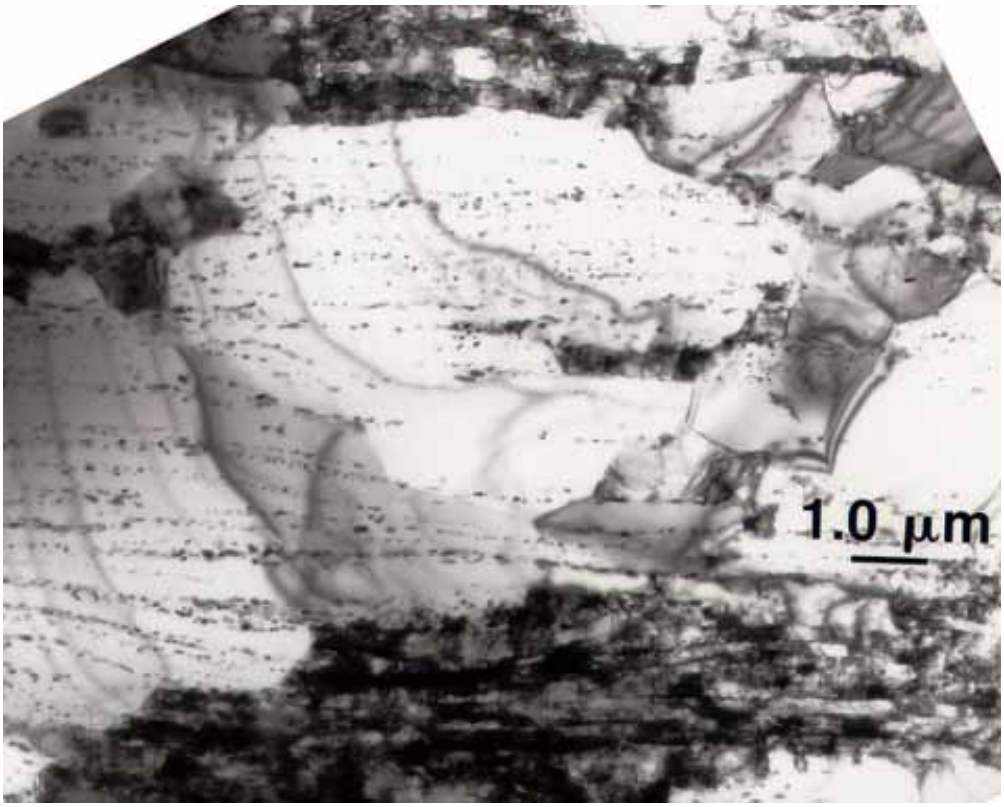

Fig. 3.10. Microstructure of annealed RBMK pressure tube (Radial direction of the tube is vertical on the page and the longitudinal direction is horizontal.)

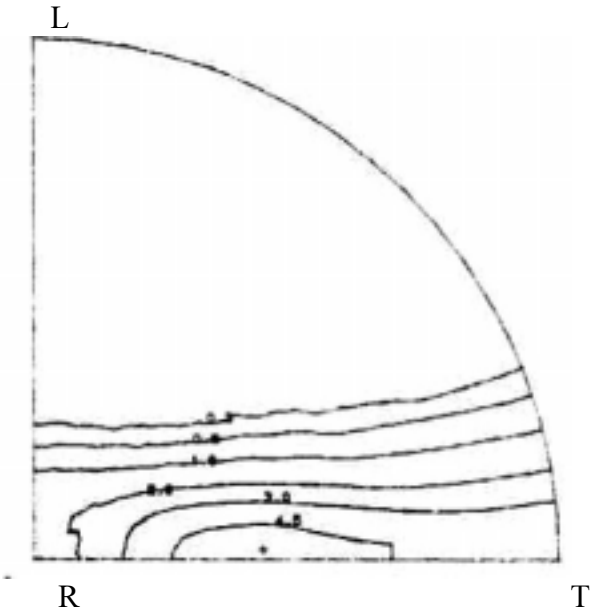

Fig.3.11. Basal pole figure for RBMK pressure tube in the annealed condition.

3.3.2. Test specimen

A detailed description of the test method [3.2] is given in Appendix 2. The test specimens were compact toughness specimens that met the requirements of ASTM E399, except for thickness and retention of the curvature, Fig. 3.12. The specimens were machined so that the crack grew in what was the longitudinal direction of the original tube on a plane with normal in the transverse direction of the original tube. A starter crack was grown about 1.7 mm from the notch by fatigue at room temperature, to give the recommended a_o/W ratio of 0.5 (where a_o is the crack length and W is the specimen width, with respect to the loading point.) K_I was calculated from equations given in ASTM E399. The maximum K_I was reduced during fatigue in up to six steps until it was less than the initial K_I for DHC testing.

3.3.3. DHC testing

To realize the maximum crack velocity, the test temperature must be attained by cooling from a peak temperature above the solvus temperature (with no under cooling), hydrides must be present at the test temperature and the maximum amount of hydrogen must be in solution. Since the latter two conditions are somewhat contradictory, the test temperature was set below the dissolution solvus temperature. A typical test sequence is given in Fig. 3.13. The full load, supplying an initial K_I of about 15 MPa√m, was applied about ½ hour after the test temperature had stabilized. After the crack extended about 1.5 mm, the load was removed and the specimen was cooled to room temperature. The end of the crack was marked by heat-tinting or post-test fatigue.

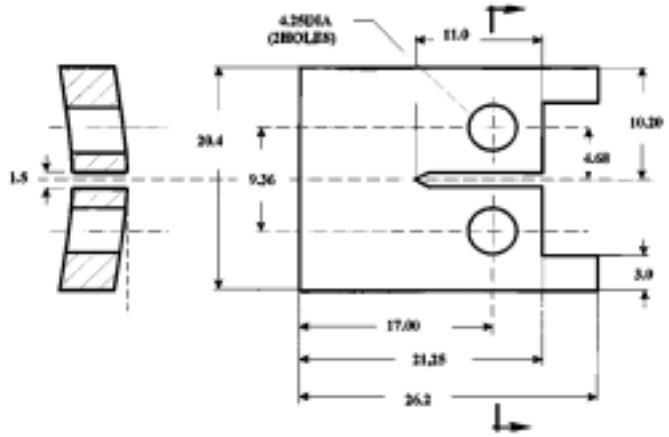

Fig. 3. 12. Schematic diagram of DHC compact toughness specimen.

The direct current, potential drop (dc pd) technique was used to evaluate the status of the crack during both fatigue pre-cracking and DHC testing. A constant current of about 8 A is large enough to provide a pd of about 5 mV across the specimen without excessive heating. The crack front tends to be curved. For fatigue, surface markers were useful to indicate the progress of the crack. After DHC, the amount of cracking was measured directly from the fracture surface once the two halves of the specimen were pulled apart. The crack length was evaluated by one of two methods. The area of DHC was estimated and the average crack length was calculated by dividing the crack area by the specimen thickness. Alternatively, the crack extension by DHC from the limit of fatigue cracking was averaged from measurements at nine equidistant intervals across the crack face.

DHC often required an incubation period, indicated by an increase in pd. The test time was taken as the difference of the total time under full load and the incubation time. DHC velocity was then crack extension by DHC divided by cracking time.

A test matrix was established where, in principle, each country measured DHC velocity on at least three specimens at three temperatures ranging from 283 °C down to 144 °C, with each temperature being covered by three countries, Table 3.5. At least nine results at each temperature were thought to provide a good statistical basis.

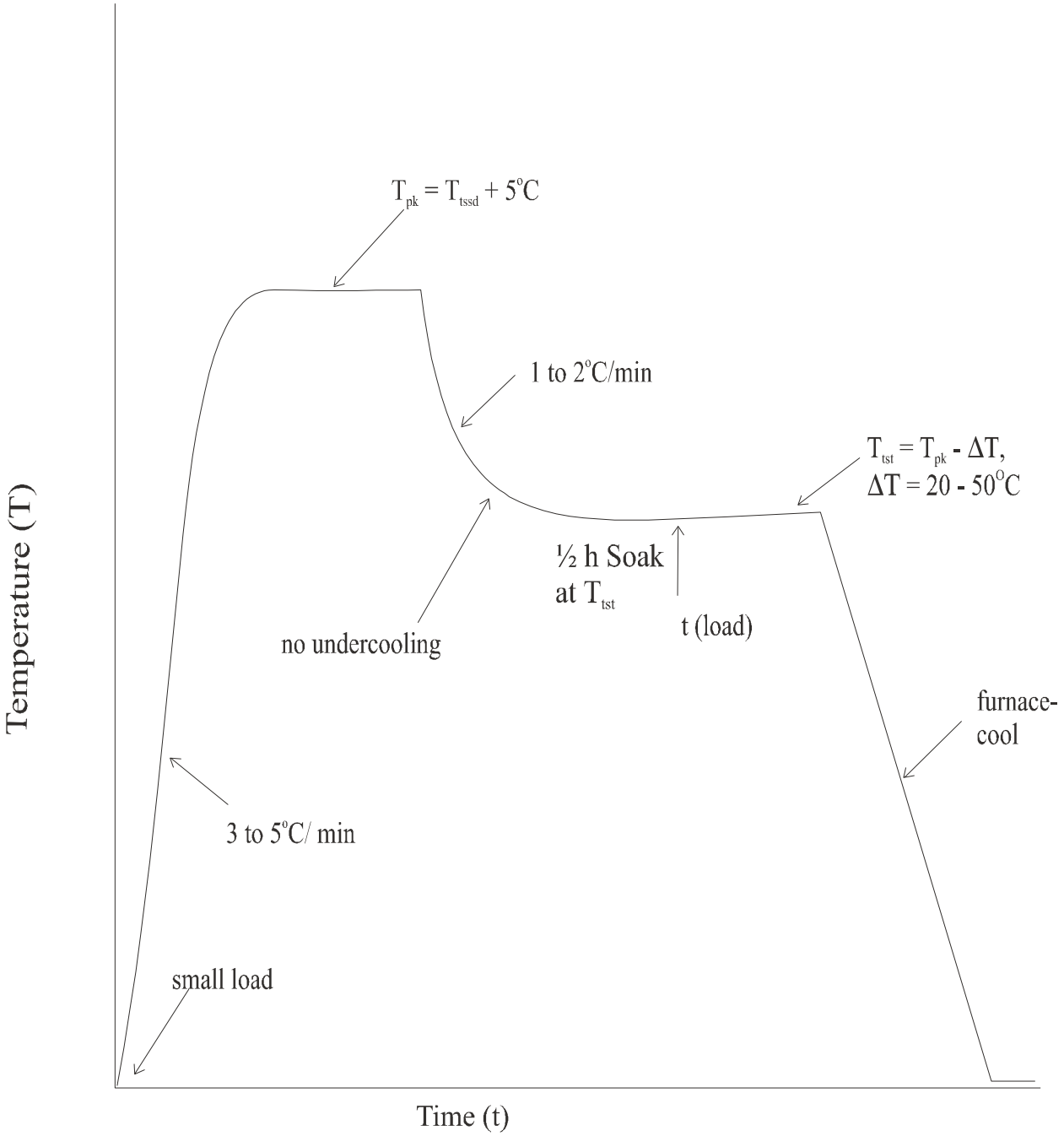

Fig. 3.13. Recommended temperature and loading history for DHC testing.

Table 3.5. Test matrix for Phases 1, 2, and 3

Peak Temperature (°C)	Test Temperature (°C)	Hydrogen Concentration, ppm	Participating Countries
330	283	72	Russia, Lithuania, Argentina
315	250	58	ALL
295	227	45	Romania, Pakistan, Canada
285	203	38	Russia, Romania, India
275	182	34	ROK, China Argentina
275	162	31	Pakistan, China, India
275	144	29	Lithuania, ROK, Canada

In practice, because of some experimental difficulties some temperatures were lightly sampled. As one example, when the hydrogen concentration was not precisely known, the thermal cycle was altered. The peak temperature was set higher than the possible solvus temperature by a large margin, then the test temperature was reduced in steps to the temperature at which cracking started.

The distribution of hydrides was examined metallographically on the planes with their normal in the transverse and longitudinal direction. The fracture surfaces were examined, and, where found, striation spacings were estimated.

3.4. Hydrogen Analysis

Knowledge of hydrogen concentration is needed when assessing the response of zirconium alloys to hydrogen. During the CRP on DHC in zirconium alloys the participants were adding specific amounts of hydrogen to their test specimens. The hydrogen concentration is critical to the tests; too much hydrogen may cause hydrides to be present at the peak temperature reached before the lower test temperature is attained, while too little hydrogen may provide insufficient hydrogen for hydride precipitation during testing and give a false, low crack velocity.

Until recently, no standards were available for hydrogen in zirconium alloys and most laboratories use hydrogen in titanium as their standard. Samples of hydrogen in zirconium are currently prepared at AECL - Chalk River Laboratories to provide standards for zirconium alloys. Such samples require testing in several laboratories to enhance their status as standards. An inter-laboratory comparison by the CRP participants helped meet this requirement.

159 pellet specimens (approximately 200 mg) were cut from Zr-2.5Nb pressure tube material and prepared individually. Each pellet was heated to 950°C under vacuum to remove most of the initial dissolved hydrogen gas. The system was isolated from the vacuum pump and a known quantity of hydrogen gas was added from a calibrated volume. The pellet quantitatively absorbed the hydrogen gas during cooling from 950°C to room temperature.

The concentration assigned to each specimen (expressed in units of ppm) was based on the known mass of the pellet and the known amount of hydrogen to which it was exposed.

The target concentration for hydrogen addition was 47 ppm for each sample. The starting material may have a residual hydrogen concentration as high as 1 ppm after pre-extraction. After the standards were made, a problem with the temperature measurement was identified that may have introduced a systematic bias as high as 1 ppm. Therefore, the hydrogen concentration in the samples was expected to range from 47 to 49 ppm. Random samples were then analysed to determine the actual mean concentration and standard deviation of the population. The specimens were made in 4 batches (up to 49 specimens per batch). Ten samples were selected at random from each batch for a total of 40 specimens. These 40 random samples were analysed by hot vacuum extraction – isotope dilution mass spectrometry (HVE – IDMS)[3.5, 3.6]. The results from the 40 samples showed that the combined population was approximately normal with a mean value of 49.8 ppm and a standard deviation of 0.5 ppm (1% rsd). Although the mean value was somewhat higher than expected, the standard deviation of the distribution was ideal for the inter-laboratory comparison.

The remaining specimens from the 4 batches were mixed, and then randomly divided into 10 bottles with 10 specimens per bottle. Each bottle was labelled with a number from 1 to 10. Based on the Canadian determination, the H concentration of the 10 random samples in each bottle is expected (from probability theory) to have a standard deviation ≤ 0.7 ppm. Bottles #1 through #10 were sent to the IAEA coordinator for distribution to the participants who were asked to analyse them using their normal laboratory procedures. The remaining 19 specimens were placed in Bottle #11 and retained in Canada for later analysis. Each specimen in the bottles was weighed to the nearest 0.1 mg and recorded. The mass served to identify each specimen, except for a few samples where the masses were indistinguishable.

REFERENCES TO CHAPTER 3

[3.1] KIDD K. V., Preparation of Material and Specimens for the IAEA Co-ordinated Research Programme on Delayed Hydride Cracking. FC-IAEA-001, T1.20.13-CAN-273.63-01, November 1998.

[3.2] CHOUBEY, R., DHC Axial Velocity Test Procedure for IAEA Round-Robin Test Program, FC-IAEA-02, T1.20.13-CAN-27363-02, November 1998.

[3.3] LEPAGE, A. D., FERRIS, W. A. and LEDOUX, G. A., Procedure for adding Hydrogen to small sections of Zirconium alloys, FC-IAEA-03, T1.20.13-CAN-27363-03, November 1998

[3.4] NIKULINA, A.V., RESHETNIKOV, N.G., SHEBALDOV, P.V., AGEENKOVA, L.E., FOMIN, V.S., SHEVNIN, Yu.P., KOCHERGIN, S.A., Fabrication Technology of RBMK Zr-2.5Nb Pressure Tubes, Voprosy Atomnoy Nauki i Tekhniki, Ser. Materials Science and Novel Materials, 1990, issue 2 (36), pp. 46–54.

[3.5] GREEN, L. W., BICKEL, G. A., LEESON, P. K., JAMES, M. W. D., LAMARCHE, T. G. and H. Michel, A Hot Vacuum Extraction Mass Spectrometric System for Determination of H and D in Zirconium, Proceedings of the 2nd Alfred O. Nier Symposium on Inorganic Mass Spectrometry, Durango, Colorado, May 1994 (Available as part of AECL-11342, Jan. 1996, pp. 95–99.

[3.6] BICKEL, G.A., GREEN, L.W., JAMES, M.W.D., LAMARCHE, T.G., LEESON, P.K., MICHEL, H., The determination of hydrogen and deuterium in Zr-2.5 Nb material by hot vacuum extraction mass spectrometry, J. Nucl. Mater., 306, (2002), 21–29.

CHAPTER 4

RESULTS AND DISCUSSION

4.1. Source of Test Data

A typical test history, Fig. 4.1, shows the change in potential drop with changes in temperature and loading and subsequent cracking.

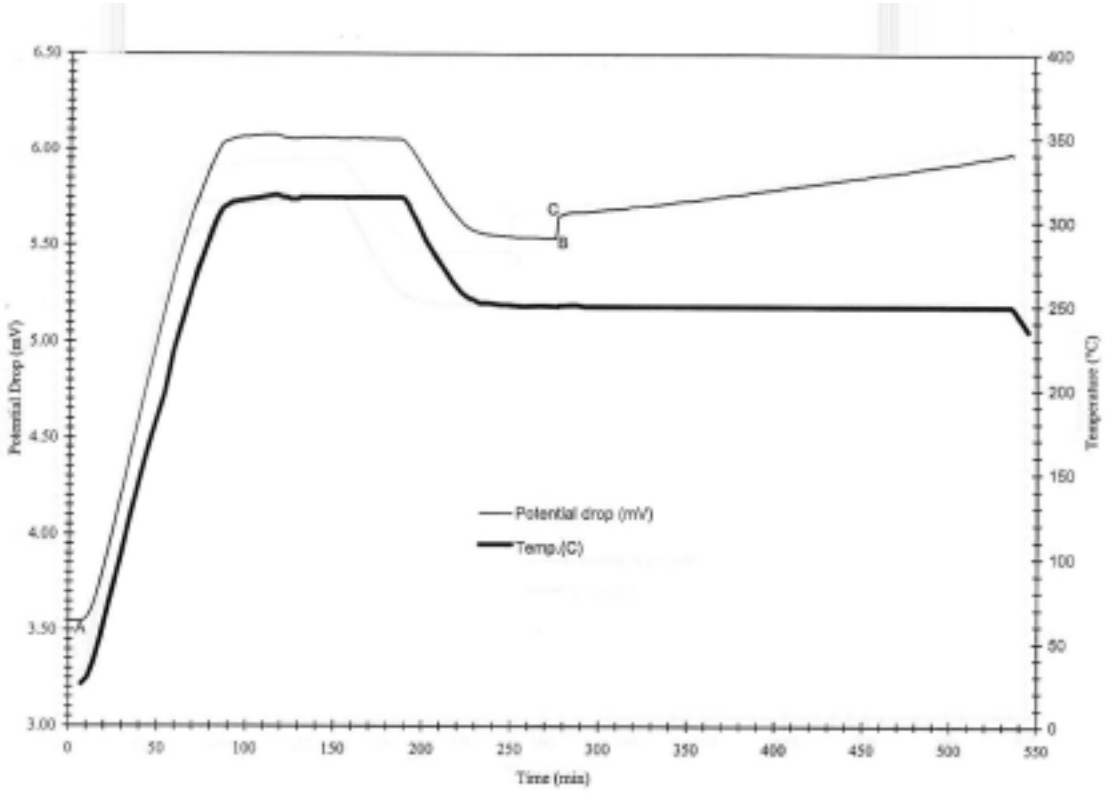

Fig. 4.1. Temperature and cracking history, as indicated by potential drop, during typical DHC test. A is start of test and the step at BC indicates the time of loading.

A typical fracture surface is depicted in Fig. 4.2 where the various stages of the test are visible as bands of different colour and roughness. Both fatigue cracks are characterized by a gently curved crack front. The DHC has a region where the crack is held up at each specimen surface corresponding to a less constrained stress state.

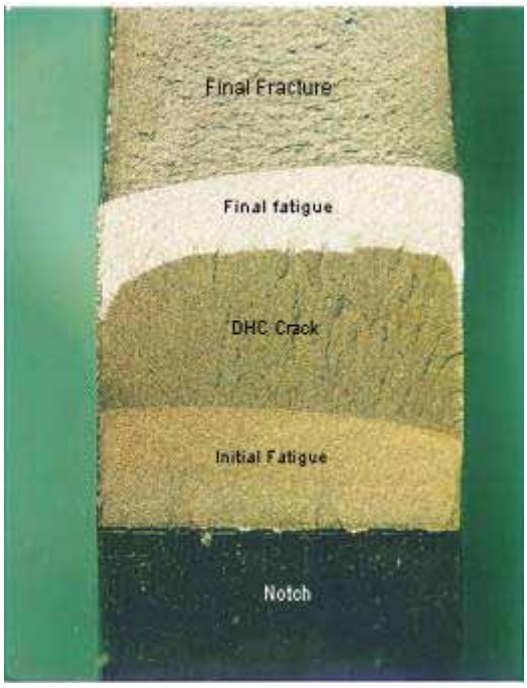

Fig. 4.2. Typical fracture surface of Zr-2.5 Nb after DHC testing.

4.2. Phase 1: Tests at 250°C on CANDU Pressure Tube

Details of each test are given in Appendix 4. The DHC velocities at 250°C are summarised in Table 4.1.

Table 4.1. Summary of DHC velocity of CANDU pressure tube at 250°C (m/s × 10^{-8}).

Argentina	Canada	China	India	ROK	Lithuania	Pakistan	Romania	Russia	Sweden
10.0	8.90	7.55	7.87	8.80	9.68	8.09	8.49	7.36	9.29
9.25	10.0	7.89	7.67	10.6	9.31	9.64	7.99	11.6	10.5
9.49	8.10	7.35	9.10	9.80	9.24	8.67	9.10	8.59	10.6
9.86	8.00	8.18	8.90	10.6	9.87	7.72	8.56	6.62	9.11
10.6	9.20	7.65	8.46	9.80	9.84	8.42	9.63	5.83	8.62
9.47	9.10	6.71	7.98	10.8	9.39	9.44	9.55	8.14	
8.95	8.30	8.62	8.50	10.2	9.86	8.63	8.96		
9.12	8.70	8.54	7.75		8.01				
8.54			7.49		8.58				
			8.14		9.35				
					7.34				
					8.89				
					8.22				
Average	9.48	8.79	7.81	8.19	10.1	9.04	8.66	8.90	8.02	9.62
Stdev	0.61	0.66	0.64	0.54	0.69	0.80	0.69	0.62	2.0	0.88

The mean value of all the data from 80 specimens is 8.86 × 10^{-8} m/s with a standard deviation of 1.07 × 10^{-8} m/s. The range of the mean value of each set of data is from 7.81 to 10.1 × 10^{-8} m/s while the standard deviation ranges from 0.54 to 2.0 × 10^{-8} m/s although most values are less than 0.7 × 10^{-8} m/s. The data can be reasonably represented by a normal distribution, Fig. 4.3. The tight distribution of the data can be attributed to the high level of control and consistency imposed by strict adherence to the test methods.

The mean value fits with data reported in the literature for tests at 250°C, Table 4.2. In early testing the importance of the various test conditions were not fully realised and, despite the specimens containing much hydrogen and K_I being large, the cracks grew more slowly than one would now expect. The main reason is that the peak temperature was too low to dissolve all the hydrogen. In later tests, with lower hydrogen concentrations but with peak temperatures greater than the solvus temperature for dissolution, the values spanned the current data.

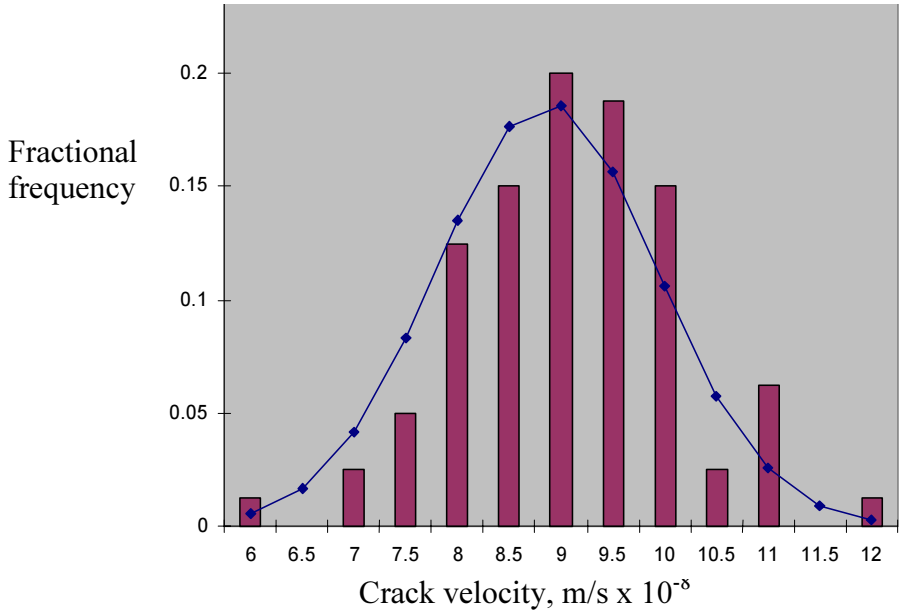

Fig. 4.3. Frequency distribution of crack velocities at 250°C. Continuous line is normal distribution.

Table 4.2. Reported values for DHC velocity in cold-worked Zr-2.5 Nb at 250°C

Hydrogen concentration (ppm)	DHC velocity range ($m/s \times 10^{-8}$)	Comment	Reference
150 to 400	0.9 to 3	K_I range from 15 to 45 MPa√m Temperature history not well characterized	4.1
140	3 to 4	K_I range from 7 to 27 MPa√m Peak temperature 290°C	4.2
55	11.8 ± 3.1	Initial K_I 17 MPa√m Peak temperature greater than solvus temperature	4.3
40	5.9 ± 0.87		

Several factors could explain the distribution of the values in Table 4.1. DHC depends on the diffusion and solubility limit of hydrogen in zirconium, the growth and fracture of hydrides, and the local variation in grain structure. Each of these factors will have statistical variability;

consequently DHC will be inherently variable. Scatter from variation in material properties may be caused by variations in microstructure in the pressure tube. The microstructure in a cold-worked Zr-2.5 Nb pressure tube varies a small amount from end-to-end because of variation in temperature during extrusion, but over the length of tube used in these tests, 800 mm, such variation would be difficult to discern. The difference in results showed no correlation with position along the tube, Table 4.3, suggesting that some of the variation was caused by experimental vagaries.

Table 4.3. DHC velocity at 250°C at various positions in Tube RX094

Specimen group (see Appendix 1)	Distance from back end of tube RX094 (mm)	Crack velocity ($m/s x 10^{-8}$)
100	1850 to 1918	8.54, 7.81
200	1920 to 1988	10.1, 9.04
300	1990 to 2058	8.66, 8.90
400	2060 to 2128	8.19, 8.02
500	2130 to 2198	9.66
1000	2480 to 2548	9.48, 9.03

Experimental factors that may affect the measurement of crack velocity are discussed below. Experiences from Phase 2 are included for completeness.

(1) Peak temperature

To maximize DHC velocity the zirconium alloy matrix should contain the maximum supersaturation of hydrogen [4.4]. This supersaturation can only be attained if all the hydrides are dissolved. Thus the peak temperature was set at least 5°C greater than the solvus temperature for hydride dissolution. For the range of hydrogen concentrations used at 250°C, the peak temperature had to be greater than between 298 and 306°C, and was set at 315°C to provide some margin on this factor. Some laboratories used peak temperatures lower than the recommended value, and consequently their values of crack velocity may be lower than expected, Table 4.4. For example, the values of crack velocity from China and India are the lowest and third lowest, respectively, and their peak temperatures were on the borderline of attaining full supersaturation.

(2) Under cooling at test temperature

Above a test temperature of about 180°C, if the test temperature is attained by heating, the crack velocity is less than the maximum value [4.4–4.8]. Hence we recommend that undercooling be avoided. In two early tests in Romania the test temperature of 250°C was attained after small undercoolings of about 2 and 2.5°C and the crack velocities were 6.3 and 5.7×10^{-8} m/s, respectively; with no undercooling the lowest value was 7.99×10^{-8} m/s. The values obtained after undercooling were excluded in determining the mean value of 8.9×10^{8} m/s.

Table 4.4. Mean crack velocity at 250°C from various peak temperatures

Country	Hydrogen Concentration (ppm)	Solvus Temperature (°C)	Peak Temperature (°C)	Mean Crack Velocity ($m/s \times 10^{-8}$)
Argentina	57,59	298-300	313-315	9.48
Canada	57,59	298-300	315-320	8.79
China	59,59	300	305-308	7.81
India	59,63	300-306	304-305	8.19
Rep. of Korea	55,56	295-296	315	10.1
Lithuania	55,56	295-296	315	9.04
Pakistan	59,59	300	315-317	8.66
Romania	59,59	300	315	8.9
Russia	59,63	300-306	311-316	8.02
Sweden	56,60	296-302	319-321	9.66

(3) Cooling rate to test temperature

If Zr-2.5 Nb containing hydrogen in solution is cooled rapidly (>100°C/s) to below the solvus for precipitation, very small hydride precipitates form. The subsequent DHC velocity is much higher than in material that has been slowly cooled [4.9]. Thus in this test programme care was taken to control the cooling rate to the test temperature. In all the laboratories the cooling rate was between 1.0 and 2.7°C/min., Table 4.5, thus variation from differences in hydride size was minimised.

Table 4.5. Cooling rates used by each laboratory

Country	Cooling rate to test Temperature °C/min
Argentina	2.2
Canada	1 to 2
China	1.5
India	1
ROK	2.7
Lithuania	1.5
Pakistan	1.1
Romania	1.8
Russia	1 to 2
Sweden	1 to 2

(4) Actual test temperature

Crack velocity is sensitive to temperature through $V = Aexp(-Q/RT)$. As an illustration, using $A = 8.74 \times 10^{-3}$ and Q=50 kJ/mole, around 250°C, V changes by about 0.2×10^{-8}m/s per °C. Canada, India and Sweden reported small deviations from a test temperature of 250°C and the consequences are depicted in Fig. 4.4.

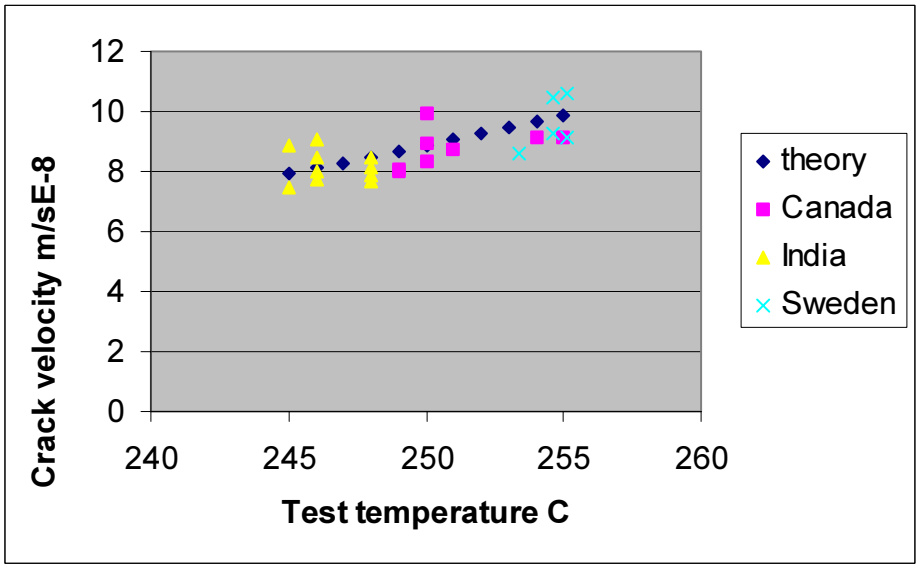

Fig. 4.4. Scatter in crack velocity as a consequence of deviation from 250℃.

(5) Measurement of crack length

The two methods for measuring crack length were evaluated by ROK on six specimens. The nine-point method tends to miss specimen edges and the occasional longitudinal slit. (These slits are probably caused by the fracture of circumferential hydrides by the component of applied stress parallel with the crack plane in the thickness direction.) Since the crack front is retarded in these areas, the area method will provide a truer picture of the extent of fracture and will tend to produce lower values of crack growth than the discrete point method. The size of this difference is between 1 and 9%.

(6) Crack length

The recommended amount of crack growth by DHC is 1.5 mm. Although DHC velocity is reported to be independent of K_I over a wide range of K_I [4.2], crack growth should be limited to prevent changing the operating stress state from mostly plane strain to one of plane stress, as illustrated by the edge-effect. Since the exact crack length after fatigue pre-cracking was uncertain, there was a variation in initial values of K_I ranging from 13.3 to 20.0 MPa√m with a mean value of 15.9 ± 1.7 MPa√m, close to the recommended value of 15 MPa√m. Most laboratories obtained seemingly valid results with crack growths in the range 0.86 to 4.0 mm; the mean crack growth by DHC in all the tests at 250°C was 1.91 ± 0.52 mm. The final K_I was in the range 19.8 to 40.3 MPa√m with a mean value of 24.1 ± 4.5 MPa√m. Two contradictory observations were made. In early tests in China, crack growth longer than 4 mm appeared to induce plasticity that interfered with the DHC and slowed the crack growth; the final K_I values were up to 55 MPa√m but the crack velocities were $<5 \times 10^{-8}$ m/s. (These results are excluded from the data set.) Alternatively, some results from Russia provide the opposite result; the crack growths varied from 1.5 to 2.28 mm and the derived velocities ranged from 5.8×10^{-8}m/s to 11.6×10^{-8}m/s. When all the results are pooled, no dependence or correlation between crack velocity and crack length or final K_I is observed, Figs 4.5 and 4.6, confirming expectations of K_I independence and suggesting that the latter results are a coincidence.

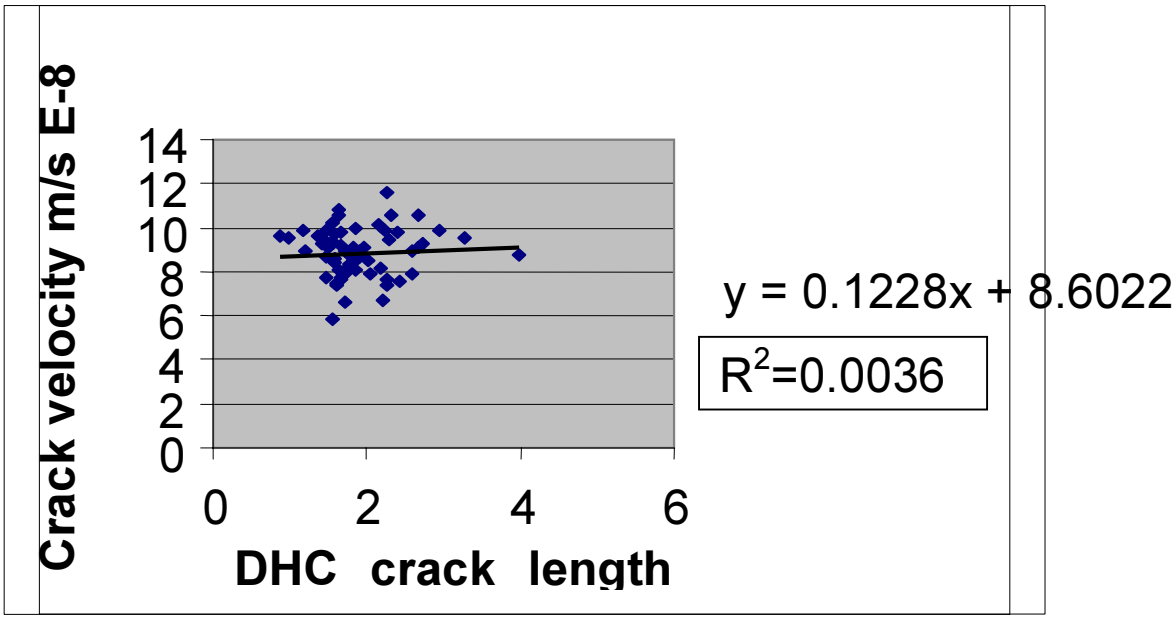

Fig. 4.5. Lack of dependence or correlation between amount of crack growth and DHC velocity at 250℃.

(7) Cracking time

Cracking starts after hydrides have grown at the initial crack tip and the conditions for cracking these hydrides has been established. Time is required to attain these conditions and a period of apparent inactivity, (for example, no change in the potential drop,) is observed between the initial application of the load and the start of cracking. This period is called the incubation time. An accurate assessment of incubation time depends on the sensitivity of the crack detection system, and in these experiments was very scattered. The time for the end of the test is established very accurately because it corresponds to the final unloading of the specimen. Thus the accuracy of the cracking time depends on observing the start of cracking. In the tests at 250°C the incubation time was usually very short, a few minutes, or even zero; occasionally cracking did not start for 20 min. and in one specimen the incubation time was 40 minutes. The mean incubation time, excluding the longest time, was 3.3±4.2 min. Since the average cracking time was 362±103 min., incubation time represents about 1% of the test time and any error in its value contributes little to the variation in crack velocity.

(8) Fatigue pre-cracking

If K_I is reduced during a test a new incubation period is required before cracking can restart [4.4, 4.5, 4.7]. Similarly if the final K_I during fatigue pre-cracking is greater than the starting K_I for the DHC test, crack initiation is much delayed. In some early tests in Romania cracks could not be initiated or the cracks propagated a small amount then stopped. This experience was attributed to pre-loading the crack by fatigue. When the final K_I of fatigue was lower than the DHC test load, the crack propagated by DHC at the expected rate. The results of these early tests are not included in the database.

(9) Loading rate

Another possible explanation of the variability in crack initiation was thought to be because of differences in specimen loading. For example, rapid application of the load may lead to plastic overload at the crack tip. A survey indicated that most laboratories used dead-weight loading that was applied manually at rates ranging from about 10 N/s up to 80 N/s. Since testing was successful with such a range of methods of loading, it was not considered further as contributing to variability.

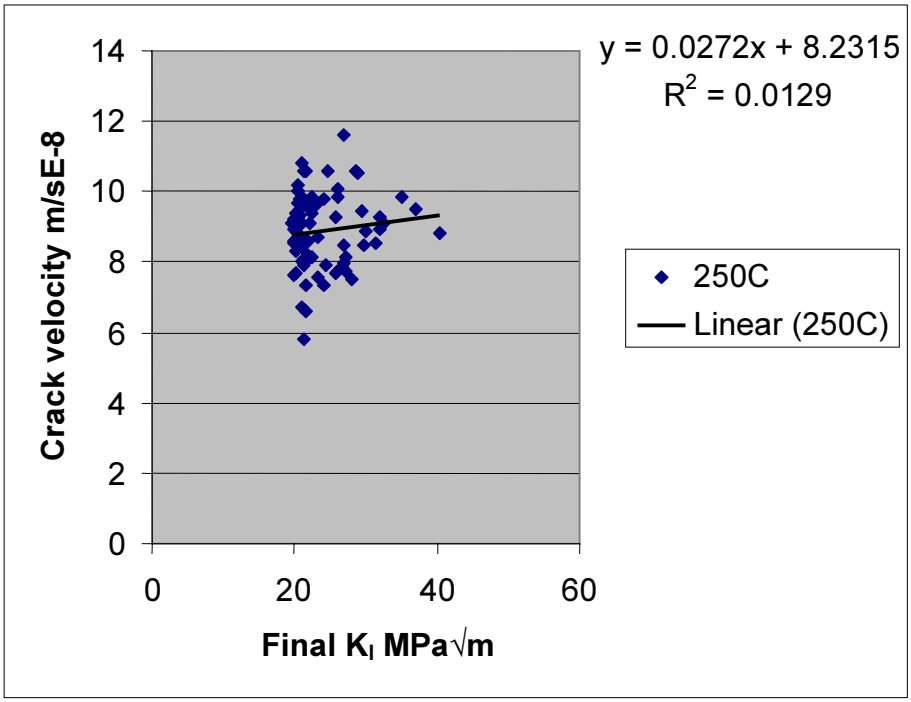

Fig. 4.6. Lack of dependence or correlation between DHC velocity and final K_I.

In summary, the chief experimental factors contributing to the variation in the values of crack velocity that have been accepted into the database, Table 4.1, appear to be variation in peak temperature and actual test temperature. The other factors considered appear to be under good control and contribute little to the scatter in data.

4.3. Phase 2: Tests at Other Temperatures on CANDU Pressure Tube

4.3.1. Specimen preparation

The formation of the hydride layer to supply hydrogen to the specimens was consistent within each laboratory but quite variable between each laboratory:

Country	Argentina	Canada	China	India	ROK	Lithuania	Pakistan	Romania	Russia
Hydriding rate µm/h	0.62	0.62	0.64 (CANDU) 2.5 (RBMK)	1.7	0.64	1.9	0.5 (CANDU) 1.6 (RBMK)	4.2	0.58

The hydriding rates of the CANDU tube RX094 could not be distinguished from those of the RBMK TMT-1 tube, except in China and Pakistan. Since the electrolyte, current density and electrolysing temperature were similar in all laboratories, the main source of variation was attributed to variation in surface preparation. For example, in Pakistan the hydriding rate after a final grinding with 1200 Emery paper was about 0.5 μm/hour while after pickling in 30% HNO_3/30%H_2SO_4/30%H_2O/10%HF the hydriding rate increased by a factor of two to four.

The final hydrogen concentration after annealing was also highly variable and did not correlate well with the expectation based on the TSSD [4.10], Fig. 4.7.

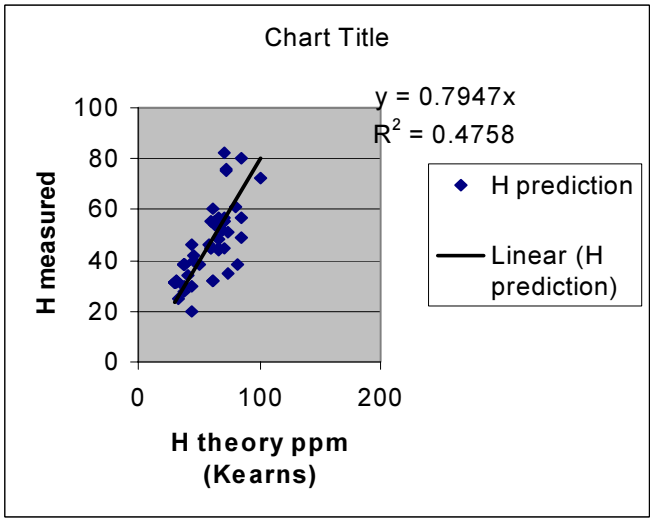

Fig. 4.7. Measured hydrogen concentrations after annealing hydride layers compared with expected hydrogen concentration based on Kearns' TSSD. Trend line forced through zero.

The sources of error are:

(a) insufficient time at the annealing temperature to allow the hydrogen concentration to approach equilibrium,
(b) errors in annealing temperature,
(c) insufficient hydride layer,
(d) retention of some hydride layer before hydrogen analysis,
(e) variation in hydrogen analysis.

Points (a), (b), c) and (e) could contribute to values of hydrogen concentration that are too low while points (b), (d) and e) could contribute to values of hydrogen concentration that are too high. It was outside the scope of this study to pursue in detail the sources of the variation although point (e) will be addressed in the section reporting on the inter-laboratory comparison of hydrogen analysis.

Typical distributions of hydrides are depicted in Figs 4.8 for CANDU material and Fig. 4 9 for RBMK TMT-1 material. In both materials the hydrides are well aligned with the direction of cold-work giving strong traces in the axial direction, as seen on the radial-axial sections. In the radial-transverse sections, the hydrides are still aligned but the traces are scattered about the transverse direction, but rarely approach the radial direction. Before testing the normals to the hydride plates are mostly in the radial direction, which is perpendicular to the expected plane of cracking. The length and breadth of the hydride traces are generally much smaller than 100 μm.

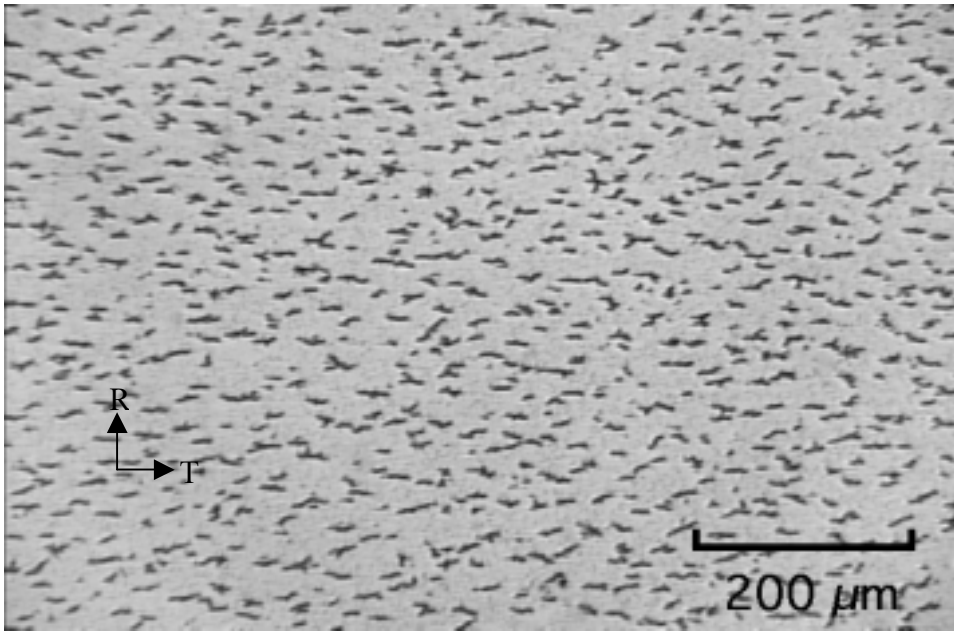

(a)

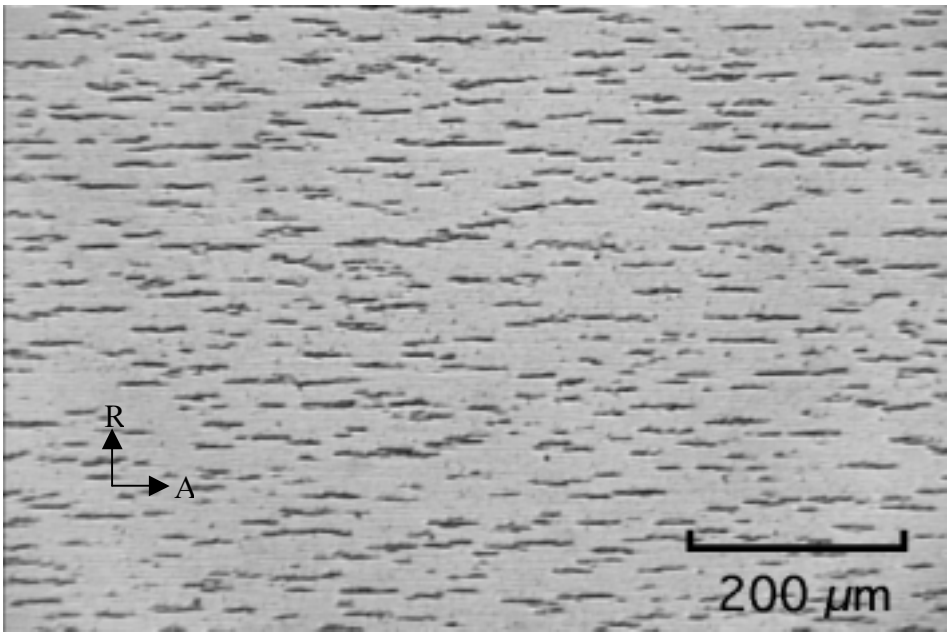

(b)

Fig. 4.8. Hydride distribution in CANDU pressure tube material with a hydrogen concentration of 79 ppm.: a - radial-transverse section; b – radial-axial section.

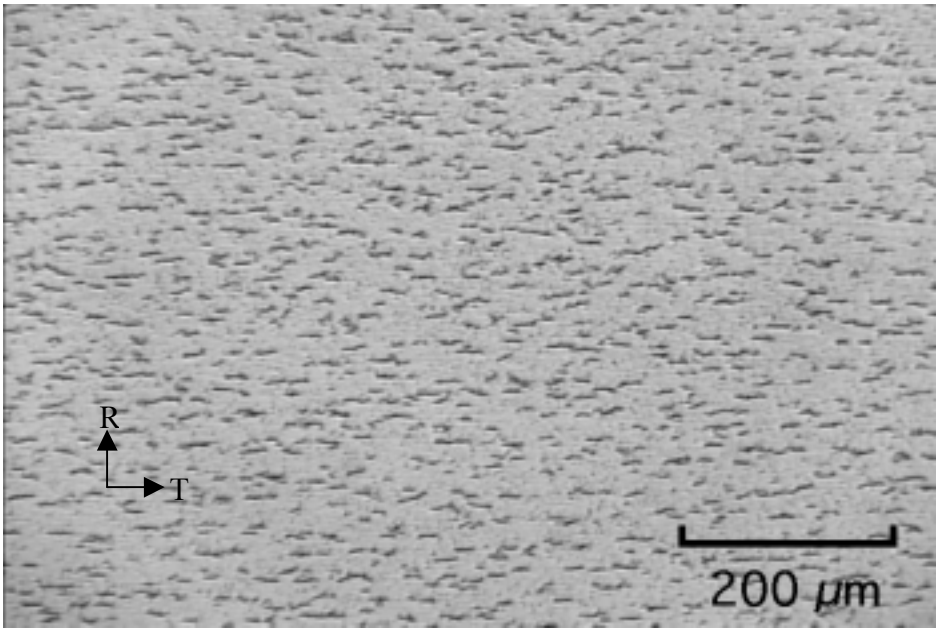

(a)

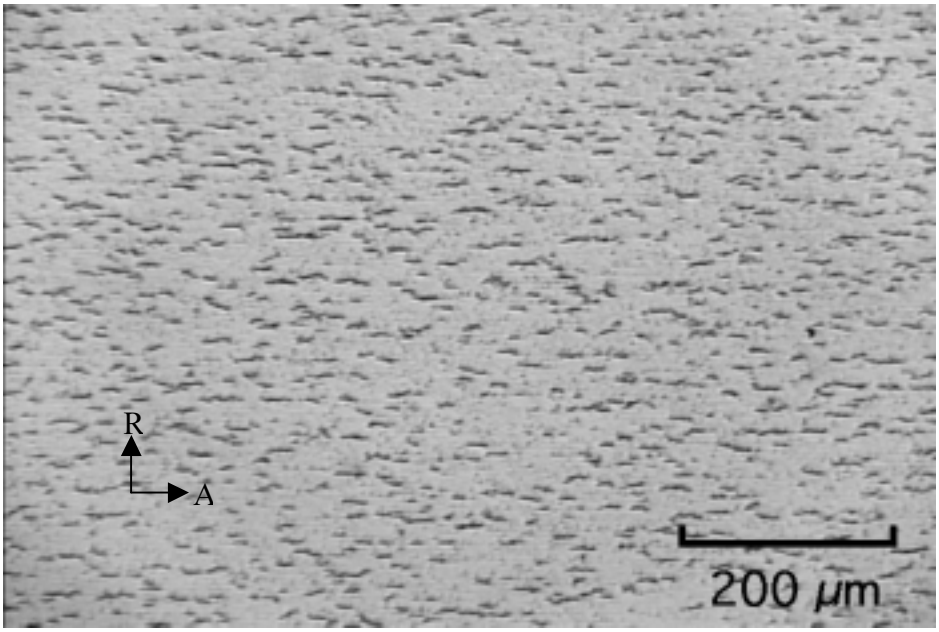

(b)

Fig. 4.9. Hydride distribution in RBMK TMT-1 pressure tube material with a hydrogen concentration of 76 ppm. a - radial-transverse section; b – radial-axial section.

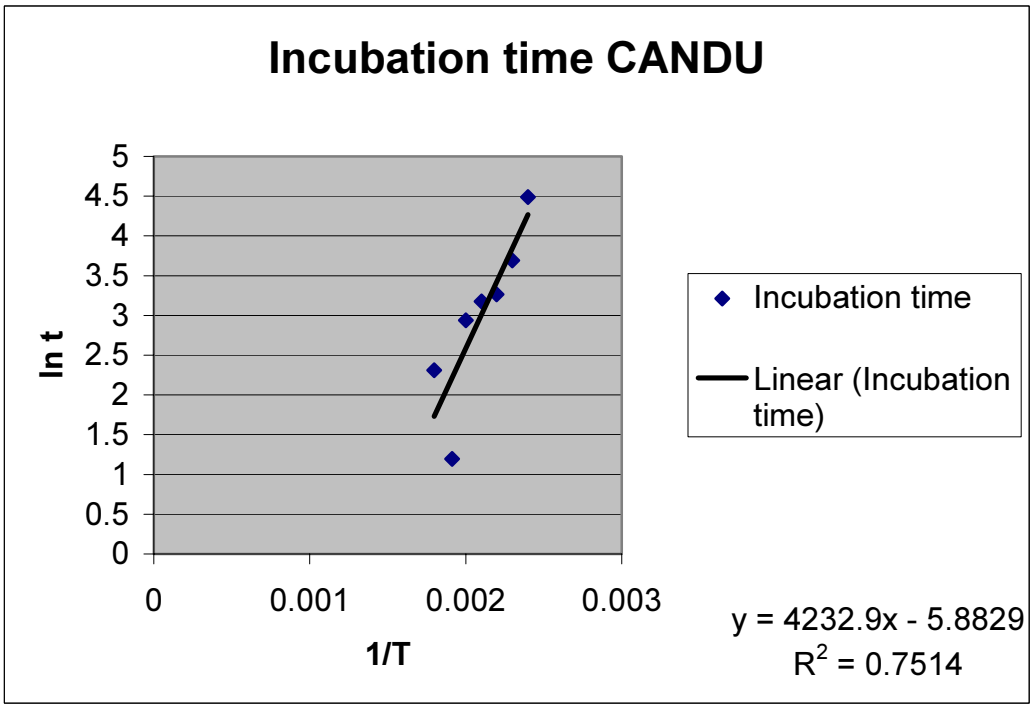

Fig. 4.10. Temperature dependence of mean incubation time for DHC in CANDU Zr-2.5 Nb pressure tube.

4.3.2. Results of DHC tests

Despite the mixed performance of the additions of hydrogen to the material, the DHC tests were successful, Appendix 4. The prescribed testing conditions were adhered to and the amounts of crack growth were not excessive. As with the first tests at 250°C, the incubation times to the start of continuous cracking were quite variable, with large dispersions, represented by the standard deviation and the range, Table 4.6. Contributing factors are the sensitivity of the crack monitoring equipment in resolving a change in potential drop and variations in the preparation of the starter-crack by fatigue. The incubation times consumed less than 5% of the total test time in all but five of the 89 tests, thus error in their determination contributed only a small error to the crack velocity.

Table 4.6. Summary of incubation times in CANDU Zr-2.5 Nb pressure tube RX094

Test Temperature °C	283	250	227	203	182	162	144
Mean value (min)	10	3.3	19	24*	26#	40	89
Standard deviation (min)	7.4	4.2	12	26*	16#	75	48
Maximum value (min)	27	40	36	84	61	190	162
Minimum value (min)	3	0	0	0.7	5	0.3	6

* Excludes values of 284 and 461 min. If these values are included, the mean value is 77 min. and the standard deviation is 138 min.
# Excludes values of 237 and 1489 min. If these values are included, the mean value is 166 min. and the standard deviation is 420 min.

The incubation time partly depends on the rate of arrival of hydrogen to the initial crack tip and thus it will tend to decrease as the test temperature is increased. This expectation is confirmed, Fig. 4.10, although the correlation is poor.
The crack velocities obtained at temperatures in the range 144°C to 283°C are summarized in Table 4.7. The standard deviations of the mean values range from 38% down to 8% of the mean while the range of values at any one temperature varies from a factor of 5.2 down to 1.3. The values of crack velocity have a clear and highly correlated temperature dependence described by V = Aexp(-Q/RT). Fig. 4.11 and Fig. 4.12 depict the temperature dependence of the mean values and total data set, respectively, including the data from the tests at 250°C. The statistical parameters of the data set are summarised in Table 4.8. Q has a value of 45.4 kJ/mol based on the mean values and 47.9 kJ/mol based on all the data. Linearity is not verified using the total data. The correlation is higher but the confidence is lower using the mean values.

In the literature the value of Q has a wide range of values, 72 to 42 kJ/mol, with the current value being at the low end of the range. The main source of the discrepancy is the variety of temperature histories involved in the tests. The temperature dependence of DHC velocity arises through the temperature dependence of the solubility limit and diffusivity, which are responsible for transporting the hydrogen to the crack tip. The product of their activation energies over predict that for crack velocity, and other factors, such as the negative temperature dependence of the yield stress, are involved in describing the temperature dependence of V. These issues will be discussed further when the data from the other materials have been presented.

4.4. Phase 3: Tests On Other Materials

4.4.1. RBMK Zr-2.5 Nb with TMT-1 heat-treatment

A similar set of tests were performed on this material in the temperature range 144°C to 283°C with results qualitatively similar to those obtained on the CANDU tube. The complete results are included in Appendix 4.

Again the incubations times were very scattered, Table 4.9, but the mean values decreased with increasing test temperature, Fig. 4.13. The incubation time occupied over 5% of the test time in only seven of the 105 tests thus errors in crack velocity from this source are very low.

Although the data for both materials are very scattered, the mean values of the incubation times appear to be different, Fig. 4.14, with those for RBMK TMT-1 tube being longer than those for the CANDU tube.

The crack velocities obtained on the RBMK tube in the TMT-1 condition at temperatures in the range 144°C to 283°C are summarized in Table 4.10. The standard deviations of the mean values range from 36% down to 7% of the mean while the range of values at any one temperature varies from a factor of 4.5 down to 1.2. As with the CANDU material, the values of crack velocity have a clear and highly correlated temperature dependence described by V = Aexp(-Q/RT). Figure 4.15 and Fig. 4.16 depict the temperature dependence of the mean values and total data set, respectively. Linearity of these plots is verified for both presentations of the data. The statistical parameters of the data set are summarised in Table 4.11. Q has a value of 54.3 kJ/mol based on the mean values and 55.5 kJ/mol based on all the data. The correlation is higher but the confidence is lower using the mean values.

Table 4.7. Summary of crack velocities in CANDU Zr-2.5 Nb pressure tube RX094

Test temperature °C	283	227	203	182	162	144
Crack Velocity 10^{-8} m/s	8.3	3.6	2.1	1.3	0.62	0.57
	6.3	4.4	2.0	1.4	0.60	0.59
	5.6	4.3	2.1	1.2	0.74	0.55
	6.9	4.0	1.8	0.58	0.87	0.52
	6.8	4.1	2.3	0.98	0.88	0.54
	17.7	3.8	1.9	2.0	0.79	0.57
	10.5	3.3	1.9	0.41	0.38	0.52
	10.8	5.7	3.2	2.2		0.59
	14.2	5.6	3.0	1.9		0.51
	9.5	6.0	2.5	1.9		0.49
	13.5	5.6	2.8	1.5		0.48
	14.1	5.2	2.1	1.5		0.45
		4.9	3.1	1.6		0.52
		4.2	1.6			0.54
		4.7	2.5			
		6.2	2.7			
		4.3	3.1			
		2.3	2.4			
			2.8			
			2.3			
			2.1			
			2.5			
Mean value	10.4	4.5	2.4	1.4	0.70	0.53
Standard deviation	3.8	0.98	0.46	0.53	0.18	0.041
Stdev/mean	0.37	0.22	0.19	0.38	0.26	0.08
Highest V/lowest V	3.2	2.6	2.0	5.2	2.3	1.3

Table 4.8. Statistical summary of DHC tests on CANDU Zr-2.5 Nb pressure tube

	Q kJ/mol	Standard Error on Q kJ/mol	Upper 95% Confidence of Q kJ/mol	Lower 95% Confidence of Q kJ/mol	A m/s	R^2
Mean values	45.4	2.76	52.5	38.3	2.33 10^{-3}	0.98
All data	47.9	1.03	50.1	45.8	8.31 10^{-3}	0.92

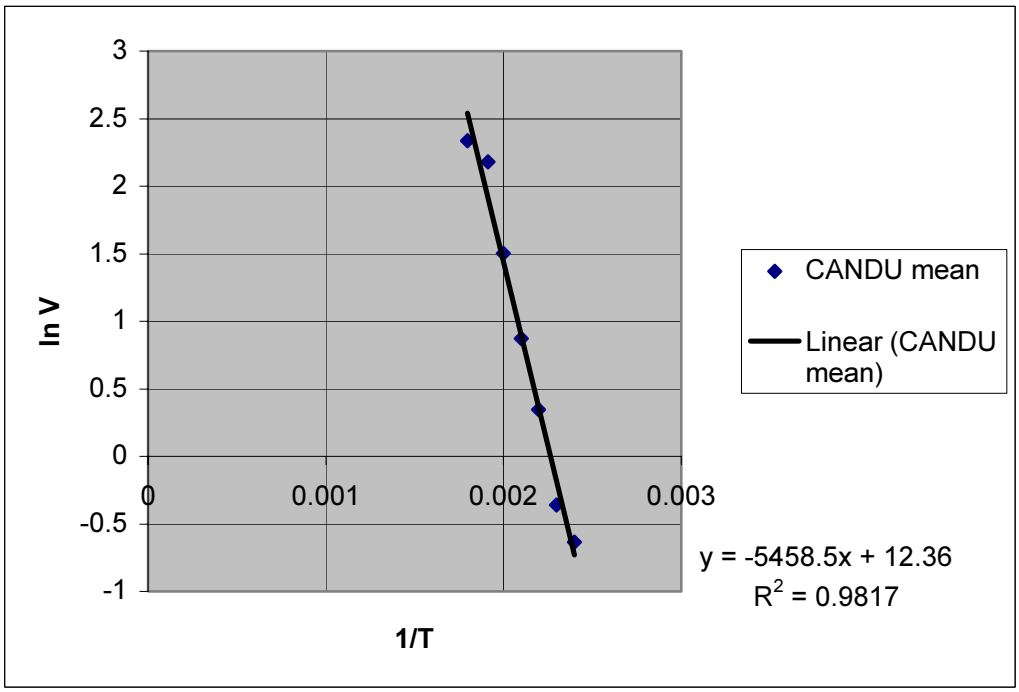

Fig. 4.11. Temperature dependence of mean velocity of DHC for CANDU Zr-2.5 Nb pressure tube RX094.

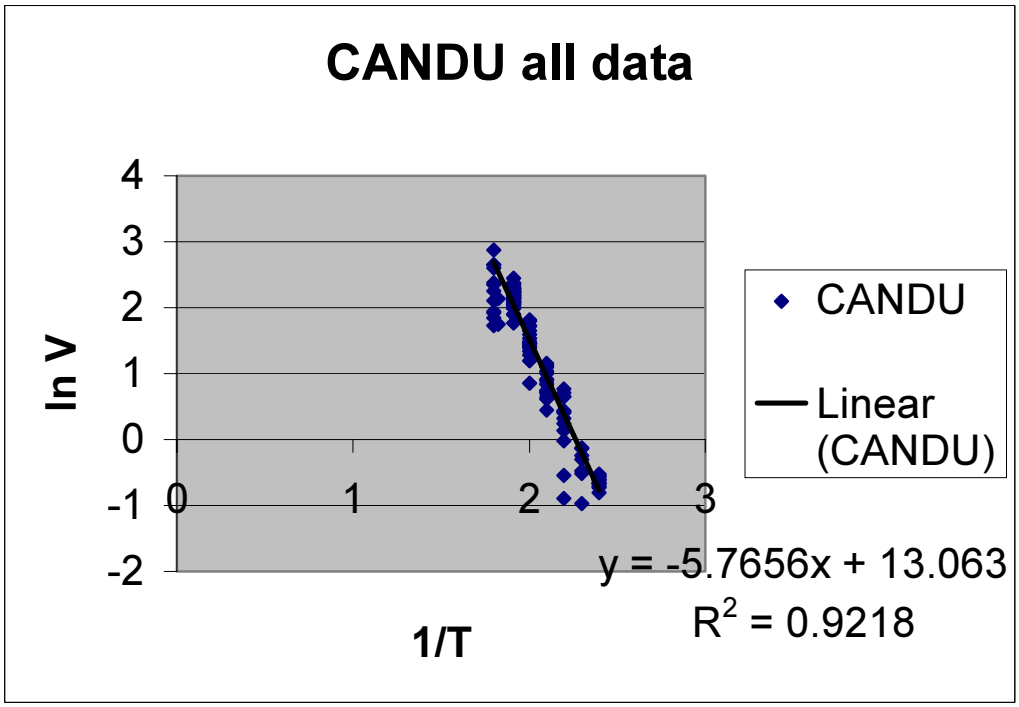

Fig. 4.12. Temperature dependence of velocity of DHC for CANDU Zr-2.5 Nb pressure tube RX094 based on all tests.

Table 4.9. Summary of incubation times in RBMK Zr-2.5 Nb pressure tube in TMT-1 condition

Test Temperature °C	283	250	227	203	162	144
Mean value (min)	37	25	29	56	123	660
Standard deviation (min.)	41	44	28	52	134	1080
Maximum value (min.)	120	172	66	148	347	3084
Minimum value (min.)	5	0	1	0	0	67

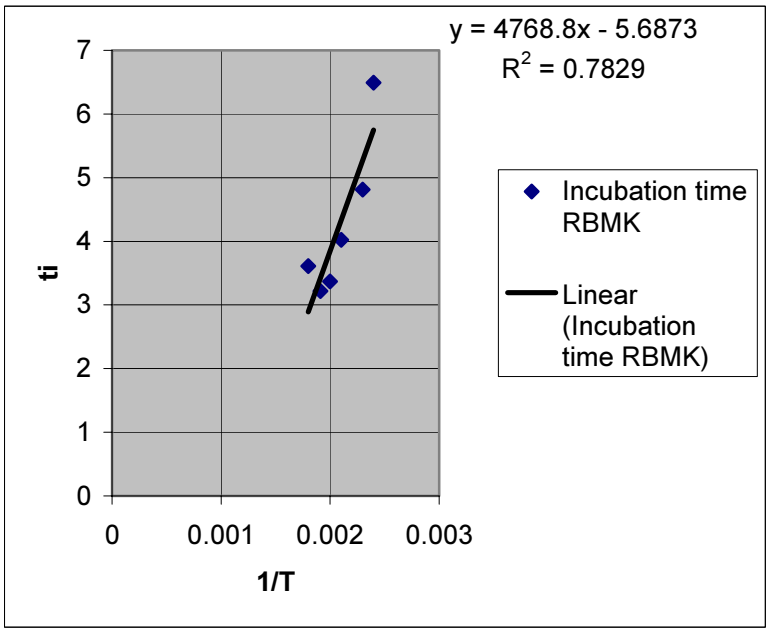

Fig. 4.13. Temperature dependence of mean incubation time for DHC in RBMK Zr-2.5 Nb pressure tube in TMT-1 condition.

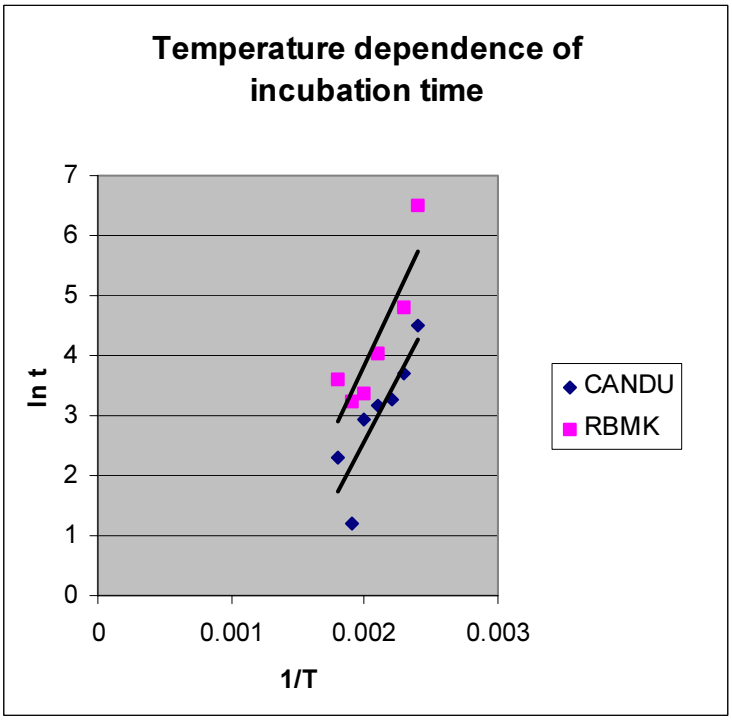

Fig. 4.14. Comparison of incubation times for DHC in CANDU and RBMK TMT-1 tubes.

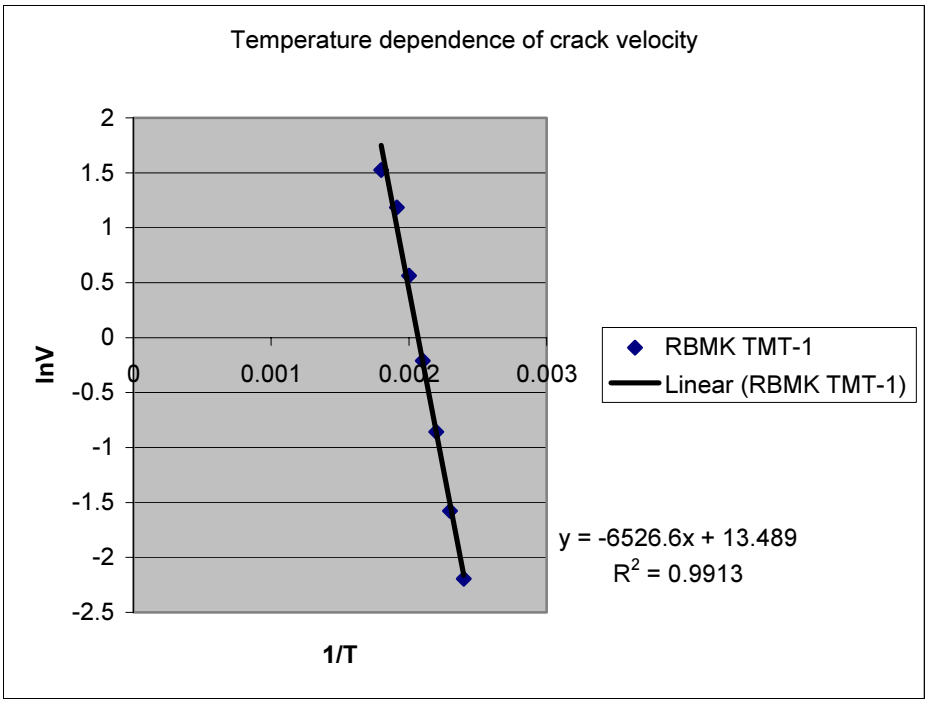

Fig. 4.15. Temperature dependence of mean velocity of DHC for RBMK TMT-1 Zr-2.5 Nb pressure tube.

Table 4.10. Summary of crack velocities in RBMK TMT-1 Zr-2.5 Nb pressure tube

Test temperature °C	283	250		227	203	182	162	144
	4.0	4.0	3.2	2.3	0.85	0.41	0.21	0.11
Crack velocity	3.7	4.0	3.0	2.0	0.54	0.44	0.23	0.11
m/s x10 ^{8}	4.8	3.8	3.3	2.1	1.0	0.43	0.20	0.12
	5.0	3.6	3.1	2.1	1.0		0.21	0.11
	4.3	3.7	3.6	2.0	1.0		0.19	0.11
	5.6	1.9	3.8	2.0	0.54		0.2	0.13
	5.9	1.6	3.7	1.9	0.80		0.22	0.13
	4.1	1.6	3.1	2.0	1.0			0.14
	4.0	1.7	3.9	2.0	0.99			0.094
	4.7	3.0	3.8	2.1	0.64			0.091
		2.6	4.0	2.0	0.71			0.095
		2.5	3.8	1.4	0.69			
		3.4	3.4	1.4	0.71			
		3.4	3.4	2.0				
		3.3	3.2	2.1				
		3.4	3.3	2.2				
		3.1	3.3	1.9				
		3.6	3.2	0.51				
		3.1	3.4	0.52				
		3.3	4.0	0.54				
			4.1					
Mean value	4.6	3.3		1.76	0.81	0.42	0.21	0.11
Standard deviation	0.74	0.64		0.63	0.19	0.013*	0.014	0.015
std.dev./mean	0.16	0.20		0.36	0.23	0.03*	0.07	0.14
Highest V/lowest V	1.6	2.7		4.5	1.9	1.1*	1.2	1.5

* Too few values to be statistically useful.

Table 4.11 Statistical summary of DHC tests on in RBMK TMT-1 Zr-2.5 Nb pressure tube

	Q kJ/mol	Standard Error on Q kJ/mol	Upper 95% Confidence of Q kJ/mol	Lower 95% Confidence of Q kJ/mol	A m/s	R^2
Mean values	54.6	2.26	60.1	48.4	7.3×10^{-3}	0.99
All data	55.5	1.4	58.3	52.7	1.01×10^{-2}	0.94

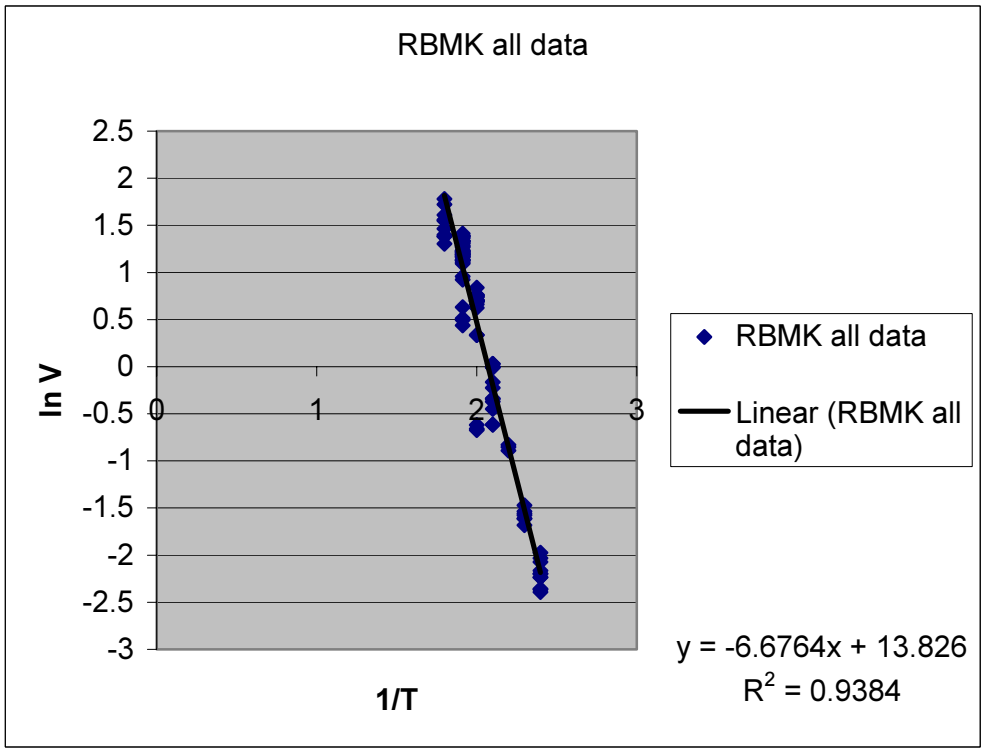

Fig. 4.16. Temperature dependence of velocity of DHC for RBMK TMT-1 Zr-2.5 Nb pressure tube based on all tests.

The mean values of crack velocity of the RBMK TMT-1 material appear much lower than those for the CANDU tube. The t-test was used to analyse both the total population and the mean values from each country at 250°C. The assumptions for validity for the t-test were examined. The DHC testing is considered to be random because each tube and the location of the test pieces were selected arbitrarily.

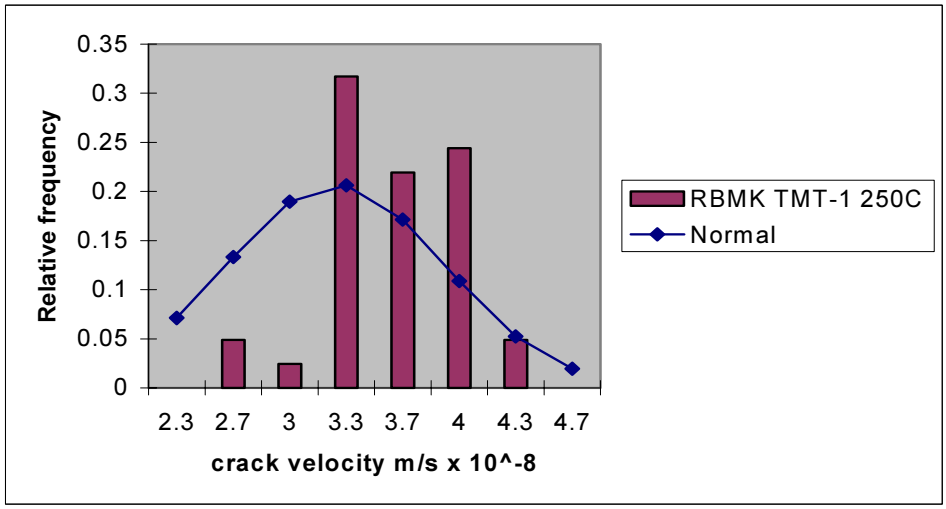

Fig. 4.17. Frequency distribution of crack velocities at 250℃ of RBMK TMT-1 pressure ube.

The data from the RBMK tube were not well represented by a normal distribution. Figure 4.17, although adherence to strict normality can be relaxed. The dispersions of the total sample population were quite distinct, so one has to be careful in case any difference is caused by the differences in dispersion rather than the means. The standard deviations of the total samples were 1.1 for CANDU and 0.64 for RBMK, while those of the means were similar, 0.74 versus 0.70. The t-values of 31 (total sample) and 17 (means) were so large and significant that the difference between the two tubes is real: the crack velocity in the CANDU tube was 2.7 times faster than in the RBMK TMT-1 tube at 250°C. This conclusion is further reinforced when the distributions of values are compared; they are clearly distinct, Fig. 4.18.

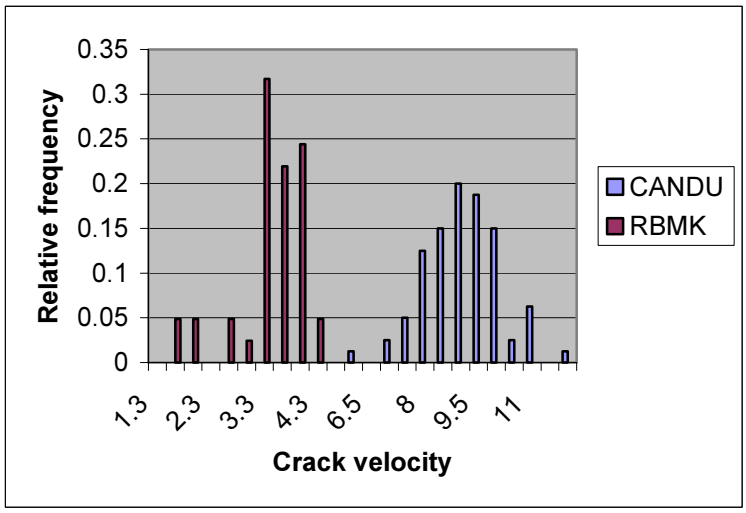

Fig. 4.18. Comparison of distributions of crack velocities at 250℃ in CANDU and RBMK TMT-1 tubes (velocities have units of m/s x 10^{-8}).

Assuming that a similar analysis is valid at the other test temperatures, crack velocities were always greater in the CANDU tube than in the RBMK TMT-1 tube, with a possible increase in the ratio of velocities as the test temperature was lowered:

Temperature °C	283	250	227	203	182	162	144
CANDU/RBMK TMT-1: means	2.25	2.71	2.71	2.95	2.91	3.37	4.75

The difference in behaviour of the two tubes is also illustrated by the Arrhenius plot, Fig. 4.19:

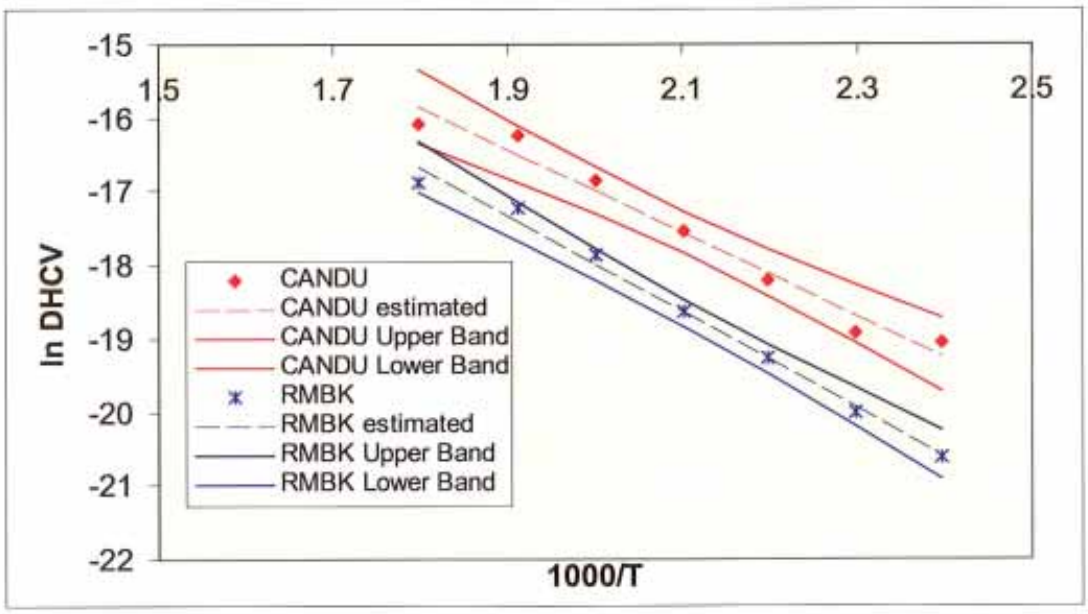

Fig. 4.19. Comparison of crack velocities of DHC in CANDU and RBMK TMT-1 tubes.

Having concluded that the crack velocities of the two tubes are clearly distinguishable over the whole range of test temperatures, we now consider their temperature dependencies. The values of Q in Tables 4.8 and 4.11, the ratios of the crack velocities and Fig. 4.19 all suggest that the RBMK TMT-1 tube has greater temperature dependence than the CANDU tube. However, statistically the temperature dependencies cannot be separated. This conclusion will be reinforced when the next sets of results are presented.

4.4.2. CANDU tube from Cernavoda

Velocity of DHC was measured at 250°C, 227°C and 203°C on specimens machined from tube 429. The results are included in Appendix 4 and summarised in Table 4.12.The values are slightly larger than those of tube RX094 although t-tests show they are essentially indistinguishable. The temperature dependence is also similar, Fig. 4.20, with an activation energy of 59.4 kJ/mol. This value is not very reliable because it is based on only three test temperatures. The technical significance of this result is that the two pressure tubes, which were chosen at random, one made from an ingot that was double melted and one from an ingot that was melted four times, have similar DHC behaviour, strongly suggesting that ingot preparation has no effect on the velocity of DHC [4.11].

Table 4.12. Summary of crack velocities in Cernovoda CANDU pressure tube 429

Test Temperature °C	250	227	203
Crack velocity m/s × 10^{-8}	10.0 9.3 9.4	6.3 5.6 5.0 5.1 5.0 4.8 5.8 4.7	2.2 2.3 2.7 3.0 2.5
Mean value	9.6	5.3	2.5
Standard deviation	0.34	0.56	0.31
Difference of means (429-RX094) %	7.9	10.8	5.3

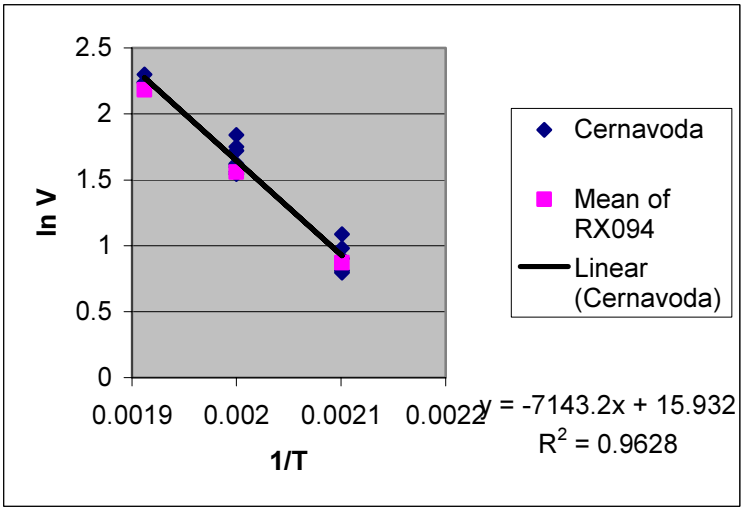

Fig. 4.20. Temperature dependence of DHC in Cernovoda Zr-2.5 Nb pressure tube 429.

4.4.3. HWR tube from India

Velocity of DHC was measured in the temperature range 283 to 162°C on specimens machined from tube 100-2-3. The results are included in Appendix 4 and summarised in Table 4.13.

Table 4.13. Summary of crack velocities in Indian HWR pressure tube 100-2-3

Test temperature °C	283	250	227	203	182	162
Crack velocity m/s × 10^{-8}	16.2 17.7	8.5 9.2 8.1 7.2 6.3 6.6 6.8 8.2	4.2 4.5 3.5	2.6 2.3 1.6 1.9 2.1 1.9	0.96 0.97 1.0	0.56 0.80 0.47
Mean value Standard deviation	16.9 -	7.6 1.05	4.1 0.49	2.1 0.33	0.99 0.043	0.61 0.17
Difference in means ((100-2-3)-RX094)%	38.5	-16.5	-10.7	-16.7	-41.3	-14.7

Except at a test temperature of 283°C, the values are slightly lower than those of tube RX094, although t-tests show they are from the same population. The temperature dependence is also similar, Fig. 4.21, with an activation energy of 56.4 kJ/mol.

Again, tubes made from ingots with different melting practice and slightly different microstructure, have similar DHC behaviour [4.12].

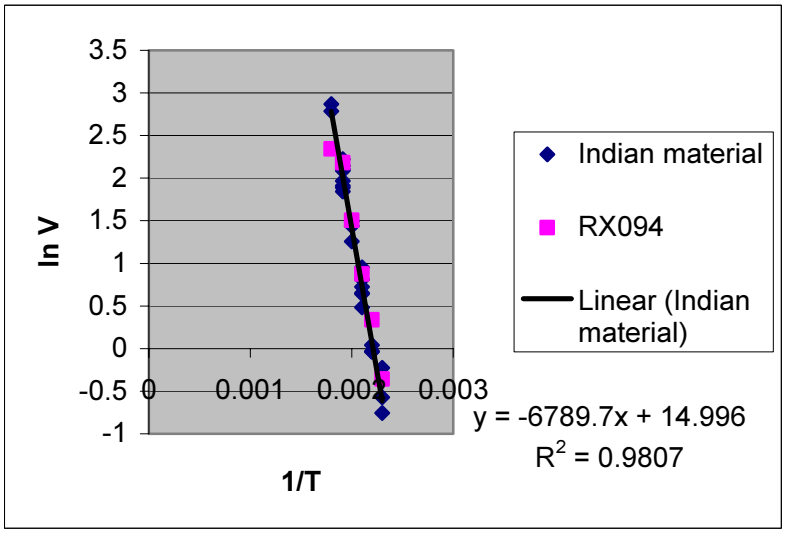

Fig.4.21. Temperature dependence of DHC in Indian Zr-2.5 Nb pressure tube 100-2-3.

4.4.4. Other RBMK materials

The velocity of DHC was measured at 250°C on specimens machined from a standard RBMK tube, from a standard tube in which the recrystallization treatment was absent and from a tube given the TMT-2 treatment. About 100 ppm hydrogen were added gaseously to all specimens. The results are included in Appendix 4 and summarised in Table 4.14.

Table 4.14. Incubation times and velocity of DHC at 250°C for three RBMK tubes

Material	RBMK Standard	RBMK no annealing	TMT-2
Incubation time	3240	29	160
Minutes	1244	18	140
	1560		197
Crack velocity	1.7	13.2	6.0
m/s 10^{-9}	3.2	17.1	6.1
	1.9		6.6
Mean value, V	2.3	15.2	6.3

Cracks were reluctant to grow in the standard RBMK material and the initial K_I used was higher than with other materials, about 21 MPa√m. The incubation times to the start of cracking were very long and the rate of cracking was low in this material. The other materials exhibited faster cracking but still lower than that in cold-worked Zr-2.5 Nb.

4.4.5. Alternative measurement method – CANDU Tube RX094

The standard method was not followed in Argentina because of difficulties in obtaining an accurate hydrogen analysis. This uncertainty led to uncertainty in what peak temperature to use and what test temperature to apply. The hydrogen concentration may be estimated by finding the temperature at which cracking starts after cooling from a temperature well above any reasonable solvus temperature for dissolution [4.13–4.15]. The test sequence was to heat to 330°C, well above the annealing temperature used for adding the hydrogen, cool to a trial test temperature, load the specimen and wait for the potential drop to indicate cracking. If no cracking was observed after a time that was several times the expected incubation time, the temperature was lowered. This process was followed until a temperature, T_c, was reached where cracking was detected, Fig 4.22. In this example, T_c was about 282°C. The value of T_c was related to the TSSP [4.15]. The crack front was marked either by overloading or heat-tinting, although the former gave erratic results in the RBMK TMT-1 material. On further lowering the test temperature, the crack grew and the velocity was estimated from the extent of cracking measured on the crack surface divided by the time of cracking as indicated by potential drop. As observed by Ambler [4.6], once cracking had initiated, with a reduction in temperature of about 10 to 20°C the crack velocity increased, passed through a maximum value then decreased as $V=Ae^{-Q/RT}$. Both of the common pressure tubes behaved in a similar manner, except cracking in the RBMK TMT-1 tube was about 2.5 times slower than in the CANDU tube, Fig. 4.23.

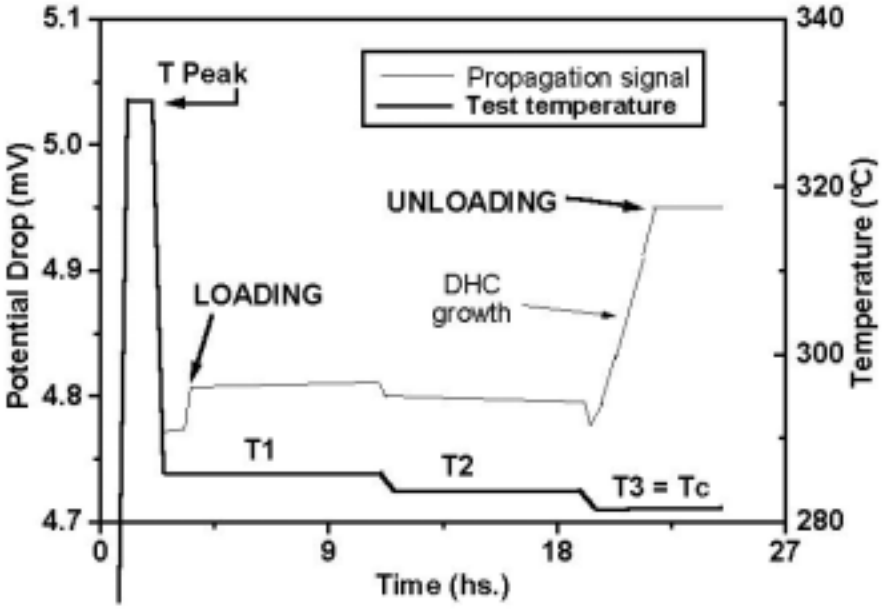

Fig. 4.22. Progressive cooling to evaluate the temperature at which DHC starts.

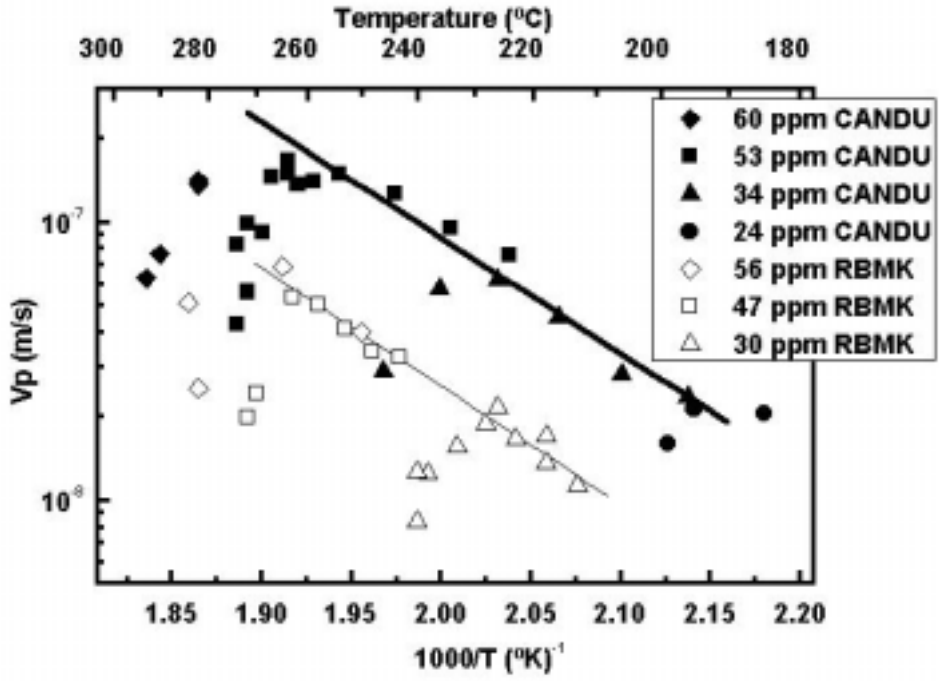

Fig. 4.23. Crack velocity as a function of inverse temperature during cooling showing maximum velocity below T_c followed by Arrhenius-behaviour at lower temperatures.

4.5. Striations

A prominent fractographic feature of DHC in Zr-2.5 Nb is the formation of striations perpendicular to the crack direction. Typical examples are shown in Fig. 4.24 for both the main pressure tubes.

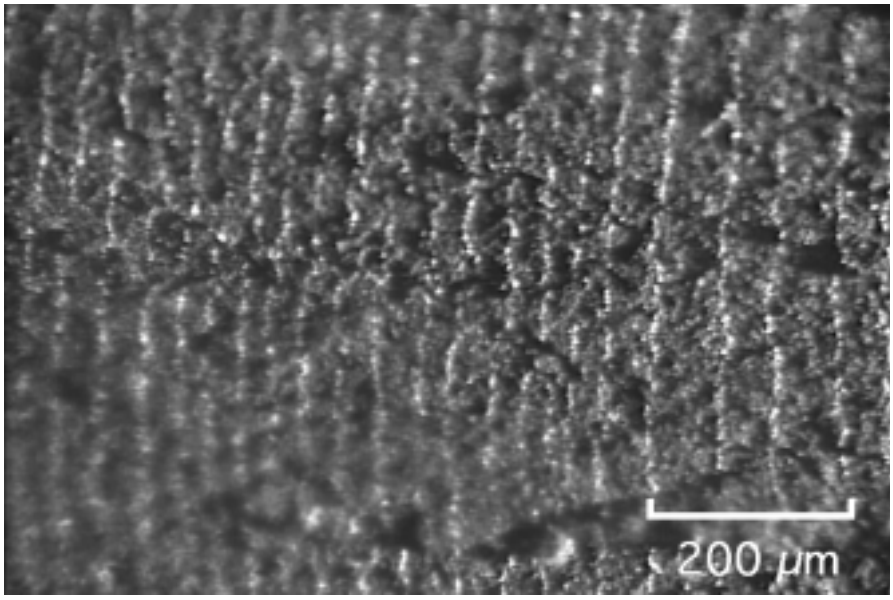

A)

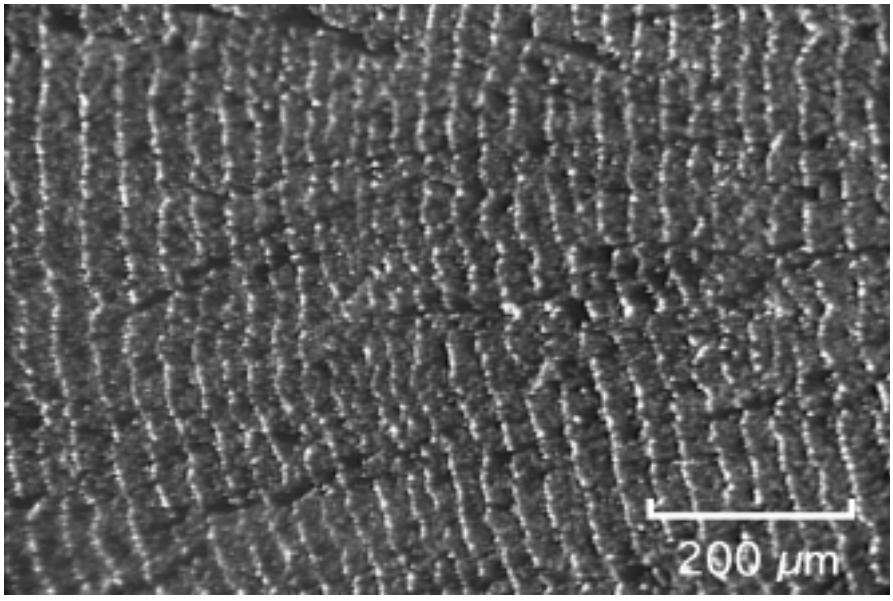

B)

Fig. 4.24. Striations formed by DHC at 283℃. A) RBMK TMT-1 containing 76 ppm hydrogen, B) CANDU containing 79 ppm.

The light contrast arises from ductile fracture while the dark contrast is produced by cleavage of hydrides. The spacing between striations was measured by counting the number of striations within a known length of cracking and the results from four laboratories (Canada, ROK, Lithuania and the Russian Federation) are summarised in Table 4.15.

Striation spacing increases with increase in test temperature and appears to be larger in the specimens of the RBMK material than in the CANDU material. When compared with published values, those from CANDU material agree exactly with those of Nuttall and Rogowski [4.16] but when later measurements by Simpson and Puls [4.2] are added, they include the current values on RBMK TMT-1 material, Fig.4.25.

Table 4.15. Striation spacing of DHC at various temperatures on the two main materials

CANDU Tube RX094

Test temperature, °C	283	275	250	227	203	182	144
Striation spacing, μm	27.9	22.5	19.8	13.1	17.2	9.53	8.8
	28.8	24.2	20.0	14.5	16.4	10.8	8.0
	32.3		20.4	17.2	16.5	9.9	13.8
	29.1		22.1	16.4	16.7	10.0	12.9
	31.6		19.3	15.9	15.8	11.3	13.7
	29.6		24.8	16.1	9.8	12.0	11.5
			21.6		10.9	11.6	9.97
			20.8		12.6	9.8	10.3
			24.3			11.2	
			22.5				
			17.8				
			21.6				
			17.3				
			21.0				
			18.8				
			20.3				
Mean value, μm	29.9	23.4	20.8	15.5	14.5	10.7	11.1
Standard deviation	1.7	-	2.1	1.5	2.9	0.90	2.2

RBMK TMT-1

Temperature,°C	283	250	144
Striation spacing, μm	41.9	27	19.6
	43.2	26.3	23.3
	37.7	30.9	21.5
		32.4	
Mean value, μm	40.9	29.2	21.5

Early in the tests at 250°C on RBMK material in the annealed condition, the striation spacing was up to 200 μm but reduced as the test continued. In stress relieved material the average spacing was 45 μm while after the TMT-2 heat-treatment, spacings averaged 75 μm. All the striation spacings in each material of the current study can be reconciled as a linear function of the yield stress, Fig. 4.26.

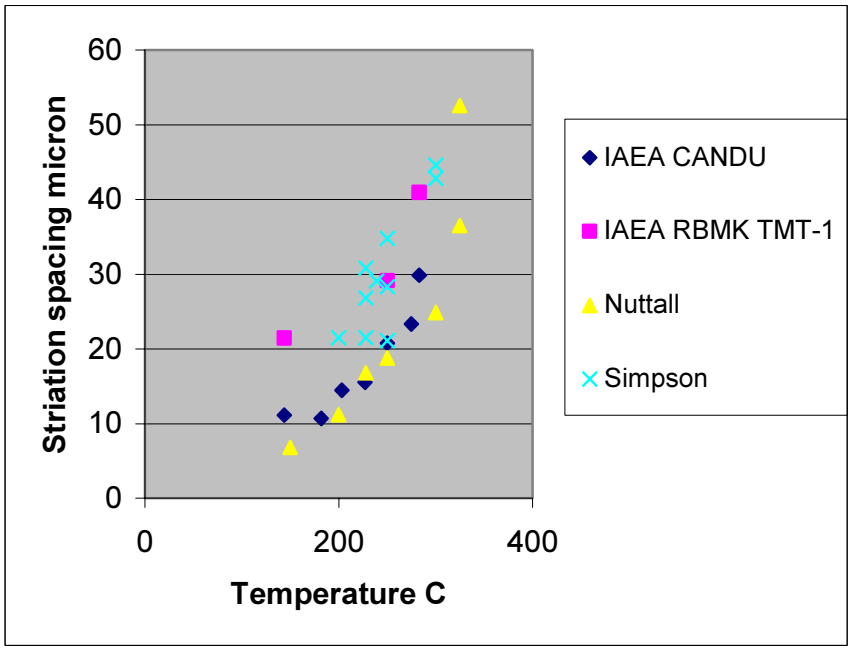

Fig. 4.25. Temperature dependence of striation spacing.

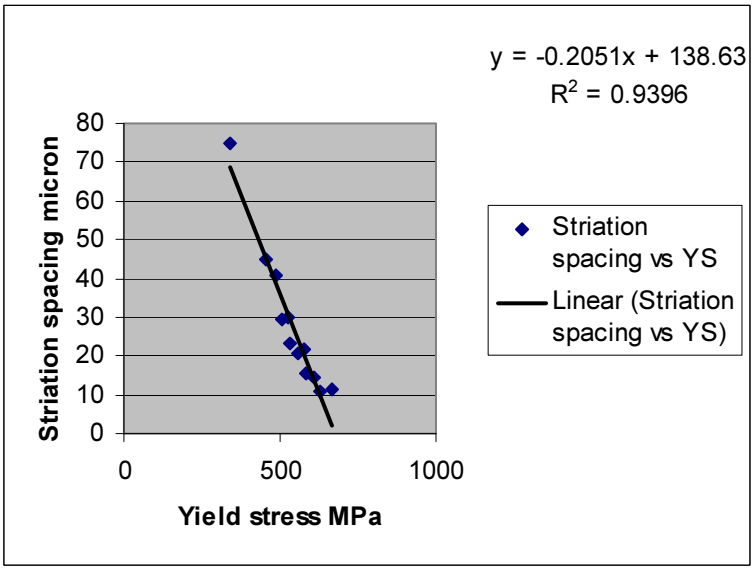

Fig. 4.26. Yield stress dependence of striation spacing.

4.6. Inter-Laboratory Comparison on Hydrogen Analysis

All of the participating laboratories (excluding Canada) used commercial inert gas fusion (IGF) instruments for the determination. (In Canada an isotope dilution method was used [4.17, 4.18] because the heat-transport fluid in a CANDU reactor is heavy water and one

needs to distinguish between deuterium and protium when estimating hydrogen ingress.) Any large variation between these instruments would reflect problems with standards, improper laboratory procedures or instrumental malfunctions. Table 4.16 is a synopsis of the instrumentation and methods used by each laboratory. The table also summarizes information on standards and blanks. Two laboratories reported that they used the ASTM analysis procedure for H in Ti [4.19]. This procedure is similar to that recommended by the instrument manufacturer. Presumably the other laboratories followed the instrument manufacturers recommended procedure.

Table 4.16. Synopsis of instruments and methods used by each laboratory

Country	Bottle	Equipment	Procedure	Standards	Blank
Argentina	1 & 3	LECO RH 404		Ti: LECO 502-154 and 762-741	
China	2	LECO RH 404		Ti	1 μg/g
India	4	LECO RH IE		Ti: LECO 762-741	1.1 ± 0.2 μg/g
ROK	5	LECO RH-404		Zr-2.5Nb: AECL 20HA and 100HA	0.05 μg/g
Lithuania	6	LECO RH-402		Ti	0.017 μg/g
Pakistan	7	STROHLIEN H-mat 251		Zr: NBS-358, Ti: AR-641	0.00001 μg/g
Romania	8 & 3	ELTRA OH-900	ASTM E 1447	Ti: AR 642	0.2 μg/g
Russia	9	LECO RH-404		Ti: LECO 762-741	0.28 μg/g
Sweden	10	ELTRA OH-900	ASTM E 1447	Ti: AR 648, NIST 352c, BCR No 318	0.4 μg/g
Canada	11	AECL HVE - IDMS	Custom	None	1.5 ± 0.4 μg/g

Results of the individual determinations are compiled in Table 4.17.

Table 4.17. Summary of analysis results from round robin on hydrogen analysis

Country	Argentina	China	India	ROK	Lithuania	Pakistan	Romania	Russia	Sweden	Canada A	Canada B
Bottle	1	2	4	5	6	7	8	9	10	11	11
H (μg/g)	41.0	48	45.8	46.6	57.9	49.5	29.3	47.6	49.8	46.7	47.1
	57.4	45	44.2	46.4	57.5	50.0	25.6	49.6	52.3	45.9	47.3
	60.1	49	46.3	47.7	57.5	50.0	25.1	48.8	50.0	46.8	46.9
	40.8	50	41.1	47.9	57.7	50.0	17.8	51.2	50.6	48.2	47.0
	61.7	45	42.3	48.7	57.9	50.0	35.0	49.2	51.2	47.3	47.3
	59.7	49	41.5	47.7	57.6	50.5	50.4	48.5	49.8	45.7	47.5
	59.9	49	44.4	47.1	59.2	50.5	32.6	48.4	50.1	47.1	47.0
	43.3	48	40.5	46.7		51.0	22.1	48.1	50.9	46.2	46.7
	46.2	49	44.2	47.1		51.0	16.5	52.9	51.2	47.0	47.1
	61.4	48	43.3	48.7			28.5	50.8	50.9	46.3	
Mean	53.2	48	43.4	47.5	57.9	50.3	28.3	49.5	50.7	46.7	47.1
Std Dev	9.1	1.7	2.0	0.8	0.6	0.5	9.8	1.7	0.8	0.7	0.2

4.6.1. Precision

The instrumental precision expected for repeat measurements is specified to be within 2% rsd (based on calibration by gas analysis) on the LECO RH-404 [4.20] and 1% rsd for the ELTRA OH-900 [4.21]. We assume that the other instrument models are competitive and offer similar precision. Considering the blank uncertainty and other uncertainties associated with the fusion step, a precision of 1–2 μg/g was anticipated from each laboratory. Most of the laboratories achieved that precision. This result confirmed that the samples were properly prepared with a small dispersion and were properly randomized. Argentina and Romania obtained a large dispersion initially. On investigation these laboratories confirmed that their instrument was malfunctioning. Five specimens from Bottle 3 were sent to these two laboratories and the subsequent results had a low dispersion:

	Hydrogen Concentration ppm					Mean	Standard Deviation
Argentina	53.3	53.2	53.1	53.0	53.4	53.2	0.16
Romania	54.3	54.4	56.2	52.8	54.3	54.4	1.2

The instrumental blank uncertainty may also contribute to the analysis precision. In Table 4.16, a wide range of blank values is reported. Some of the very low values reported are probably the residual blank after instrument compensation. The actual size of the blank should be determined and monitored routinely. The uncertainty on the blank must be known to calculate the precision of the sample analysis.

4.6.2. Bias

Assessment of the bias is hindered somewhat by the ambiguity in the known hydrogen concentration. The initial analysis of the 40 samples in Canada indicated the mean value was 49.8 μg/g. After 2 months of storage, the specimens in bottle #11 were analysed on two different HVE - IDMS instruments. The combined mean hydrogen concentration was found to be 46.9 μg/g. Such large systematic shifts are not seen on these instruments for analyses of deuterium in Zr standards, so it is thought that the original analysis was contaminated by background water from humid air providing an incorrect blank. High humidity may bias values since H_2O adsorbed on the surface of the sample reduces to H_2 during the fusion. The system blank does not account for this excess hydrogen introduced by the sample itself. However, there was no evidence that the observed relative biases correlate with differences in humidity.

Fig. 4.27 shows the results plotted relative to the mean value obtained in Canada (46.9 μg/g) and illustrates the relative biases between the laboratories. The results from Romania and Argentina are from the extra five specimens. Since all of the hydrogen in the Zr-2.5 Nb specimens came from the same source, the biases reflect differences in the performance of the individual laboratories.

The use of the standards may be the source for much of the bias. The standard deviation on some of the Ti standards is large. The laboratory operators must run a sufficient number of calibration standards to ensure that the calibration is not biased. For example, using LECO 762-741 certified with a standard deviation of 10 %, at least 16 calibration standards would

have to be analyzed to ensure that the calibration bias was < 5% at a level of confidence of 95%. Also Ti may not be a good surrogate for Zr. All laboratories used hydrogen in Ti as standards, except ROK. Zr standards had been provided to ROK by AECL under a commercial contract. Those standards were produced in the same way that the inter-laboratory specimens were produced. Therefore the agreement between Canada and ROK is expected to be good. More importantly, the differences between ROK and the other laboratories may be indicative of a real difference between Zr and Ti standards. For example, ROK measured the calibration factors for their instrument using both Ti and Zr standards, and obtained values of 1.3672 and 1.2591, respectively. The results suggest that more hydrogen is released from Zr than Ti. If the results with the high bias are corrected by the ratio of the two calibration factors, 0.9209, most of the values approach those of Canada and ROK, Fig. 4.28. The calibration factor for the Lithuanian results was reported as both 1.5366 and 1.3769 with the results being presented with the higher value in Fig. 4.27. These results were revised by 0.8194 in Fig. 4.28. The results from India tended to be slightly lower than those from Canada and ROK so they were not modified in Fig. 4.28.

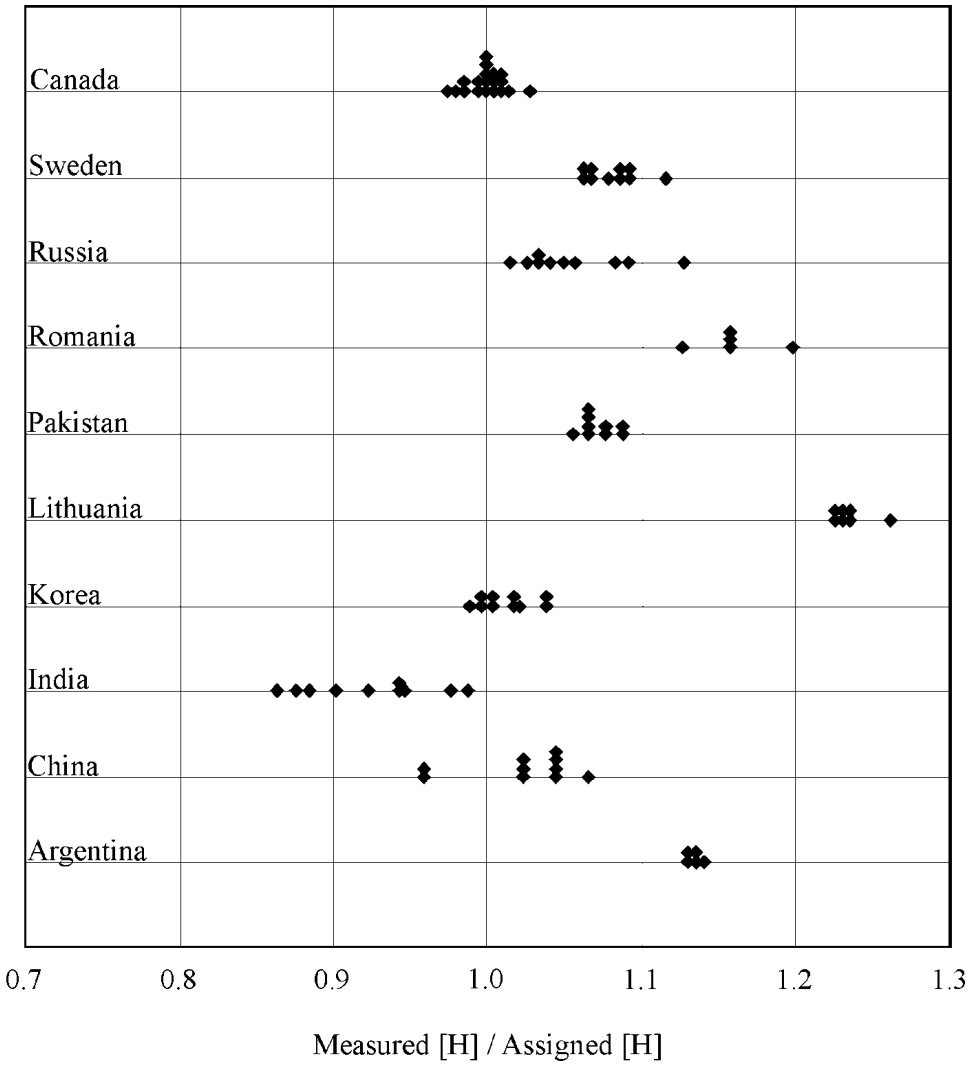

Fig. 4.27. Hydrogen analysis in each country relative to Canadian results.

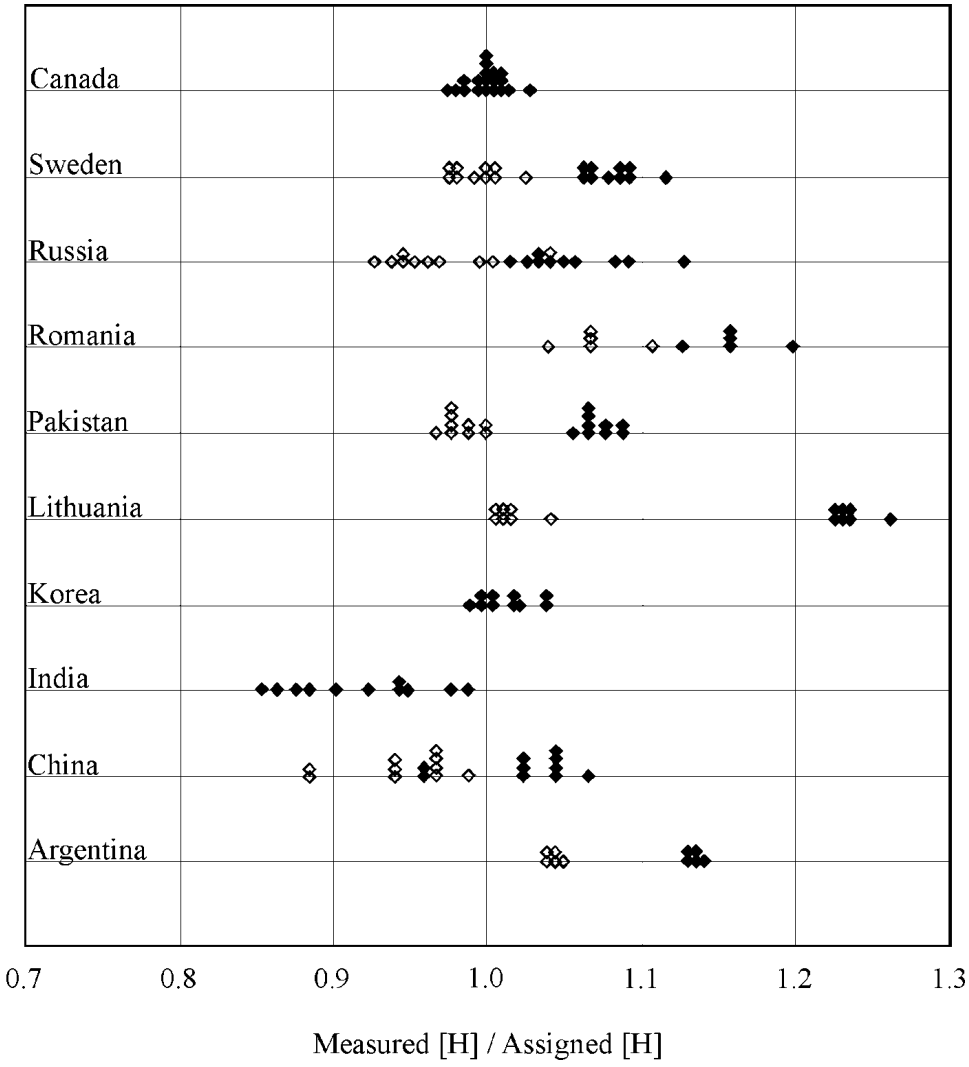

Fig.4.28. Hydrogen analysis results modified by the ratio of the calibration factors for Ti and Zr standards: open points; initial results from Fig. 4.27 are closed points.

The above corrections will not be exact because the calibration factors for Ti and Zr in the specific instruments will likely be different from those quoted, but the corrected results comply with those derived using Zr as a standard and with the initial hydrogen additions. If this approach is correct, standards appear to be specific to the particular metal. Thus measurements of hydrogen in Zr should use hydrogen in Zr for standards rather than hydrogen in Ti.

4.7. Discussion

The results presented in the previous sections show that this Co-ordinated Research Project has met its objectives. The methods for performing consistent measurements of DHC velocity in Zr-2.5Nb developed in Canada have been transferred to other countries. The general agreement on the values between the different laboratories on the two main test materials demonstrates the success of this transfer.

The main areas of inconsistency are with the additions of hydrogen and its analysis. Some latitude is available for DHC measurements so long as the temperature history of the tests meets the criteria for maximum crack velocity:

(a) The peak temperature must be equal to or exceed the solvus temperature for hydrogen dissolution, T_d [4.4].

This criterion is met so long as the peak temperature is greater than the annealing temperature used to diffuse the hydrogen into the specimen. Examination of the reported test conditions shows that this criterion was met, with the exceptions mentioned in Section 4.2. Some tests on other tubes may not have fully met this criterion. Three Indian tests at 250°C on tube 100-2-3 on specimens containing 80 ppm used a peak temperature of 306°C; depending on which TSSD is used [4.10, 4.22–4.24] T_d is between 317 and 329°C so hydrides would still have been present at the peak temperature. The crack velocities of these specimens were slightly lower, 6.3 to 7.15 $\times 10^{-8}$ m/s, than in similar specimens containing 60 ppm (T_d between 295 and 306°C) that had a peak temperature >319°C, 8.06 to 9.24 $\times 10^{-8}$ m/s. The peak temperature in the tests on the other RBMK materials, Table 4.14, were 325 to 330°C whereas with a hydrogen concentration of 100 ppm the preferred peak temperature is 335 to 348°C, thus the reported values of crack velocity may be slightly too low.

(b) The test temperature must always be attained by cooling.

Results of tests were rejected in which there was known undercooling before the test temperature, T_t, was reached and therefore the test temperature was attained by heating (Section 4.2).

(c) Hydrides must be available at the test temperature.

DHC can start when the solubility limit for precipitation is exceeded at the crack tip because of the transport of hydrogen into this high stress region. Thus the temperature at which cracking is possible, T_c, is between T_d and T_p, the solvus for precipitation. Over the current range of test conditions, based on crack incubation time detected by acoustic emission, [4.13, 4.14], T_d-T_c is in the range 6 to 17°C and T_c-T_p is in the range 41 to 52°C while the same quantities derived from cracking detected by potential drop [4.15] are 16 to 28°C and 30 to 42°C. To obtain the maximum crack velocity (minimum incubation time), the test temperature should be ≥ 15°C lower than T_c, that is, about 35 to 45°C below T_d or within 15 to 25°C of T_p. The results in Section 4.4.5, Figs 4.22 and 4.23, illustrate this situation. As the test temperature was lowered cracking was detected; this is T_c. As the temperature was lowered further the crack velocity increased to a maximum value; let us call this temperature T_m. With subsequent temperature reduction the crack velocity followed the Arrhenius relationship with all these values being the maximum value for that temperature. The relationship between T_c, T_m, T_d and T_p is summarised for these tests in Table 4.18. Included is a similar test on irradiated Zr-2.5 Nb, which fits the pattern [4.25].

A second illustration of the need to exceed a critical hydrogen concentration is the lower two results in Table 4.2. The test temperature of 250°C for the specimens containing 40 ppm did not meet the (T_c-15°C) criterion and thus the crack velocity was less than the maximum possible value; the specimens containing 55 ppm had sufficient hydrogen to crack at the maximum velocity because $T_t < T_c$-15°C.

Table 4.18. Test results indicating the temperature where the DHC velocity is maximized, T_m, and the relationship to the hydrogen solvus temperatures

Material	H ppm	T_c °C	T_m °C	T_c °C Literature	T_d °C	T_p °C
CANDU	24	201	189	218-227	234-242	175-206
	34	246	232	238-249	256-265	198-226
	53	276	263	268-278	286-296	232-254
	60	{300}	275-280	276-287	295-305	243-262
CANDU Irradiated	105	320-325	300-310	319-330	340-352	291-296
RBMK TMT-1	30	240	228	231-241	248-257	190-218
	47	275	263	260-270	277-287	223-246
	56	{284}	{278}	271-282	290-300	237-257

Having a test temperature below T_p guarantees the maximum crack velocity because hydrides are available throughout the specimen while the maximum hydrogen concentration in solution (supersaturated from cooling) is also available.

For the current tests, based on the reported hydrogen concentrations, maximum crack velocities were measured since the T_p criterion was met in all specimens tested at 203°C and below. In tests at 250 and 227°C the (T_c-15°C) criterion was met while in some tests at 283°C the (T_c-15°C) criterion was apparently borderline, which may account for some of the low values of crack velocity and the large standard deviation that were observed in the CANDU material, Table 4.7. In retrospect, the target hydrogen concentration for testing at 283°C should have been a little higher, say 85 to 90 ppm, to guarantee maximum velocities.

In Section 4.4.1 we concluded that DHC was 2 to 5 times slower in the RBMK TMT-1 material than in the CANDU tube. To judge whether these results represent members of the same population or not we need data from other tubes made to each representative specification. No further data are available on the RBMK material but several tests that met the criteria for maximum crack velocity have been done at 250°C on CANDU tubes other than the three reported here (Sections 4.2, 4.4.2, 4.4.3.) The results are summarised in Table 4.19. The best we can do is show whether or not the results on the RBMK TMT-1 tube are outside the distribution of the samples of CANDU data.

If so, and since these tubes were selected at random, we can conclude that the difference is because they were sampled from separate populations. The mean value of the results at 250°C on the RBMK TMT-1 tube was $3.3 \times 10^{-8} \pm 0.64$m/s (Table 4.10) which has less than 5% chance of being part of the distribution of results on CANDU material, that is: $(9.52–(2 \times 2.2)) > (3.3+(2 \times 0.64))$. We conclude that the results from each type of tube come from different populations.

Table 4.19. DHC velocity at 250°C in several CANDU tubes

Material	H ppm	Yield stress Mpa Transverse 250°C	Mean crack velocity $m/s \times 10^{-8}$	Standard deviation (number of specimens) $m/s \times 10^{-8}$	Reference
RX094	55 - 63	567	8.86	1.07 (80)	This report
429	65 - 67	585	9.6	0.34 (3)	This report
100-2-3	60 - 80	531	7.6	1.05 (8)	This report
"SMIRT-17"	170	606	7.0 (Interpolated value)		4.25
Tube A front	72	Not available	8.4	0.41 (6)	Choubey private communication
Tube A back	72	600	8.5	0.54 (6)	Choubey private communication
Tube B front	69	Not available	9.4	0.33 (6)	Choubey private communication
Tube B back	69	600	8.8	0.58 (6)	Choubey private communication
Tube C front	72	Not available	12.1	0.35 (6)	Choubey private communication
Tube C back	72	602	9.2	0.73 (6)	Choubey private communication
Tube D front	73	Not available	8.9	0.23 (6)	Choubey private communication
Tube D back	73	614	14.6	0.60 (6)	Choubey private communication
Tube E middle	63 - 71	567	6	0.30 (6)	Choubey private communication
Tube F	60	559	7.6 - 8.8		Shek private communication
Zr conference	55	Not available	11.8	3.1 (5)	4.3
		Mean value	9.52		
		Standard deviation	2.2		

The crack velocity is controlled by the solubility limit, C, diffusivity of hydrogen, D, and the ability to form and crack a hydride. The sources of the difference between the tube types are the parameters that affect each of the controlling factors: grain structure, crystallographic texture and strength. The interactions are complicated because strength is determined by the grain structure and texture as well as the chemical composition while grain structure and texture can affect DHC independently of strength. As examples:

(a) if the β-phase is continuous it can provide a pathway for rapid hydrogen diffusion and high crack velocities [4.26, 4.27],
(b) a tensile stress parallel to the basal plane normal promotes precipitation of hydrides with their platelet normals parallel with the stress and facilitates cracking whereas cracking is difficult when the tensile stress is perpendicular to the basal plane normal, [4.27–4.30],
(c) a high yield stress produces a high stress gradient at the crack tip and reduces the size of the hydride required for cracking and therefore facilitates DHC [4.4, 4.8, 4.31]. The latter effect is reflected in the dependence of the striation spacing on yield stress, Fig. 4.26.

The crack velocity was expected to be lower in the RBMK TMT-1 tube than in the CANDU tube because:

— it did not contain a continuous β-phase film in its grain boundaries as in the CANDU tube,
— the fraction of basal plane normals in the transverse direction was much lower in the RBMK
TMT-1 tube than in the CANDU tube,
— the yield stress was lower in the RBMK TMT-1 tube than in the CANDU tube.

To judge the relative importance of the microstructural features and strength, we compare the results on a CANDU tube given the same heat-treatment as TMT-1 [4.32]. The microstructure was similar to the RBMK tube but the strength was higher than in a cold-worked tube (estimated at 250°C by interpolation). The crack velocity (estimated by extrapolation of a fitted Arrhenius line) was intermediate between the values of the current two materials, Table 4.20. With the warning that only one tube is being sampled from each potential population, the results demonstrate that both microstructure and strength can independently affect crack velocity.

Table 4.20. Comparison of the factors affecting DHC velocity in Zr 2.5 Nb

Material	F_T	Continous β-phase	Yield stress, Mpa Transverse, 250°C	Crack velocity m/s × 10^{-8}
CANDU CW	0.6	Yes	567	8.9
CANDU HT	0.42	No	≈700	≈5.5
RBMK TMT-1	0.42	No	494 - 524	3.3

Difference in strength seems to be the main reason why the crack velocity in the standard annealed RBMK tube, (yield stress of 255-314 MPa) was about ten times slower than when the tube was only stress-relieved rather than annealed, providing a strength of 455 MPa, Table 4.14. Since texture is mostly established during extrusion, the texture of the two tubes should be similar. The β-phase stringers would be mostly decomposed by the intermediate anneal at 580°C so they should not play a major role in enhancing hydrogen diffusion. The importance of yield stress in controlling DHC velocity at 250°C is illustrated in Figure 4.29. Included in the figure are the current results, those in Tables 4.19 and 4.20 as well as the early results demonstrating the effect of strength [4.4] and results from a well-controlled irradiation [4.33] assuming the increase in strength is the main factor. Although the correlation holds over this wide range of yield stresses, it can be improved by taking into account the microstructure differences. To account for the temperature dependence of hydrogen migration V is normalized [4.31] by the solubility limit, ($C=1.2 \times 10^5 \exp(-35900/RT)$) [4.10] and diffusivity ($D = 2.17 \times 10^{-7}\exp(-35100/RT)$) [4.34].

The equation for the solubility limit was chosen because it provides a good representation of many data sets. To represent the materials where the β-phase was not continuous, the pre-exponential term in D was reduced by 50%. The activation energy was not changed to acknowledge that Q for crack velocity was similar for all the materials. To take into account texture, V was normalized by F_T, Table 3.4 [4.29]. The results, Fig. 4.30, show that the correlation is improved by 10%.

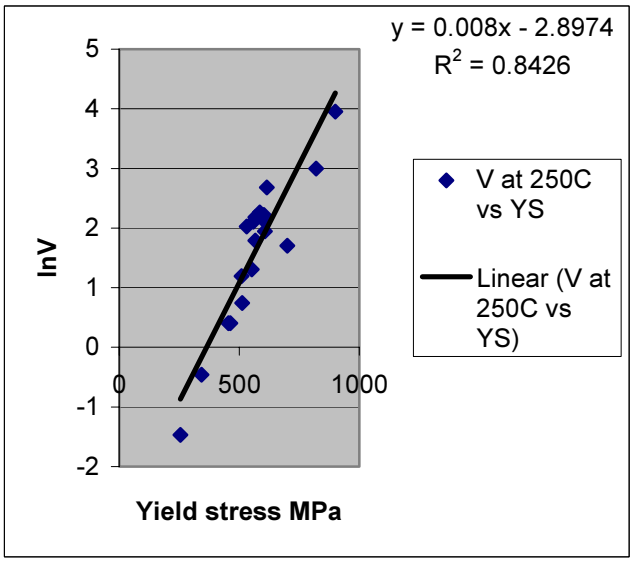

Fig. 4.29. Dependence of DHC crack velocity at 250°C in Zr–2.5 Nb on yield stress.

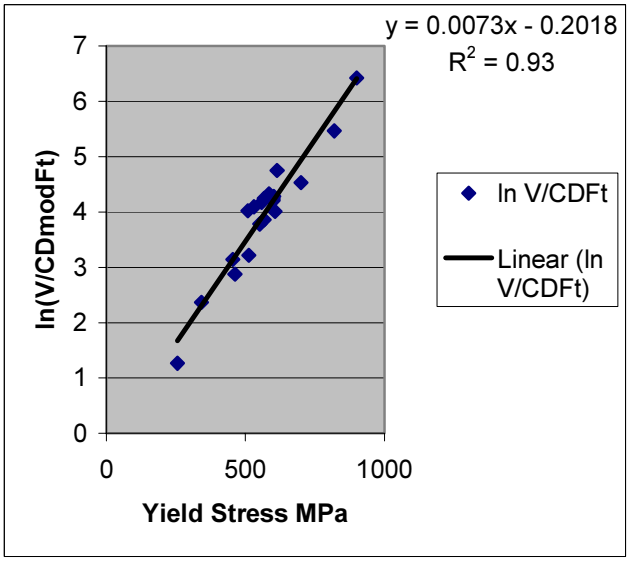

Fig.4.30. Dependence of normalized DHC crack velocity at 250°C in Zr–2.5 Nb on yield stress.

Despite the assumptions required because of lack of detailed information on some of the materials and the need to use representative values of C and D rather than values for the actual tubes, the analysis appears to depict the important factors in DHC velocity at one temperature.

The need for the normalization is more apparent when all the results at other test temperatures from this programme are plotted against strength, Fig. 4.31.

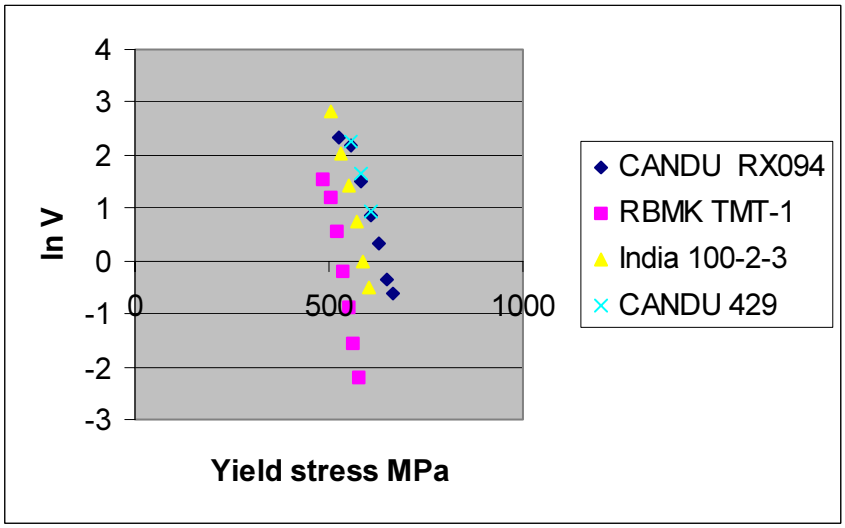

Fig.4.31. DHC velocity for the four test materials at various test temperatures as a function of yield stress.

Using the same normalization as above with the same equations for C and D, and the same values of F_T, the data are united, Fig. 4.32, although a better correlation is attained if the effect of texture is ignored, Fig. 4.33.

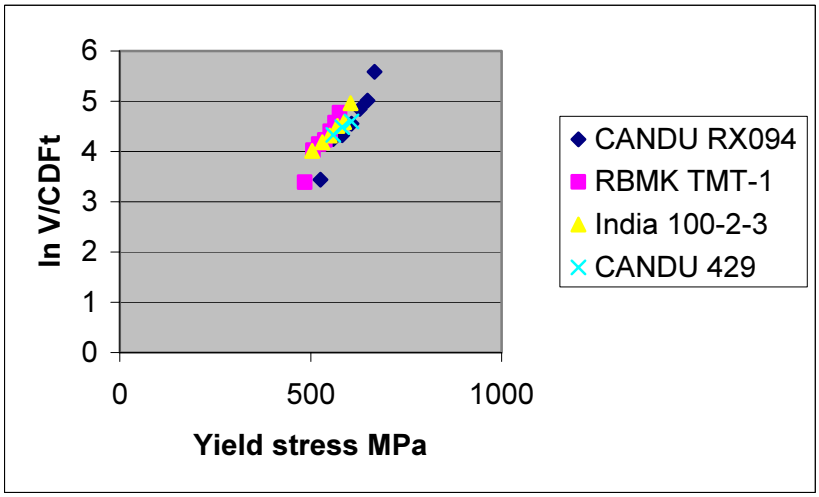

Fig. 4.32. Dependence on yield stress of normalized DHC velocity in the Zr-2.5 Nb tubes used in the current study.

When the data presented in Fig. 30 are combined with those in Fig. 4.32, they exhibit a clear but modest correlation with yield stress, Fig. 4.34. Thus the results of the test programme on Zr-2.5 Nb tubes made by different fabrication routes from material of different compositions and performed in different countries can be rationalized empirically through the expected temperature dependence of the main factors important to DHC — solubility limit of hydrogen, diffusivity of hydrogen and strength, and by taking into account microstructural features such as the distribution of β-phase and crystallographic texture.

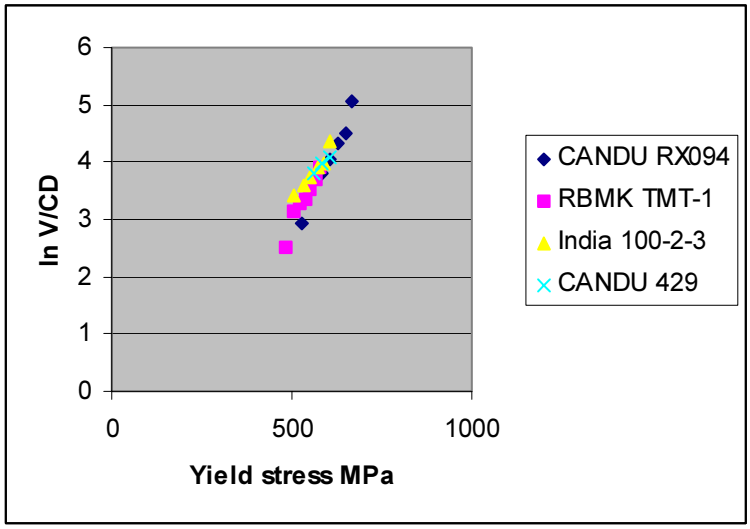

Fig. 4.33. Dependence on yield stress of normalized DHC velocity in the Zr-2.5 Nb tubes used in the current study, ignoring differences in texture.

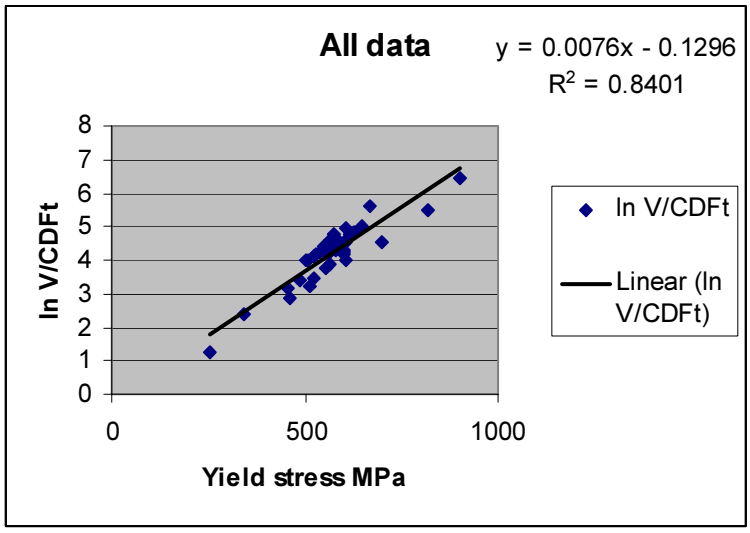

Fig. 4.34. Dependence on yield stress of normalized DHC velocity of all the various Zr-2.5 Nb materials tested over a wide temperature range.

REFERENCES TO CHAPTER 4

[4.1] DUTTON, R., NUTTALL, K., PULS, M.P., SIMPSON, L.A., Mechanisms of hydrogen induced delayed cracking in hydride forming materials, Met. Trans., 8A, (1977), 1553–1562.

[4.2] SIMPSON, L.A., PULS, M.P., The effects of stress, temperature and hydrogen content on hydride-induced crack growth in Zr-2.5 pct Nb, Met. Trans., 10A, (1979), 1093–1105.

[4.3] SAGAT, S., COLEMAN, C.E., GRIFFITHS, M., WILKINS, B.J.S., The effect of fluence and irradiation temperature on delayed hydride cracking in Zr-2.5 Nb, Zirconium in the Nuclear Industry-10th International Symposium, ASTM STP 1245, eds. A.M. Garde and E.R. Bradley, ASTM, West Conshohocken, PA, (1994), 35–61.

[4.4] SHEK, G.K., GRAHAM, D.B., Effect of loading and thermal maneuvers on delayed hydride cracking in Zr-2.5 Nb alloys, Zirconium in the Nuclear Industry-8th International Symposium, ASTM STP 1023, eds. L.F.P. Van Swam and C.M. Eucken, ASTM, West Conshohocken, PA, (1989), 89–110.
[4.5] AMBLER, J.F.R., COLEMAN,C.E., Acoustic emission during delayed hydrogen cracking in Zr-2.5 wt.%.Nb alloy, Proc. 2nd International Congress on Hydrogen in Metals, Paris, Pergamon Press, Oxford, (1977) Paper 3C10.
[4.6] AMBLER, J.F.R., Effect of approach to temperature on the delayed hydride cracking behavior of cold-worked Zr-2.5 Nb, Zirconium in the Nuclear Industry-6th International Symposium, ASTM STP 824, eds. D.G. Franklin and R.B. Adamson, ASTM, West Conshohocken, PA, (1984), 653–674.
[4.7] COLEMAN, C.E.,.CHEADLE,B.A., AMBLER, J.F.R., LICHTENBERGER, P.C., EADIE, R.L., Minimising hydride cracking in zirconium alloys, Can. Met. Quart., 24, (1985), 245–250.
[4.8] KIM, Y.S., KIM, S.S., CHEONG, Y.M., KIM, I.S., Governing factors for delayed hydride cracking in Zr-2.5 Nb tubes, Presented at Canadian Nuclear Society, June, 2003.
[4.9] AMOUZOUVI, K.F., CLEGG, L.J., Effect of heat treatment on delayed hydride cracking in Zr-2.5 wt pct Nb, Met. Trans., 18A, (1987), 1687–1694.
[4.10] KEARNS, J.J., Terminal solubility and partitioning of hydrogen in alpha zirconium, Zircaloy-2 and Zircaloy-4, J. Nucl. Mater., 20, (1967), 292–303.
[4.11] ROTH, M., CHOUBEY, R., COLEMAN, C.E., RITCHIE, I., Measurement of DHC in CANDU pressure tubes, 17th Int. Conf. Structural Mechanics in Reactor Technology, Prague, 2003, Paper G350.
[4.12] SINGH, R.N., KUMAR, N., KISHORE, R., ROYCHAUDHURY, S., SINHA, T.K., AND KASHYAP, B.P., Delayed hydride cracking in Zr-2.5Nb pressure tube material, J. Nucl. Mater., 304, (2002), 189–203.
[4.13] COLEMAN, C.E., AMBLER, J.F.R., Measurement of effective solvus temperature of hydrogen in Zr-2.5 wt% Nb using acoustic emission, Can. Met. Quart., 17, (1978), 81–84.
[4.14] COLEMAN, C.E., AMBLER, J.F.R., Solubility of hydrogen isotopes in stressed hydride-forming metals, Scripta Met., 17, (1983), 77–82.
[4.15] SHI, S.-Q., SHEK, G.K., PULS, M.P., Hydrogen concentration limit and critical temperature for delayed hydride cracking in zirconium alloys, J. Nucl. Mater., 218, (1995), 189–201.
[4.16] NUTTALL, K., ROGOWSKI, A.J., Some fractographic aspects of hydrogen-induced delayed cracking in Zr-2.5 wt. Percent Nb alloys, J. Nucl. Mater., 80, (1979),279–290.
[4.17] GREEN, L. W., BICKEL, G. A., LEESON, P. K., JAMES, M. W. D., LAMARCHE, T. G. and H. Michel, A Hot Vacuum Extraction Mass Spectrometric System for Determination of H and D in Zirconium, Proceedings of the 2nd Alfred O. Nier Symposium on Inorganic Mass Spectrometry, Durango, Colorado, May 1994 (Available as part of AECL-11342, Jan. 1996, pp. 95–99.
[4.18] BICKEL, G.A., GREEN, L.W., JAMES, M.W.D., LAMARCHE, T.G., LEESON, P.K., MICHEL, H., The determination of hydrogen and deuterium in Zr-2.5 Nb material by hot vacuum extraction mass spectrometry, J. Nucl. Mater., 306, (2002), pp. 21–29.
[4.19] ASTM E 1447, “Standard Test Method for Determination of Hydrogen in Titanium and Titanium Alloys by the Inert Gas Fusion Thermal Conductivity Method.
[4.20] LECO Corporation RH-404 Hydrogen Determinator Specification Sheet, LECO Corporation Application Bulletin: Determination of Hydrogen in Titanium.

[4.21] ELTRA GmbH Oxygen/Hydrogen Determinator OH900 Specifications, (www.eltragmbh.com).
[4.22] SLATTERY, G., "The Terminal Solubility of Hydrogen in Zirconium Alloys between 30 and 400 °C", J. Inst. Met., 95, (1967), 43–47.
[4.23] PAN, Z.L., Ritchie, I.G., Puls, M.P., The terminal solid solubility of hydrogen and deuterium in Zr-2.5Nb alloys, J. Nucl Mater., 228, (1996), 227–237.
[4.24] McMINN, A., DARBY, E.C., SCHOFIELD, J.S., Terminal solid solubility of hydrogen in zirconium alloys, Zirconium in the Nuclear Industry-12th International Symposium, ASTM STP 1354, eds. G.P. Sabol and G.D. Moan, ASTM, West Conshohocken, PA, (2000), 173–195.
[4.25] SAGAT, S., PULS, M.P., Temperature limit for delayed hydride cracking in Zr-2.5Nb alloys, 17th Int. Conf. Structural Mechanics in Reactor Technology, Prague, 2003, Paper G311.
[4.26] SIMPSON, L.A., CANN, C.D., The effect of microstructure on rates of delayed hydride cracking in Zr-2.5% Nb alloy., J. Nucl. Mater., 126, (1984), 70–73.
[4.27] COLEMAN, C.E., SAGAT, S., AMOUZOUVI, K.F., Control of microstructure to increase the tolerance of zirconium alloys to hydride cracking, AECL Report, AECL-9524, 1987.
[4.28] COLEMAN, C.E., Effect of texture on hydride reorientation and delayed hydrogen cracking in cold-worked Zr-2.5Nb, Zirconium in the Nuclear Industry-5th International Symposium, ASTM STP 754, eds. D.G. Franklin, ASTM, West Conshohocken, PA, (1982), 393–411.
[4.29] KIM, S.S., KWON, S.C., KIM, Y.S., The effect of texture variation on delayed hydride cracking behavior of Zr-2.5%Nb plate, J. Nucl. Mater., 273, (1999), 52–59.
[4.30] KIM, Y.S., KIM, S.S., KWON, S.C., IM, K.S., CHEONG, Y.M., Anisotropic threshold stress intensity factor, K_{IH} and crack growth rate in delayed hydride cracking of Zr-2.5Nb pressure tubes, Met. & Mat. Trans., 33A, (2002), 919–925.
[4.31] OH, J.Y., KIM, I.S., KIM, Y.S., A normalization method for relationship between yield stress and delayed hydride cracking velocity in Zr-2.5Nb alloy, J. Nucl. Sci. and Tech., 37 (2000), 595–600.
[4.32] CHOW, C.K., COLEMAN, C.E., KOIKE, M.H., CAUSEY, A.R., ELLS, C.E., HOSBONS, R.R., SAGAT, S., URBANIC, V.F., RODGERS, D.K., Properties of an irradiated heat-treated Zr-2.5Nb pressure tube removed from the NPD reactor, Zirconium in the Nuclear Industry-11th International Symposium, ASTM STP 1295, eds. E.R. Bradley and G.P. Sabol, ASTM, West Conshohocken, PA, (1996), 469–491.
[4.33] HOSBONS, R.R., DAVIES, P.H., GRIFFITHS, M., SAGAT, S., COLEMAN, C.E., Effect of long-term irradiation on the fracture properties of Zr-2.5Nb pressure tubes, Zirconium in the Nuclear Industry-12th International Symposium, ASTM STP 1354, eds. G.P. Sabol and G.D. Moan, ASTM, West Conshohocken, PA, (2000), 122–138.
[4.34] SAWATZKY, A., The diffusion and solubility of hydrogen in the alpha-phase of Zircaloy-2, J. Nucl. Mater., 2, (1960), 62–68.

CHAPTER 5

MEASUREMENT OF DHC VELOCITY IN FUEL CLADDING USING THE PIN-LOADING TENSION TEST

As indicated in Chapter 1, DHC is implicated in the development of long splits in some fuel cladding. A potential method for evaluating DHC is described below.

5.1. Method

The Pin-Loading Tension (PLT) technique has been used to characterise the fracture toughness in the axial direction of irradiated cladding [5.1-5.3]. A notched PLT-specimen is manufactured from the cladding tube, Fig. 5.1. The specimen is axially notched at both edges, with the notches at the front edge of the specimen being sharpened by fatigue.

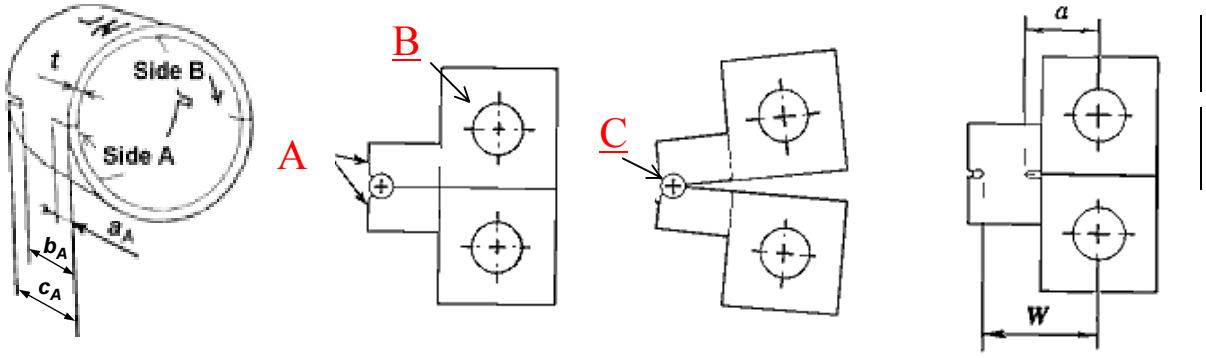

Fig. 5.1. Schematic diagram of the PLT specimen, fixture, and specimen-fixture assembly.

The PLT-fixture consists of two halves, which when placed together form a cylindrical holder A (see Fig. 5.1). The diameter of the holder allows it to be inserted into the tubular PLT-specimen, while maintaining a minimal interfacial gap. The fixture halves are loaded in tension through the pins B and have the capability of mutual rotation around the axis determined by a small pin C placed between the fixture halves at the end of the cylindrical holder. The rotation of the fixture halves is similar to the rotation of the halves of a compact specimen (CT) under tension, except that in the PLT-fixture, the rotation axis does not change its position when the crack propagates in the specimen.

The PLT specimen, pre-cracked by fatigue, can be used both for the fracture toughness evaluation and for the measurements of DHC velocities in fuel cladding materials. The crack extension during the testing can be monitored by measurement of DC potential drop, Fig. 5.2.

In the fracture toughness test the load and load-point displacement are monitored during the loading to plot the load-displacement record (LDR). After unloading, the crack extension area is marked by short-term fatigue, and the crack extension is measured on the both sides of the specimen. The average value of the crack extension is used for toughness evaluations.

The *J*-integral values are calculated from the LDR and plotted against the corresponding crack extensions. That plot represents a *J*-resistance curve of the specimen. The *J*-resistance curve is used to establish a crack initiation point, $J_{0.2}$, which is the *J*-integral value at the intersection of the 0.2 mm offset line and the *J*-resistance curve. The initial crack growth toughness, dJ/da, is obtained as a linear regression slope of the *J*-resistance curve between the 0.15- and 1.5-mm offset lines, Fig. 5.3.

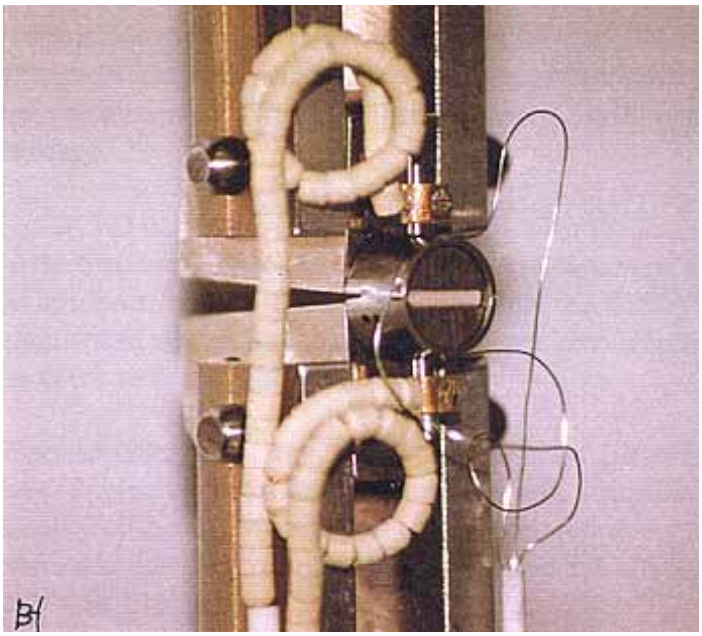

Fig. 5.2. The PLT specimen with attached DCPD probes mounted in the testing machine.

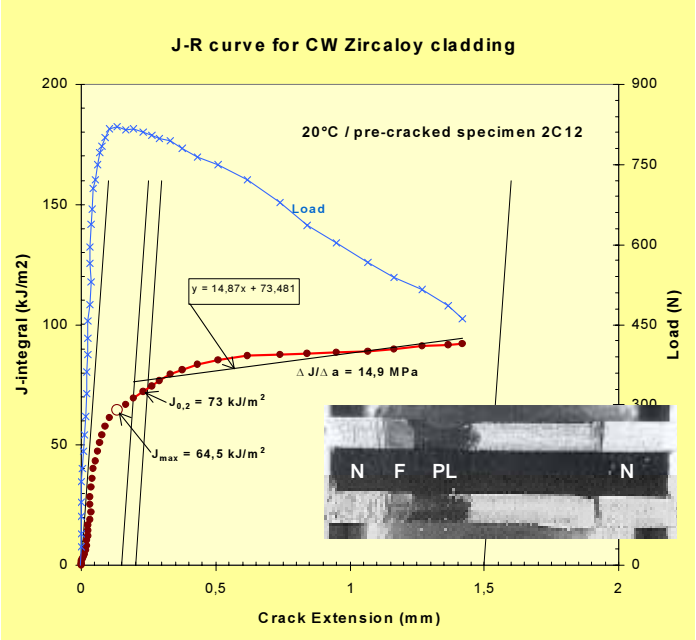

Fig. 5.3. An example of J-resistance curve and fracture surface of hydrided Zircaloy specimen (200 ppm) tested at 25°C.

The same experimental set-up has been used for the measurements of delayed hydride cracking velocity in Zircaloy cladding [5.4]. The PLT-specimens with two different lengths, 9 and 13 mm, were machined from Sandvik Zircaloy-4 lot 86080 (see Fig. 5.1). The tubing had an outside diameter of 9.5 mm and a wall thickness of 0.57 mm. The material had a final anneal of 480°C for 3.5 h and had a recovered cold-worked structure with 5 to 10% recrystallisation. The yield stresses at 20 and 385°C were 553 and 355 MPa, respectively. About 200 ppm hydrogen were added to the tubing electrolytically. The pre-cracked

specimens were heated in air to 315°C for one hour, cooled to the test temperature of 250°C, then loaded after a hold time of about one hour. To monitor crack growth under the constant load applied to the specimen, the DCPD technique was used. The loading of the specimen was usually accompanied by a step-wise increment of the DCPD reading followed by a gradual increase of the DCPD values, Fig. 5.4. Cracking was allowed to continue until the crack had grown about 2 mm. The load was then removed, the furnace opened and the specimen cooled down to room temperature. The unloading of the specimen was usually accompanied by a step-wise decrease of the DCPD reading (see Fig. 5.4). The end of the crack was marked by means of short-term fatigue. An example of specimen fracture surface obtained after the DHC test is also shown in Fig. 5.4.

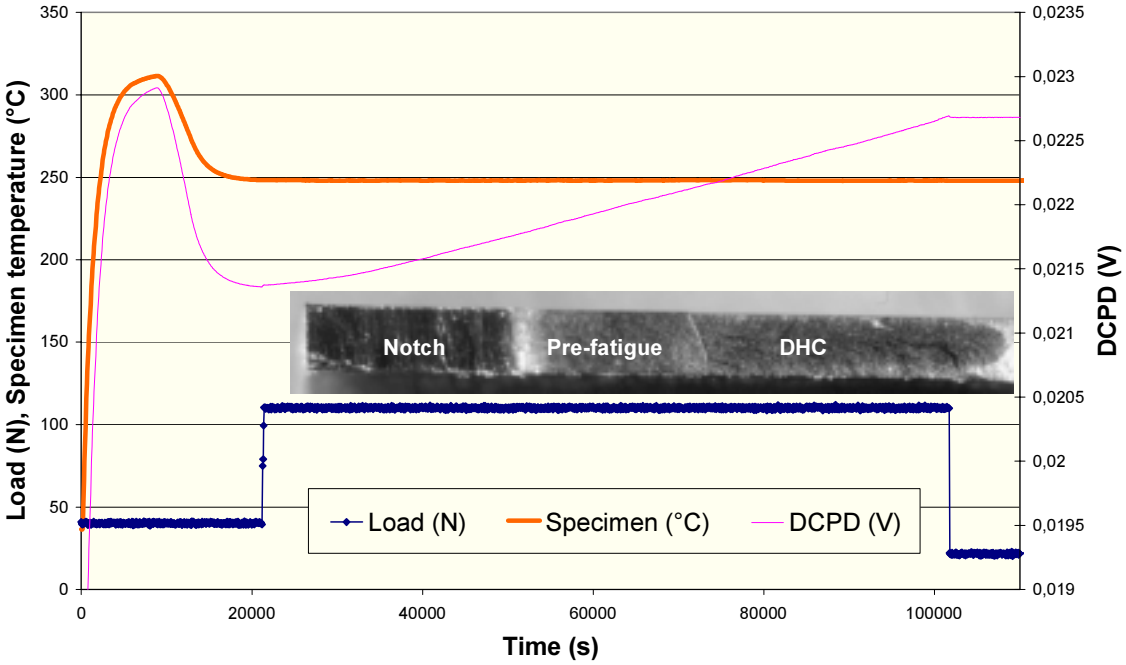

Fig. 5.4. An example of the data record for entire DHC test performed for hydrided Zircaloy cladding (200 wtppm). The DHC-crack area extended during the time under constant load of 110 N is clearly distinguished at the specimen fracture surface (one side of the specimen is shown).

5.2. Results

Independently of the specimen length, 9 or 13 mm, good reproducibility of the axial crack velocity, V_{DHC}, was observed, Table 5.1.

Table 5.1. Results of DHC tests at 250°C on Zircaloy-4 fuel cladding

Specimen	Test temp (°C)	Test temp 1000x(K^{-1})	DHC-crack (mm)	Incubation time (min)	Cracking time (min)	DHC velocity (m/s)
13-4	247.9	1.920	2.4	24	1398.0	2.8E-08
13-5	249.5	1.914	1.6	119	1032.5	2.6E-08
13-6	249.9	1.912	2.4	30	1294.0	3.0E-08
9-4	250.2	1.911	1.7	21	962.0	3.0E-08
9-5	248.1	1.919	2.1	14	1324.0	2.7E-08
9-6	251.1	1.908	1.6	19	875.0	3.0E-08

The V_{DHC}-values for identically tested specimens fell within the interval of 2.6×0^{-8} m/s to 3.0×10^{-8} m/s. Compared with the axial crack velocities obtained at 250°C in the Zr-2.5Nb pressure tube material, this range of values is below those for CANDU material, Table 4.1, but similar to those for RBMK TMT-1 material, Table 4.10. Contributors to the low value of V_{DHC} would be the low peak temperature that did not allow all the hydrogen to be dissolved and the moderate yield strength (430 MPa at 250°C,(by interpolation)), but separating these factors is beyond the scope of this report

The DHC-crack surface topography obtained in the present work for unirradiated cladding, Fig. 5.5, appears to reproduce the main topographical features observed for axial splits in failed fuel rods:

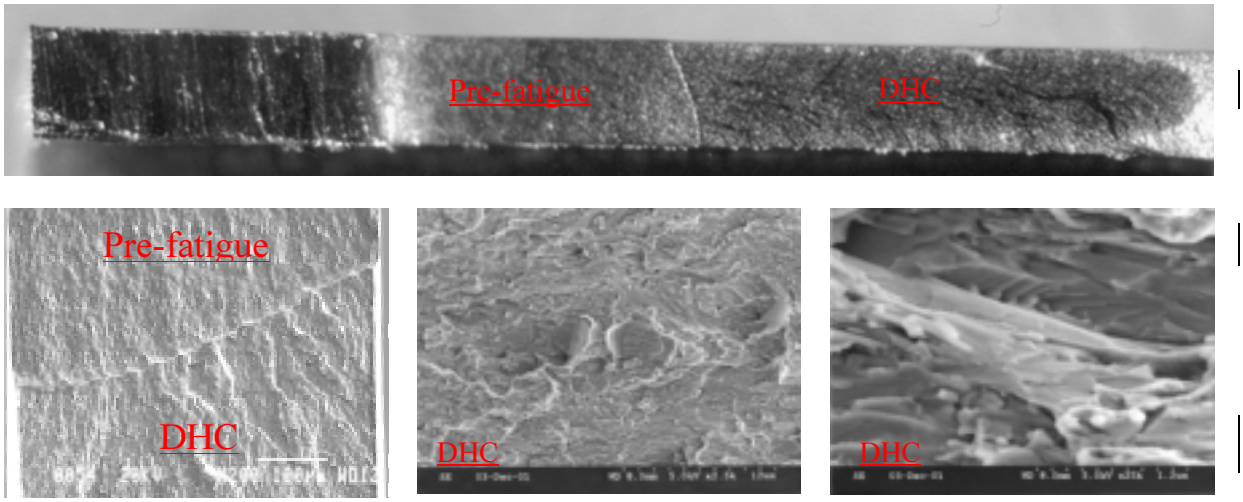

Fig. 5.5. Typical macroview of DHC fracture surface in unirradiated hydrided Zircaloy cladding and SEM photos of the same fracture surface (the SEM photos are the courtesy of K. Pettersson).

— the crack surface is macroscopically flat and oriented along the radial-axial plane of cladding;
— the clear "chevron" pattern is observed along the entire DHC-crack length;
— the notch length and fatigue crack length are longer at the inner surface of the specimen, while the DHC-crack propagates faster in the outer layers of the specimen;
— the fatigue crack propagates without specimen thinning while the specimen wall is thinned along the DHC-crack.

5.3. Summary

A method has been developed and demonstrated to measure the crack velocity of DHC in fuel cladding. The method is based on a previous method used for evaluating fracture toughness of fuel cladding and incorporates the knowledge developed in this CRP.

REFERENCES TO CHAPTER 5

[5.1] GRIGORIEV, V., JOSEFSSON, B., ROSBORG, B., Fracture toughness of Zircaloy cladding tubes. ASTM STP 1295, American Society for Testing and Materials, PA, 1996, pp. 431–447.

[5.2] GRIGORIEV, V., JOSEFSSON, B., ROSBORG, B., BAI, J., A novel fracture toughness testing method for irradiated tubing - Experimental results and 3D numerical evaluation. Transactions of the 14-th International Conference on Structural Mechanics in Reactor Technology (SMiRT-14), Vol. 2, Division C-4, 1997, pp. 57–64.

[5.3] LYSELL, G., GRIGORIEV, V., EFSING, P., Axial splits in failed BWR fuel rods. Presented at ANS International Topical Meeting on Light Water Reactor Fuel, Park City, Utah, USA, April 10–13, 2000.

[5.4] GRIGORIEV, V. JAKOBSSON, R., Application of the Pin-Loading Tension test to measurements of Delayed Hydride Cracking velocity in Zircaloy cladding. Report SKI-00:57 (November 2000).

CHAPTER 6

CONCLUSIONS AND RECOMMENDATIONS

6.1. Conclusions

1. The techniques for performing measurements of the rate of delayed hydride cracking in zirconium alloys have been transferred from the host laboratory to other countries.
2. By following a strict procedure, a very consistent set of values of crack velocity were obtained by both individual laboratories and between the different laboratories.
3. The results over a wide range of test temperatures from materials with various microstructures fitted into the current theoretical framework for delayed hydride cracking.
4. An inter-laboratory comparison of hydrogen analysis revealed the importance of calibration and led to improvements in measurement in the participating laboratories.
5. The success of the CRP in achieving its goals has led to the initiation of some national programmes.

6.2. Recommendations

1. Future work on delayed hydride cracking should be on equally well-characterized material with similarly controlled experimental procedures.
2. Based on the success of this CRP, it is recommended that further research should be initiated with the objective of evaluating delayed hydride cracking in fuel cladding to support understanding of long splits observed in some fuel.
3. Zirconium standards rather than titanium standards are recommended for calibration when analysing hydrogen in zirconium alloys.

LIST OF PARTICIPANTS

Alvarez, A.	Studsvik Nuclear, Sweden
Banerjee, S.	Bhabha Atomic Research Center, India
Bickel, G.A.	Atomic Energy of Canada Limited, Canada
Choubey, R.	Atomic Energy of Canada Limited, Canada
Coleman, C.E.	Atomic Energy of Canada Limited, Canada
Dobrea, D.	Institute for Nuclear Research, Romania
Gou, Yuan	Nuclear Power Institute of China, China
Grigoriev, V.	Studsvik Nuclear, Sweden
Grybenas, A.,	Lithuanian Energy Institute, Lithuania
Haddad, R.	Comision Nacional de Energia Atomica, Argentina
Jakobsson, R.	Studsvik Nuclear, Sweden
Kanwar Liaqat Ali	Pakistan Institute of Nuclear Science and Technology, Pakistan
Kim, Y.S.,	Korea Atomic Energy Research Institute, Republic of Korea
Leger, M.	Atomic Energy of Canada Limited, Canada
Levinskas, R.,	Lithuanian Energy Institute, Lithuania
Makarevicius, V.	Lithuanian Energy Institute, Lithuania
Markelov, V.A.	A.A. Bochvar All-Russian Scientific Research Institute of Inorganic Materials, Russian Federation
Pitigoi, V.	Institute for Nuclear Research, Romania
Radu V.	Institute for Nuclear Research, Romania
Ritchie, I.	International Atomic Energy Agency
Roth, M.	Institute for Nuclear Research, Romania
Singh, R.N.	Bhabha Atomic Research Center, India